

# Loughborough University Institutional Repository

---

## *Lens design for manufacture*

This item was submitted to Loughborough University's Institutional Repository by the/an author.

**Additional Information:**

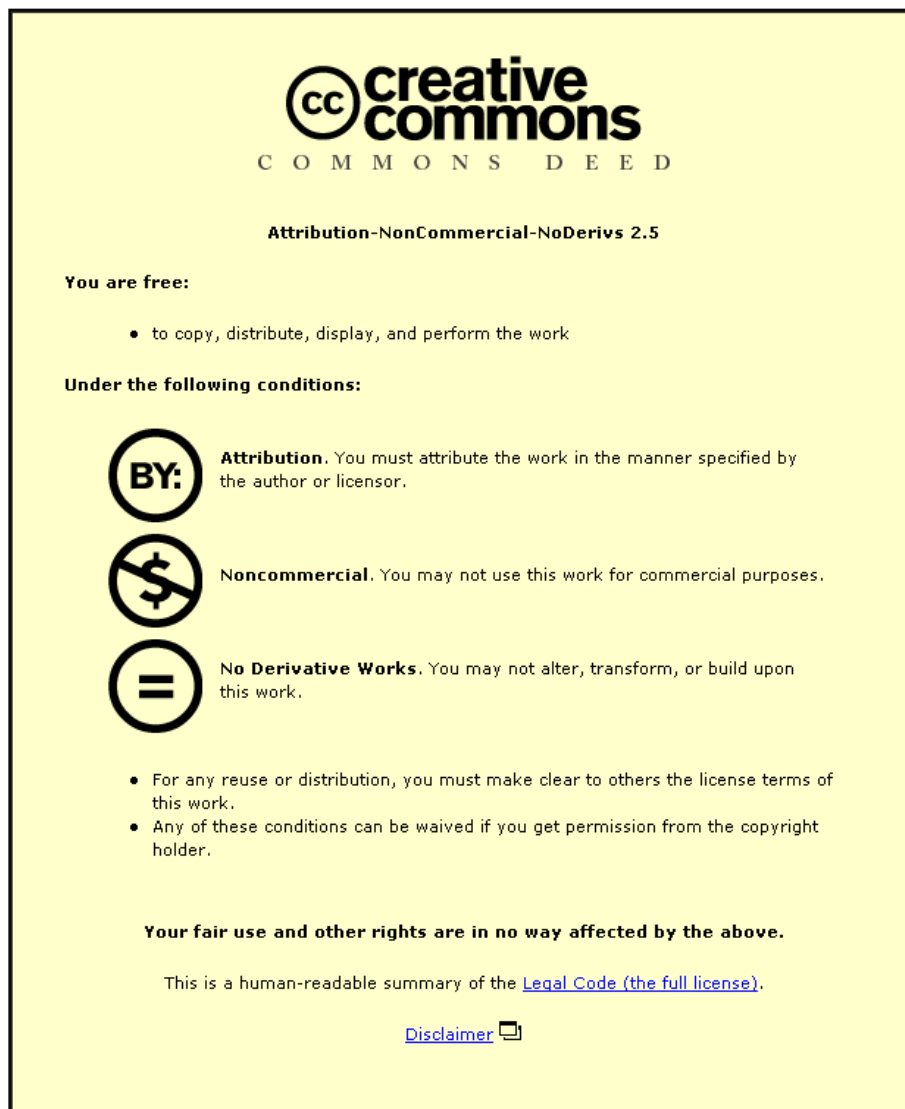
- A Doctoral Thesis. Submitted in partial fulfilment of the requirements for the award of Doctor of Philosophy of Loughborough University.

**Metadata Record:** <https://dspace.lboro.ac.uk/2134/14554>

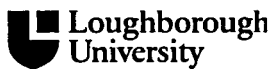
**Publisher:** © Richard John Tomlinson

Please cite the published version.

This item was submitted to Loughborough University as a PhD thesis by the author and is made available in the Institutional Repository (<https://dspace.lboro.ac.uk/>) under the following Creative Commons Licence conditions.



For the full text of this licence, please go to:  
<http://creativecommons.org/licenses/by-nc-nd/2.5/>



**University Library**

Author/Filing Title ..... TOMLINSON, RICHARD

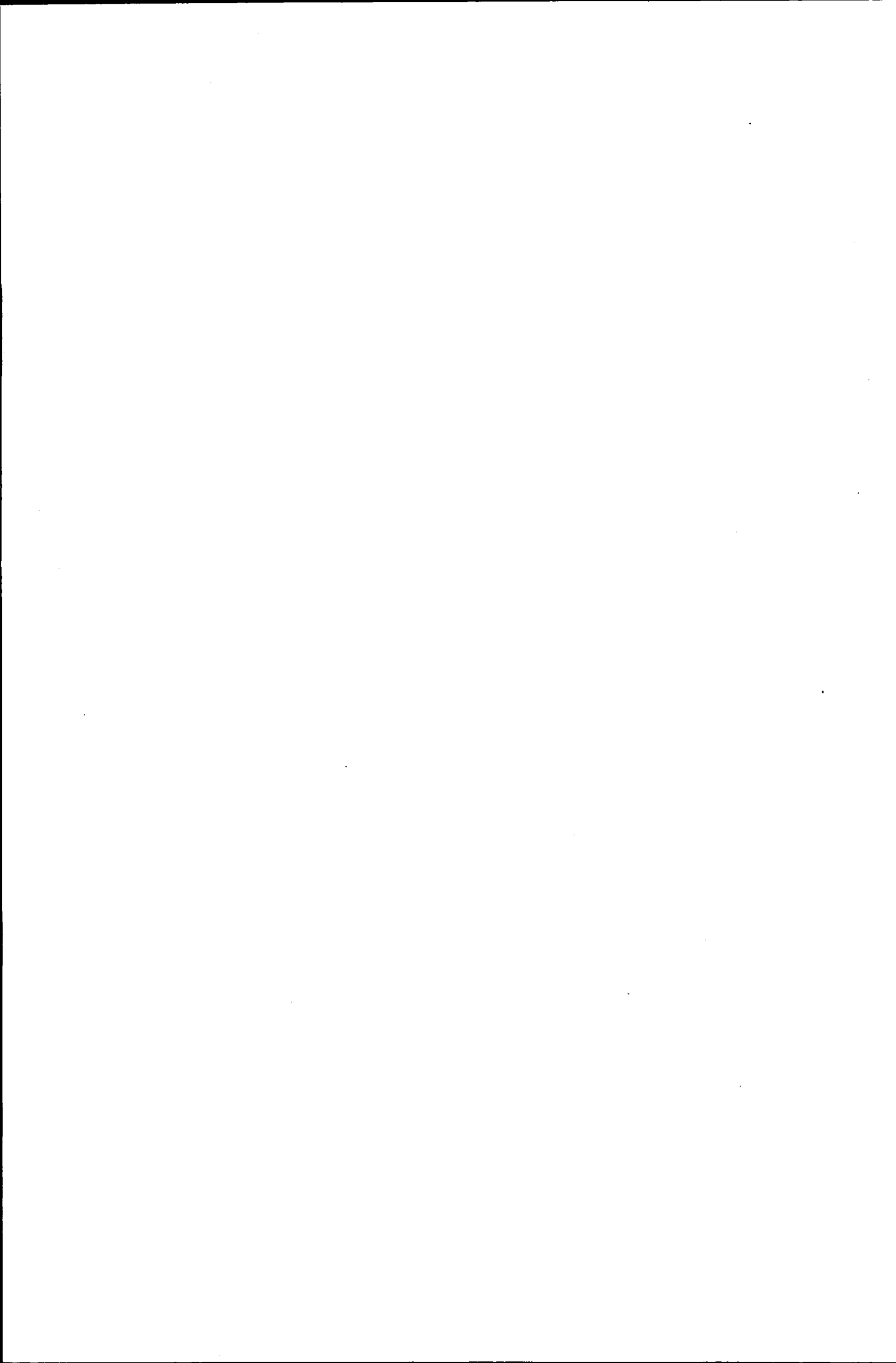
Class Mark ..... T

Please note that fines are charged on ALL  
overdue items.

FOR REFERENCE ONLY

040319136X





**Lens Design for Manufacture**

by

**Richard John Tomlinson**

**A Doctoral Thesis submitted in partial fulfilment of the  
requirements for the award of**


**Doctor of Philosophy**

**of the Loughborough University**

**December 2004**

**Research Supervisor: Dr. J M Coupland  
Dr. J Petzing**

**© Richard John Tomlinson**

	<b>Loughborough University</b> Pilkington Library
Date	JAN 2005
Class	T
Acc No.	040319136X

## Abstract

The manufacture of complete optical systems can be broken down into three distinct stages; the optical and mechanical design, the production of both optical and mechanical components and finally their assembly and test. The three stages must not be taken in isolation if the system is to fulfil its required optical performance at reasonable cost.

This report looks first at the optical design phase. There are a number of different optical design computer packages on the market that optimise an optical system for optical performance. These packages can be used to generate the maximum manufacturing errors, or tolerances, which are permissible if the system is to meet its design requirement. There is obviously a close relationship between the manufacturing tolerances and the cost of the system, and an analysis of this relationship is presented in this report. There is also an attempt made to optimise the design of a simple optical system for cost along with optical performance.

Once the design is complete the production phase begins and this report then examines the current techniques employed in the manufacture, and testing of optical components. There are numerous methods available to measure the surface form generated on optical elements ranging from simple test plates through to complex interferometers. The majority of these methods require the element to be removed from the manufacturing environment and are therefore not in-process techniques that would be the most desirable. The difficulties surrounding the measurement of aspheric surfaces are also discussed. Another common theme for the non-contact test techniques is the requirement to have a test or null plate which can either limit the range of surfaces the designer may choose from or increase the cost of the optical system as the test surface will first have to be manufactured. The development of the synthetic aperture interferometer is presented in this report. This technique provides a non-contact method of surface form measurement of aspheric surfaces without needing null or test plates.

The final area to be addressed is the assembly and test stage. The current assembly methods are presented, with the most common industry standard method being to fully assemble the optical system prior to examining its performance. Also, a number of active alignment techniques are discussed including whether the alignment of the individual optical elements is checked, and if need be adjusted, during the assembly phase. In general these techniques rely upon the accuracy of manufacture of the mechanical components to facilitate the optical alignment of the system. Finally a computer aided optical alignment technique is presented which allows the optical alignment of the system to be brought within tolerance prior to the cementing in place of an outer casing. This method circumvents the need for very tight manufacturing tolerances on the mechanical components and also removes the otherwise labour intensive task of assembling and disassembling an optical system until the required level of performance is achieved.



Acknowledgements

Many thanks to Jeremy Coupland for both his guidance and patience throughout this project.

Huge thanks to Jon Petzing for all his support and advice.

Thanks to all of the technical and workshop staff without whose assistance many of the mechanical components would not have been manufactured.

Thanks also to Ben, Emma, Adrian, Anton, Candi, and John for making coming to work such a pleasure.

Thanks to Mum, Dad, Andy and Leanne for their support.

And finally, thanks to Sarah for everything.

## TITLE: Lens Design for Manufacture

## Contents

Chapter 1. Introduction	1
1.1 Motivation	2
1.2 Background	2
1.3 The Design Process	3
1.4 Manufacture and Surface Testing	4
1.5 Synthetic Aperture Interferometry	4
1.6 Multi Element Lens Alignment	5
1.7 Outline	5
References	7
 Chapter 2. The Lens Design Process	 8
2.1 Introduction	9
2.2 Lens Design and Optimisation for Optical Performance	10
2.2.1 Basic Paraxial Optics and Thin Lens Theory	14
2.2.2 Ray Tracing	18
2.2.3 Aberration Theory	19
2.3 Aspheric Optics	23
2.4 Conclusions	25
Figures	26
References	30
 Chapter 3. Tolerancing and the Inclusion of a Cost Function within Optimisation	 34
3.1 Introduction	35
3.2 The Tolerance Parameters	35
3.2.1 Introduction to Tolerancing	41
3.3 Practical Considerations in Lens Design: The Application of Tolerancing at the Assembly Stage	45
3.4 Lens Building Example	49
3.5 The Development of a Cost Model	50

3.6 Existing Optimisation Tools that include Cost	63
3.7 A Global Cost Model	64
3.8 Conclusions	70
Chapter 3. Figures	72
References	82
Chapter 4. Optical Element Production and Testing	86
4.1 Introduction	87
4.2 The Manufacture of Optical Elements	87
4.2.1 The Production of Curved Optical Surfaces	88
4.2.2 The Problems Presented by Aspheric Surfaces	91
4.3 Surface Form Testing with Particular Reference to Aspheric Surfaces	92
4.3.1 Simple Test Plates	92
4.3.2 Contact Techniques	94
4.3.3 Interferometric Techniques and other Optical Non-Contact Techniques	95
4.4 An Ideal Surface Test System for Aspheric Optics	101
4.5 Conclusions	102
Chapter 4. Figures	103
Chapter 4. References	105
Chapter 5. Synthetic Aperture Interferometry	110
5.1 Introduction	111
5.2 Background to the Synthetic Aperture Technique	112
5.3 Synthetic Aperture Interferometer Configurations	113
5.4 Theory	115
5.5 Implementation and Experiment	119
5.6 Discussion of Synthetic Aperture Interferometry and Further Improvements	120
5.7 Conclusions	121
Chapter 5. Figures.	123

References	131
Chapter 6. Computer-Aided Lens Assembly (CALA)	132
6.1 Introduction	133
6.2 The CALA Method	134
6.3 The Design of the Test Set-up	138
6.4 Experimental Method	139
6.5 Results	140
6.6 Discussion and Conclusions	143
Chapter 6. Figures	144
References	149
Chapter 7. Conclusions and Further Work	150
7.1 Summary	151
7.2 Conclusions	152
7.3 Further Work	154
Chapter 7. Figures	157
References	158

CHAPTER 1  
INTRODUCTION

## Chapter 1. Introduction

### 1.1 Motivation

This thesis is concerned with improving the processes, and reducing the cost of the manufacture of complex multi-element lens systems. A global view of the process is presented beginning with the production of a lens specification, and a discussion of the design and tolerancing stages. The manufacture of optical components is then addressed with a review of surface form measurement techniques that are currently employed to check the quality of the optics at this stage. Particular reference is made to methods that can be applied to the production and measurement of aspheric surfaces. The final step of the production process is the build and system test stage where the individual optical and mechanical components are assembled into the finish saleable product. These last stages can have a very large impact on the overall cost of the system. By some estimates the cost of the design and optical manufacture stages can represent as little as 10% of the overall cost of the system.<sup>1</sup>

### 1.2 Background

This thesis builds upon practical experience of lens building and testing, gained whilst undertaking a Knowledge Transfer Partnership (KTP) project (formerly TCS) in the workshops of Van Diemen Ltd of Earl Shilton, Leicestershire, UK. For the most part Van Diemen was involved with the design and production of mechanical housings for cinematic lenses. However, the company had a small production facility for polishing and testing spherical elements.

Initially the author worked in the service department where he was soon responsible for the repair and re-alignment of complex lens systems from a wide variety of manufacturers. This work illustrated the range of fixing methods that are used in these types of lenses and the degree of precision afforded by each. The work also demanded knowledge of the methods used to specify lens elements so that replacement parts could be manufactured.

Once built, complete lens systems were characterised using a variety of qualitative and quantitative tests and external markings were specified. Working in this area illustrated the physical consequences of misalignment and the importance of sound mechanical design.

Returning to Loughborough University, the lens design and manufacture processes were reconsidered as a whole and a number of key areas were identified for possible improvements. In the following paragraphs these areas are briefly discussed before presenting details of this work in the main body of the thesis.

### 1.3 The Design Process

Traditionally the lens design process was very labour intensive requiring the tracing of rays using mechanical calculators and trigonometric tables. Currently, the vast majority of the design of optical systems is carried out purely on optical performance until an acceptable solution is reached and then the system is toleranced to examine the accuracies to which the system must be manufactured and assembled in order to realise the desired performance criteria. Using this approach the design may well have to be redesigned if the tolerances are too restrictive, or, indeed, are uneconomic to reach in the production environment. Even if the tolerances are possible at a commercially acceptable cost there is no guarantee that the most economic solution to the design problem has been found. Given this, it is clearly desirable to consider the tolerance data and its impact on cost, along with optical performance criteria, at the optimisation stage of the design process as this would result in both optically satisfactory and economic solutions to the design problem. To achieve this aim comprehensive cost models are required that accurately estimate the costs of manufacture and assembly of competing designs, and a balance between cost and optical performance parameters must be reached. The practical implementation of this approach is the first task considered in this thesis.

## 1.4 Manufacture and Surface Testing

There are a large number of methods available for the production of optical elements ranging from the traditional grinding and polishing techniques<sup>2</sup> to the modern Magnetorheological Finishing<sup>3</sup> method employing computer controlled generation of optical surfaces. The lenses must also be tested to ensure that they have been produced to specification. A number of different test methods are available to the optical workshop including various interferometric techniques, and contact and non-contact profilers. Currently, for aspheric surfaces, the surface form testing is carried out after the lens has been manufactured and is therefore a consecutive not a concurrent process. In order to reduce the rejection rate and aid the manufacture of aspheric surfaces, especially by the newer single point and computer controlled manufacturing techniques, it is desirable to run the production and test phases concurrently and on the same machine to enable corrective adjustment of the surface. In most cases current on-machine, in-process measurement techniques are of the profiler type and so only sample distinct areas rather than the whole surface.

## 1.5 Synthetic Aperture Interferometry

Surface shape measurement using a novel synthetic aperture interferometer is the second method introduced and discussed in this thesis. Synthetic Aperture Interferometry effectively produces a surface shape by knitting together a large number of measurements that are taken across the entire aperture of the surface under test. This process has the potential to be included as an in-process, on-machine technique that can be fitted to CNC polishing machines. The method does not require the use of separate null or test plates and is inherently tolerant of vibration such as might be experienced in an on-machine application. However, the technique does use the rear surface of the component as a reference surface and as such this surface must be calibrated in the same way that any test plate or null surface. This is a potential disadvantage as in effect every component has its own un-calibrated reference surface. The technique can be used to measure aspheric surfaces as well as conventional spherical surfaces.



## 1.6 Multi Element Lens Alignment

After the component production and measurement phases, the lens system must be assembled in a manner that satisfies the tolerances placed upon it. At present the lens systems are generally fully assembled prior to testing. This has obvious cost and time implications if the system does not meet the required performance level, and has to be disassembled and rebuilt. A method of Computer-Aided Lens Assembly (CALA) is presented here in which the individual lens elements are aligned by following computer instructions. Adjustments which can be made are decentrations in two orthogonal directions, tilt about two orthogonal axes and in the axial position (the airspace between the elements). The process continues iteratively until the system is aligned to within tolerance and low tolerance mechanical fixturing is then used to secure the elements. The CALA method is the third manufacturing innovation considered in this thesis.

## 1.7 Outline

In Chapter 2 of this thesis, the lens design process is examined in detail. Generic lens specification is presented, followed by a discussion of the optical design optimisation process. A number of different optimisation methods are outlined along with a comparison of their relative merits. These different optimisation tools all have one thing in common in that they optimise the design solely on its optical performance. The optical theory required by a designer to make the best use of optical design software is described, beginning with basic paraxial optics and ray tracing through to a description of the aberrations that degrade the performance of optical systems.

Chapter 3 describes the tolerancing of optical systems. The parameters to be toleranced are detailed and computer aided tolerancing is described. A discussion of how the cost of an optical system is affected by the tolerances placed upon it, and various models of how these costs change, is presented. Finally cost parameters are introduced into an optimisation routine, along with the usual performance criteria, in order to find a more cost effective solution to a simple optical design problem of a cement doublet lens.

Chapter 4 introduces the various methods by which optical elements are manufactured with particular interest paid to aspheric surfaces generated on optical glass. The current methods by which the surface form of these lenses is tested are then discussed. A profile of what would constitute an ideal surface test method for the production environment is then developed as an aid to the design of a new type of interferometer.

The design and testing of a new type of interferometer is discussed in Chapter 5. This technique is similar in concept to Synthetic Aperture Radar where a picture of the ground is constructed from a large number of smaller images. In this case there is an analogous interferometric technique, termed Synthetic Aperture Interferometry,

In Chapter 6, a novel method of lens alignment and build is presented, termed Computer-Aided Lens Assembly, CALA. This technique employs real and computer generated ray tracing through the optical system combined with an optimisation routine that provides corrective displacements for the system.

Chapter 7 concludes the thesis and details the main achievements presented in it. Areas for further investigation are then highlighted and discussed.

References

---

1. R.E. Hopkins, "Optical design 1937-1988...Where to from here?", *Optical Engineering*, Vol. 27, No. 12, pp 1019-1026, (1988).
2. Frank Twyman, "Chapter 3, The Nature of Grinding and Polishing", in *Prism and Lens Making*, Adam Hilger, London UK, pp 49-66, (1988).
3. Harvey M. Policove, "Next Generation Optics Manufacturing Technologies", *Advanced Optical Manufacturing and Testing Technology, Proceedings of SPIE* Vol. 4231, pp 8-15, (2000)

CHAPTER 2  
THE LENS DESIGN PROCESS

## Chapter 2. The Lens Design Process

### 2.1 Introduction

The lens design process is a very complex and involved task of many steps, requiring a wide range of skills and experiences. Before the lens design can begin in earnest, a specification of the desired performance must be drawn up. The specification contains information concerning the mechanical interface, mounting system, environmental performance and cost, in addition to the desired optical performance<sup>1</sup>. The following is a list of the most common criteria to be considered before lens design begins; it is by no means an exclusive or exhaustive list, but is meant as a basic guide.

Focal Length	Weight
Zoom Requirement	Field of View
Aperture size/position	Size
Cost	Operating Wavelength
Mounting System	Use of Optical Coatings
Image Height	Resolution.

Other parameters may be added to this list depending on the specific system required, and different weightings may be applied to these headings according to their relative importance to the success of the design. For example, if the designer is producing a film lens, then the image height must fill the film frame otherwise the lens will not be useful to the cameraman, so this parameter would have a high weighting applied to it.

Once the specification has been produced the design of the lens system may begin. The design process involves finding the optimum performance/cost balance with respect to the initial specification.

## 2.2 Lens Design and Optimisation for Optical Performance

The majority of lens design presently carried out is concerned with the optical performance delivered to the end user. The optimisation routines within the lens design packages optimise designs by minimizing a parameter known as an error function (or maximizing a merit function). An error function is a combination of numerous separate parameters that attempt to describe the performance or quality of the system within this single value. Error functions vary greatly in type and complexity and can involve simple generalized models or include large user edited components that tailor it for a specific use. Error functions can include terms to limit a design to a particular focal length,  $f\#$  number, magnification or physical dimensions such as lens aperture or edge thickness whilst attempting to minimise wavefront optical path difference (OPD), or spot size at the focal point or at many points around the field. Each of the separate parameters within the error function is assigned a weight based on its relative importance, and it is these weights that drive the optimisation package towards a particular result.

The main lens design software used during the research for this thesis has been the Sinclair Optics OSLO lens design package<sup>2</sup>. When constructing an error function within OSLO, the first choice to be made is what type of error function is the most appropriate, the RMS (Route Mean Squared) spot size, or the RMS wave front error type. The method of field and pupil sampling has to be selected, as does the number of field points. A field point is defined as the coordinate that the ray emanates from, and so the number of field points defines the minimum number of rays that will be traced through the system. In general the more field points that are generated the more accurate the analysis. However, the complexity of the error function is often limited by the available computing power. Other considerations may be included within the error function; examples of some included in the OSLO package are automatic colour correction, and the correction of distortion at full field. A limit may be put on the distortion and the error function will attempt to abide by this limit during the optimisation process.

After the generation of the desired lens specification, the next step is the choice of a suitable starting point for the optimisation. In all but the simplest cases, lens design packages are incapable of producing acceptable results when starting from a blank design, without a good starting point and human input from the designer throughout the optimisation procedure<sup>3</sup>. In the future, it may be possible to start the optimisation with flat plates and achieve a viable solution<sup>4</sup> by employing sufficient computing power. However it is not current best practice. At present the designer must still choose fundamental parameters such as how many surfaces to begin with and also be able to determine whether the design represents the best possible solution to the problem. This approach also ignores the fact that there may be an existing design that with only slight modifications could fulfil the new specification. Indeed the starting point used for the design is usually taken as an existing design that has similar optical performance to that required. Optical elements can then be added and subtracted and other design parameters altered until the new design specification is realised. Modern lens design packages often include a lens library specifically to be used as starting points in new lens designs<sup>5</sup>.

The optimisation variables are now selected. There are many potential variables including airspace, element thickness, lens curvature, optical glass type and the use of aspheric curves. The choice of variables greatly affects the progress of the optimisation, and it is often wise to constrain the optimisation to a limited number of variables at any one time. Some of the benefits and drawbacks inherent in the more commonly employed variables will now be discussed.

The airspace between lenses can be a very useful tool because it is a continuously variable parameter that can have a large effect on the overall optical performance. Element thickness, however, is a very different variable. In the majority of designs it is an ineffective variable and, unless tightly constrained, often results in unfeasibly thick elements in an attempt to significantly alter the system optical performance<sup>6</sup>. Careful limits must also be placed upon the element edge thickness and centre thickness, in the case of negative elements, if the lens is not to become prohibitively

difficult to manufacture and assemble. This will be discussed further in Chapter 3. There are still some lenses where element thickness is a useful variable, such as the older meniscus lenses like Protar and Dagor (where thickness is used to control the Petzval Curvature and higher order aberrations)<sup>7</sup>.

Lens curvature is a powerful variable that has a significant effect on the system performance for relatively small alterations. This is because it is a combination of the glass type and curvature that defines the power of the optical element. In most cases the surface curvature is treated as a continuously variable parameter within the lens design until the design nears completion. Often these curvatures are then limited to the curvatures for which the company's optical workshops already have the tooling and test plates, in order to reduce the cost of the finished design and the lens is then re-optimised with the new curvatures.

The glass type is an interesting parameter when considered as a variable. For the purposes of the optimisation, it can be considered as a continuously varying parameter even though, in reality, the designer (except in exceptional circumstances) is limited to the glass types already on the market. In this process the optimisation is allowed to alter the refractive index and dispersion of the glass to reach the highest level of performance, though they are normally altered in such a way that the design is limited to non-exotic glass types. Once an acceptable solution has been reached the theoretical glass types are substituted with their closest equivalent catalogue glass type and the design is reoptimized with the glass type fixed to produce a high quality yet manufacturable solution.

The use of aspheric curves within the optimisation can produce very effective results in terms of optical performance though the optimisation can be very difficult to constrain, especially as there is a desire to constrain the surface with as few variables as possible<sup>8</sup> since the speed of optimisation is approximately related to the square of the number of variables involved, and the lens becomes very expensive to manufacture. Despite this, aspheric elements are increasingly important in modern



lens design and the benefits and manufacturing implications are discussed in detail elsewhere in this thesis.

Numerous different optimisation techniques are available to the optical designer and an understanding of their differences and relative strengths is useful when selecting which method to use. One of the most common optimisation methods is known as the Damped Least Squares method<sup>9</sup>. The software will typically alter each of the specified variables by a small amount, (often the magnitude of the alterations can be specified by the designer), and then recalculate the error function to determine whether the performance of the system has been improved. This process will continue through numerous iterations until the program has reached a suitable end point or the maximum number of iterations has been reached. There is a simple landscape analogy<sup>10</sup> that can be applied to describe the process, in which the latitude and longitude are the variables chosen and the elevation represents the value of the error function. The initial design represents a location on this landscape and the optimisation routine will move the design through this landscape along a path of decreasing elevation until a minimum is reached. However, the landscape may have many depressions and the "local minima" that the program has reached may not be the best achievable, known as the "global minimum". The minimum that is arrived at often depends upon the starting position of the design. The design can be shifted out of local minima by manually introducing a significant change in the variables, effectively starting the design from a different point in the landscape. Similarly if part of the design is "frozen" then the design moves away from a local minima and towards another region of the landscape and hopefully a more acceptable solution.

A more modern method of optimisation is referred to as Simulated Annealing<sup>11</sup>. This is a random search type optimisation method that attempts to find a global minimum. Before the optimisation routine can begin upper and lower limits must be placed on all of the variables within the design. The optimisation routine then randomly selects, with reference to distribution models, values for the variable lens design parameters within the specified limits and the performance of the resulting

design is analysed. If the lens performs better than the preceding design then it is accepted. If not, it is rejected. In either case the program continues until the change in the merit function per step falls below a predetermined level. This method has the advantage over the Damped Least Squares method in that it jumps from point to point around the landscape and so does not get caught in local minima. This behaviour is controlled by a property known within the optimisation routine as temperature,  $T$ , as it is broadly analogous to the temperature in the annealing process. The level of  $T$  is determined by the lens designer and is lowered throughout the lens optimisation. At the start of the optimisation,  $T$ , has a large value allowing the optimisation routine to escape from local minima and explore the entire optimisation region. As the process continues the value of  $T$  is slowly lowered until the optimisation terminates at the global minimum. The rate at which  $T$  is reduced is termed the cooling rate. If the cooling rate is too fast then there is an increasing possibility that the optimisation will get caught in a local minimum and the performance of the resulting design will suffer. However, this method takes a great deal of computing power and is therefore much slower than the Damped Least Squares method.

Whatever method of optimisation is chosen, with the exception of simulated annealing, a high degree of optical design ability is still required to produce high quality results. The designer must choose a suitable start position, select and put sensible limits on the optimisation variables, and construct an error function that is tailored to the requirements of the lens specification. The designer must also be able to determine whether the design has been optimised to its maximum potential or if a local minima has been found.

### 2.2.1 Basic Paraxial Optics and Thin Lens Theory

In order to be able to achieve a high performance result, the designer must understand the optical theory that the lens design packages employ when analysing the designs. The majority of optical design is based on a process known as ray

tracing, where the progress of a number of rays is traced through an optical system. However, before ray tracing can be addressed, basic optical calculations need to be performed and are reviewed here for clarity. The first calculations on any optical system are generally carried out in the paraxial region of the optical system<sup>12</sup>. The paraxial region is defined as being close to the optical axis, and paraxial rays are parallel or almost parallel to the optical axis, such that they make only small angles to it. The ideal optical system can be defined by its cardinal points, consisting of the focal points, principal planes and nodal points<sup>13</sup>. This simplified optical system can be thought of as a *black box* defined between the two principal planes. A diagram depicting the simplified optical system is provided in Figure 2.1. If the system is bounded by air on both sides then the first and second nodal points lie on the principal planes and this case will be assumed for the examples presented here. Important properties of the system are effective focal length (EFL), defined as the distance from the rear principal plane to the second focal point; the back focal length (BFL) is the distance from the rear lens surface to the second focal point, and the front focal distance (FFL) corresponding to the distance from the first focal point to the front surface of the optical system. Thin lens theory is employed during the early stages of optical system design as it enables the designer to quickly estimate the basic properties of the optical system such as the height and position of an image formed by the system. The focal length of a single, thin lens with two spherically curved surfaces can be derived using equation 2.1 sometimes referred to as the lensmaker's formula<sup>14</sup>.

$$\frac{1}{f} = (n-1)\left(\frac{1}{R_1} - \frac{1}{R_2}\right) \quad 2.1$$

Where

- f = focal length of system
- n = refractive index of optical glass
- R<sub>1</sub> = radius of curvature of front surface
- R<sub>2</sub> = radius of curvature of rear surface.

The radius of curvature is considered to be positive when the centre of curvature is to the right of the vertex of the surface, analogous to a convex surface, and negative when the centre of curvature is to the left of the vertex.

When a lens with a finite thickness is considered, the positions of the focal points relative to the first and second principal planes have to be considered, and these are termed  $f_1$  and  $f_2$  respectively. These parameters along with the principal planes and further dimensions are depicted in Figure 2.2. The property  $f_1$  can be calculated using equation 2.2<sup>15</sup>.

$$\frac{1}{f_1} = \frac{n_1 - n_3}{n_1 R_2} - \frac{n_2 - n_1}{n_1 R_1} - \frac{(n_2 - n_1)(n_2 - n_3)}{n_1 n_2} \frac{t}{R_1 R_2} \quad 2.2$$

Where  $f_1$  = front focal point, relative to front principal plane  
 $n_1$  = refractive index of medium in front of lens  
 $n_2$  = refractive index of lens  
 $n_3$  = refractive index of medium following  
 $t$  = lens thickness.

And  $f_2$  can be calculated by employing equation 2.3.

$$f_2 = -\frac{n_3}{n_1} f_1 \quad 2.3$$

Where  $f_2$  = second focal point, relative to second principal plane

The next stage is to calculate the locations of the two principal planes. The location of the first principal plane is derived using equation 2.4.

$$r = \frac{n_2 - n_3}{n_2 R_2} f_1 t \quad 2.4$$

Where  $r$  = distance between lens front surface and first principal plane

The location of the second principal plane can be calculated using equation 2.5.

$$s = \frac{n_2 - n_1}{n_2 R_1} f_2 t \quad 2.5$$

Where  $s$  = distance between lens rear surface and second principal plane

In most cases  $n_1$  and  $n_3$  will be air and so will have the same refractive index and  $f_1$  and  $f_2$  have the same magnitude and are given the single notation  $f$ . Once the principal planes and focal points of the system have been located, as shown in Figure 2.2, the image position and size can be calculated. The position of the image from the second principal plane  $s_i$  can be calculated using equation 2.6.

$$-\frac{1}{s_o} + \frac{1}{s_i} = \frac{1}{f} \quad 2.6$$

Where  $s_o$  = the distance from the object to the first principal plane

$s_i$  = the distance from the second principal plane to the image.

In this case distances to the right of the principal plane are considered positive.

The image height is a function of the lateral magnification of the system,  $m$ . The magnification can be found by employing equation 2.7, where  $x'$  is the distance from the second focal point to the image, as defined in Figure 2.2.

$$m = \frac{x'}{f} \quad 2.7$$

The image height,  $h'$ , can then be found using equation 2.8.

$$h' = h.m$$

2.8

Where  $h$  = object height  
 $h'$  = image height.

With the above equations, the basic parameters of the system (the focal length, image position and size) can be determined. In order to learn more about the performance of an optical system, rays must be traced through it from object to image points.

### 2.2.2 Ray Tracing

The basis of ray tracing is the refraction of light at an optical surface. Snell's law governs the propagation of light rays through an optical surface, and is defined in equation 2.9 and Figure 2.3.

$$n_1 \sin \theta_i = n_2 \sin \theta_r \quad 2.9$$

Where  $\theta_i$  = angle of incidence  
 $\theta_r$  = angle of refraction  
 $n_1$  = refractive index of first medium  
 $n_2$  = refractive index of second medium.

Figure 2.4 shows how Snell's Law can be applied to calculate the refraction of a light ray at a single spherically curved surface.

Ray tracing is the basis of optical design analysis. It involves translating rays from one surface to the next through an optical system starting at the object surface and terminating at the image plane. The translation stage involves the calculation of the intercept point on the next surface and then Snell's law, equation 2.9, is applied at this point of interception.

The detail of ray tracing is beyond the scope of this introduction. However, it is worth noting if the sine function in Snell's law can be defined to arbitrary precision by accepting terms of increasing order in a series expansion, equation 2.10.

$$\sin \theta = \theta - \frac{\theta^3}{3!} + \frac{\theta^5}{5!} \dots \quad 2.10$$

If, for example, the series is cropped to first order, the paraxial formulae that defines the position and height of the image (equations 2.1-2.8) can be deduced. If the third order term is taken into account, the primary image aberrations can be defined and these are outlined in the following section.

### 2.2.3 Aberration Theory

The aberration characteristics of an optical system can be determined by tracing a large number of rays through it, and then looking at the amount they deviate from the paraxial image point. This said, by separating the aberrations into distinct image flaws, the amount of work required to analyse a system, and the number of rays that need to be traced, is reduced. Most lens systems currently employ only spherically polished lens surfaces, so this section refers to spherical surfaces unless otherwise stated. The primary monochromatic optical aberrations were analysed and defined by Seidel<sup>16</sup> and are often termed Seidel Aberrations. With reference to Figure 2.5 an equation defining the five primary Seidel Aberrations can be seen below<sup>17</sup>, in equation 2.11.

$$a(r, \theta) = {}_0C_{40}r^4 + {}_1C_{31}h'r^3 \cos\theta + {}_2C_{22}h'^2r^2 \cos^2\theta + {}_2C_{20}h'^2r^2 + {}_3C_{11}h'^3r \cos\theta \quad 2.11$$

Where  $a(r, \theta)$  = wavefront aberration  
 $r, \theta$  = the position in polar coordinates  
 $h'$  = the image height in the exit pupil from the optical axis.

In this case  $a(r,\theta)$  is the wavefront aberration and is defined in the exit pupil as the deviation from a spherical surface centred on the ideal (paraxial) image point. The  $C$  terms are constants, displayed in the form  ${}_aC_{bc}$  where  $a$ ,  $b$  and  $c$  are the powers of the  $h'$ ,  $r$  and  $\theta$  terms respectively. The five aberrations described by this equation are:  $r^4$ -spherical aberration;  $h'r^3\cos\theta$ -coma;  $h'^2r^2\cos^2\theta$ -astigmatism;  $h'^2r^2$ -field curvature, and  $h'^3r\cos\theta$ -distortion. A discussion of each of these aberrations follows, describing the causes of each aberration and their effects on the optical performance of the system.

The first aberration to be considered in detail is spherical aberration,  ${}_oC_{40}r^4$ , as it is one of the simplest to understand and analyse. This is the only one of the primary aberrations that is independent of image height, and its effect is solely dependent on the position of the ray intercept in the exit pupil. A single double convex lens with large spherical aberration can be seen in Figure 2.6. The rays passing through the centre of the lens, the paraxial region, are focused at the paraxial image plane. As the ray height above the optical axis increases, the rays are focused closer and closer to the lens as they effectively encounter a larger curvature and therefore a stronger refractive effect. If the aberration is measured along the optical axis, it is known as longitudinal spherical aberration. The aberration can also be measured in the lateral direction to provide the image blur radius. For a specified focal length, the spherical aberration of a lens will be eight times that of a lens that is only half the diameter. At a fixed aperture, spherical aberration is dependent upon the object distance and the curvature of the lens, when considering spherical lenses. This means that by altering the radius of curvature of both surfaces of the lens, and keeping its focal length constant, the spherical aberration can be reduced. This process is known as "bending" the lens<sup>18</sup>. Splitting powerful elements in the design into two or more elements can also reduce spherical aberration. This effectively reduces the angle of incidence at each surface. It is also noted that an aspheric surface can be free of spherical aberration as discussed in Section 2.3.



The next aberration to be considered is coma. Coma can be thought of as a change in the magnification of the lens as a function of aperture, and so it causes the off-axis rays to arrive at different image points, as can be seen in Figure 2.7 (a). The corresponding wavefront diagram is shown in Figure 2.7 (b). The aberration is dependent on the aperture cubed, and image height. The effect of the aberration is to produce a comet like tail on the image of a point source. Coma is an important aberration to control because it causes an asymmetric distribution of energy, which causes images to appear misshapen rather than out of focus, which tends to be the case with the symmetric aberrations. As in the reduction of spherical aberration, decreasing the bending of the lens can also reduce coma. Moving the position of the aperture can reduce coma, as can reducing the diameter of the aperture, though this causes a loss in light levels through the system. This aberration is an off-axis problem if the lens is correctly mounted.

Astigmatism occurs when the lens has a different focal position in the sagittal and tangential planes. For example if the tangential image is closer to the lens than the sagittal image, then at the tangential image plane, the sagittal image will be defocused, and at the sagittal image plane the tangential image will be defocused. Between these positions the image will be blurred. It can be seen that astigmatism is an off-axis problem because when the image height,  $h'$ , is zero, the aberration is zero. In order for astigmatism to be corrected, the tangential and sagittal images must be made to coincide. Assembling lenses such that the astigmatism in individual lenses is compensated for, to a degree, by the astigmatism of the system's other lenses, can reduce overall astigmatism in complex lens systems.

Related to astigmatism is field curvature. The image formed by a positive lens is naturally curved as can be seen in Figure 2.8. This result is intuitive as the power of the lens alters as we move off-axis. This curvature causes obvious problems in applications such as cinematography, where an image has to be put onto a flat film. However, it is not of great importance when considering viewing systems such as eyepieces, as the eye compensates for the curvature by adjusting its focus<sup>19</sup>. Like

astigmatism, field curvature is a completely off-axis problem. However, unlike astigmatism, field curvature is an axially symmetric aberration as can be seen from the lack of a  $\cos\theta$  term in its definition (see equation 2.11). Field curvature is a difficult aberration to correct and the approach taken by optical designers is to minimize the effect of the field curvature inherent in the system. This can be achieved by moving the image plane to a compromise position. Taking the example from Figure 2.8, the optical designer would move the image plane from its current position, back towards the lens. However, this would degrade the on-axis performance. A different approach to minimising the effect of field curvature is to introduce an element close to the image plane known as a field flattening element<sup>20</sup>. The term used to define the amount of field curvature inherent in an optical system is the Petzval curvature. The Petzval surface is that which the image would lie on if the astigmatism of the system were taken as zero.

Distortion is the final monochromatic Seidel aberration and is only present for off-axis image points. It is dependent on the ray height and position, with respect to the optical axis. Distortion can be thought of as a lateral variation in the magnification of the lens. Figure 2.9 shows pincushion and barrel distortion of a square grid pattern. Pincushion distortion is when the magnification increases with distance from the optical axis. If the magnification decreases with distance from the optical axis, then the image suffers from barrel distortion. Distortion is generally measured as a percentage of the calculated paraxial image height, at full field, with 1 to 2% being generally acceptable for non-measurement systems such as camera lens systems<sup>21</sup>.

Axial chromatic aberration, also termed axial colour, is caused by the fact that blue light is refracted more than red light, if the lens is made with glass that has inherent positive dispersion. Dispersion relates to the variation of refractive index with changes in wavelength. Generally the refractive index of optical glass will decrease with an increase in wavelength causing the red light to be refracted less than the blue in the same optical element. Therefore, for a positive lens the blue light is imaged

closer to the lens than the red light. This aberration is dependent upon the dispersion of the different glasses used in an optical system. Specifically chosen combinations of optical glasses, such as occur in achromatic doublets, are used to correct this aberration<sup>22</sup>. In this case a single positive lens is split into two lenses with differing dispersions. The front element is a positive lens with low dispersion, called the crown glass. The second element is a negative lens of lower power than the first lens so the net power of the lens is still positive. This second glass is made of a high dispersion glass known as flint glass, and corrects most of the chromatic aberration caused by the first element. Both elements together are known as an achromatic doublet. The achromatic doublet can also be designed to adopt the opposite form, where the high dispersion lens constitutes the front element and these are known as flint leading achromatic doublets<sup>23</sup>.

Related to axial chromatic aberration is the lateral colour<sup>24</sup>. If the lens system suffers from this aberration, then the colour of the light at the image plane varies with image height off-axis. If again, a simple positive lens after, and separated from, the aperture stop is considered as an example, the blue light is refracted towards the optical axis more than the red light. This aberration causes a coloured edge at the extremes of the field and can be difficult to correct<sup>25</sup>, especially in wide-angle applications. This aberration may be corrected by either adopting a lens construction which is close to (or exactly) symmetric about the aperture stop, or by achromatising each component individually.

In general it is an impossible task to design a complex real world lens that is completely free from the effects of all aberrations. It is the task of the lens designer to minimise and balance the overall combined effect of the individual aberrations, to produce a solution that meets the specified performance requirements, for as low a cost as possible.

### 2.3 Aspheric Optics

Traditionally, the vast majority of lens systems consist only of spherical or plano optical surfaces. However, as manufacturing technologies have improved, aspheric optics are becoming more common, especially in low precision applications, though their use is still rare. The desirability of aspheric components stems from their ability to reduce image aberrations produced by optical systems. The asphericity of a surface can be defined in a number of different ways including as a conic surface of revolution<sup>26</sup>, or as a polynomial function<sup>27</sup>. The paraxial focal length is determined by the spherical radius and the terms of the polynomial are selected to reduce the aberrations in the system.

Aspheric optics can also be useful in reducing the physical size and weight of lens systems as they can eliminate the need for the additional elements that are used to reduce the aberrations inherent in a system. Up until the end of the 19<sup>th</sup> century, aspheric optics were generally used to correct for spherical aberration<sup>28</sup>, and indeed, a single aspheric surface located close to the aperture stop can in general totally eliminate spherical aberration of all orders<sup>29</sup>. As manufacturing technologies have improved, aspheric lenses can be employed to reduce not only spherical aberration but astigmatism, distortion, coma and chromatic aberrations. Aspheric mirrors are employed in the design of high quality reflecting telescopes.

The low precision applications tend to employ aspheric optics that are made from plastics rather than optical glass, and have been injection moulded as opposed to polished or diamond turned. These optics generally have small diameters, sub 50mm, and surfaces are only generated to an accuracy of a few microns<sup>30</sup>. Higher precision aspheric components are manufactured by a variety of different means including polishing with complex tools, diamond turning and Magnetorheological Finishing (MRF), where the surface shaping is carried out by a polishing abrasive suspended in a magnetic liquid<sup>31</sup>, the application of which is directed by a magnetic field. Because of the difficulty in producing accurate aspheric test pieces, the

accurate measurement of surface figure on aspheric components can also dramatically increase their cost over spherical ones. The manufacture and test of optical components, and aspheric optics in particular, is discussed in greater detail in Chapter 4, and a new method of measuring the surface figure aspheric lenses is presented in Chapter 5.

Given the dramatic benefits that the use of aspheric surfaces can bring to optical design, the temptation for optical designers to use them can be great. However, it should be noted that the cost of a single high precision aspheric element can be greater than that of the several spherical components it is replacing<sup>32</sup> and unless there are pressing size or weight restrictions on the design specification, it may be better to stay with spherical components.

## 2.4 Conclusions

Complex lens design is a lengthy and complicated process requiring of the designer a high degree of optical knowledge and experience if the results are to be acceptable. The majority of optical design software is based on ray tracing to gain an appreciation of optical performance. With a few rare exceptions, the design optimisation and tolerance phases are separate and consecutive. The optimisation is based solely on optical performance with no method of including relative manufacturing costs and tolerances when comparing competing design solutions. The use of aspheric surfaces holds many attractions to the optical designer though they can still prove prohibitively expensive particularly in high precision applications. The following chapter contains a discussion of lens tolerancing, and its impact on complex lens manufacture, combined with an appreciation of how the manufacturing costs increase as the tolerances are tightened.

Chapter 2. Figures

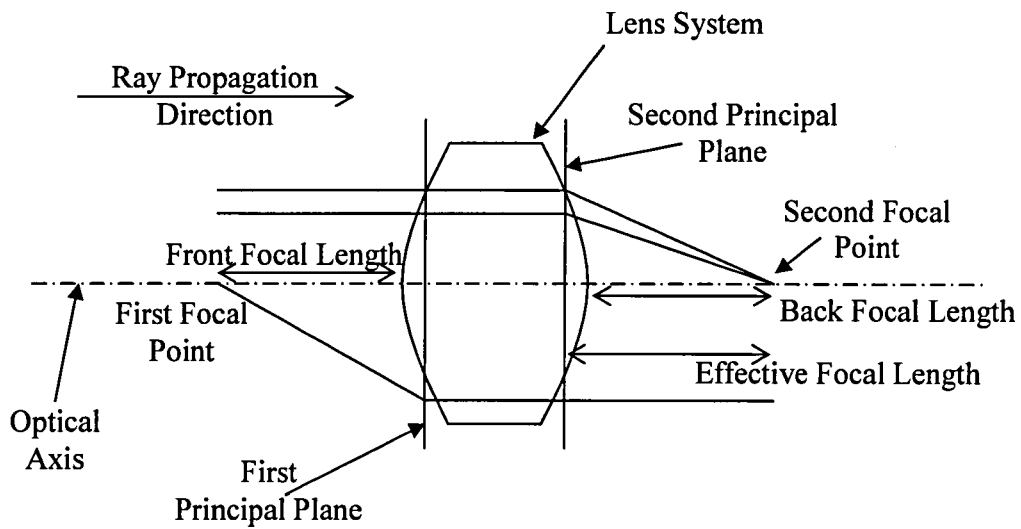


Figure 2.1. Basic Optical Layout for a Generalised System

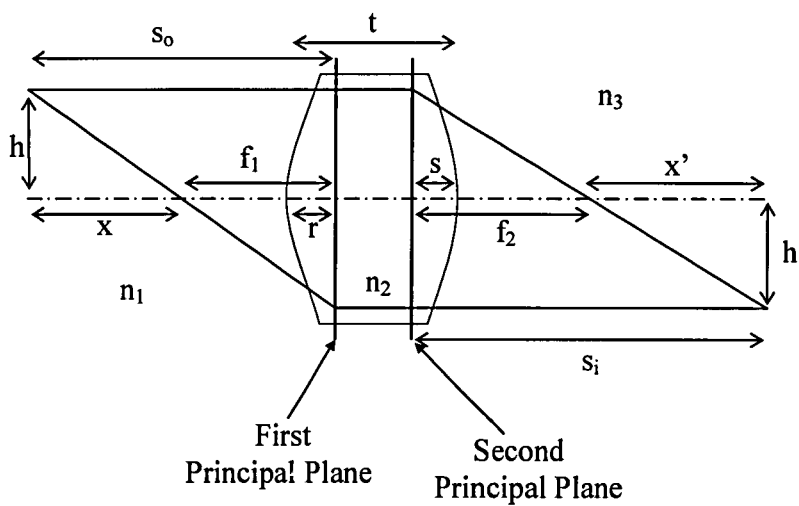


Figure 2.2. Image Height and Position

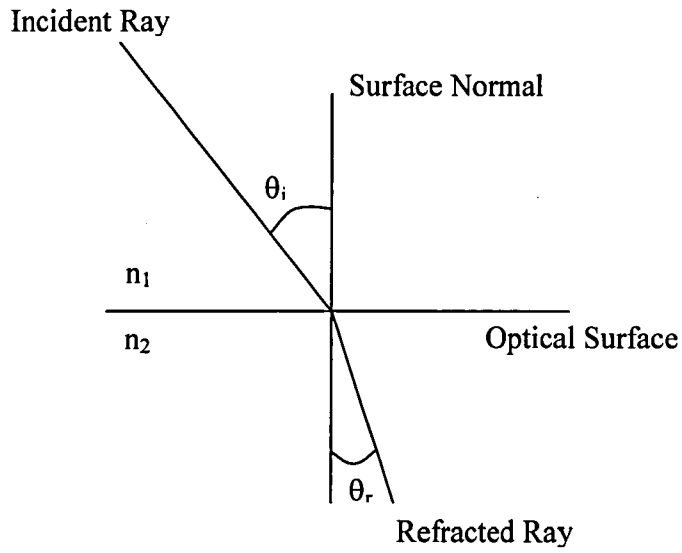


Figure 2.3. Snell's Law Refraction at a Plane Surface

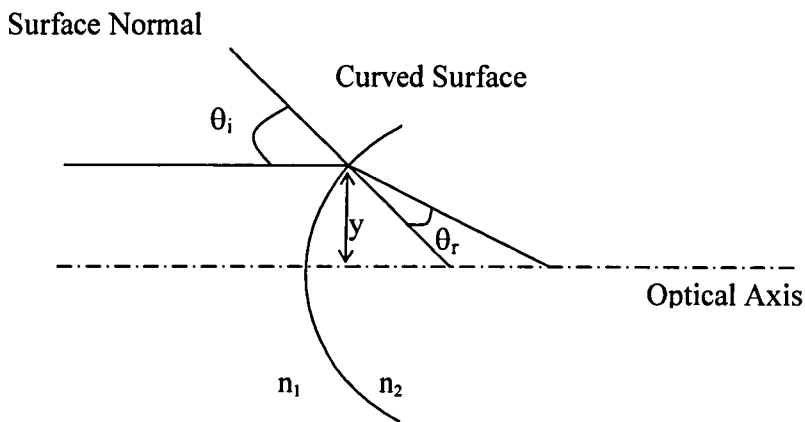


Figure 2.4. Refraction at a Single Curved Surface

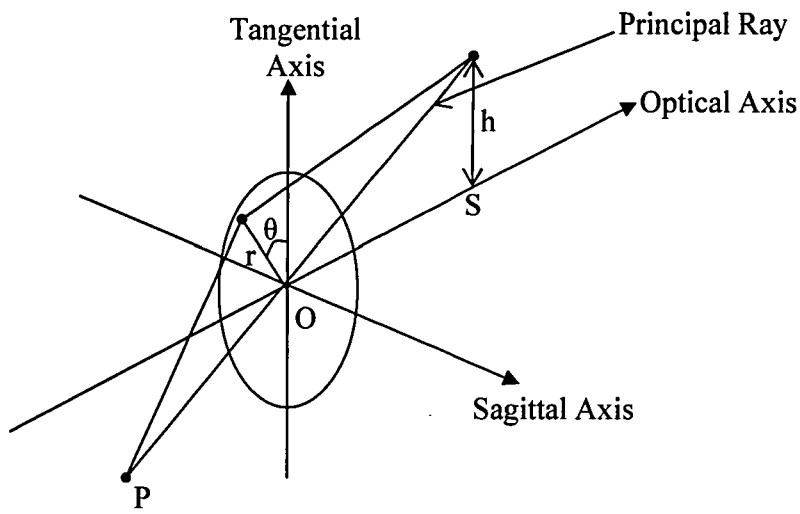


Figure 2.5. Off-Axis Ray Geometry

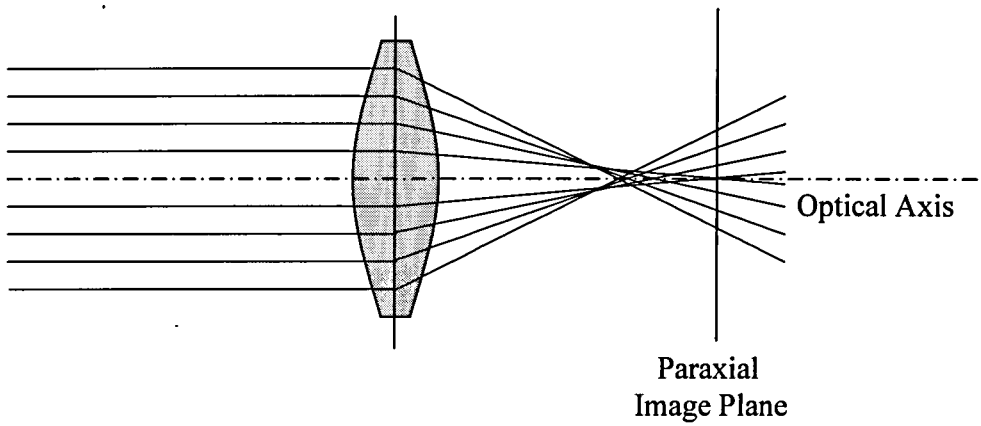


Figure 2.6. Spherical Aberration.

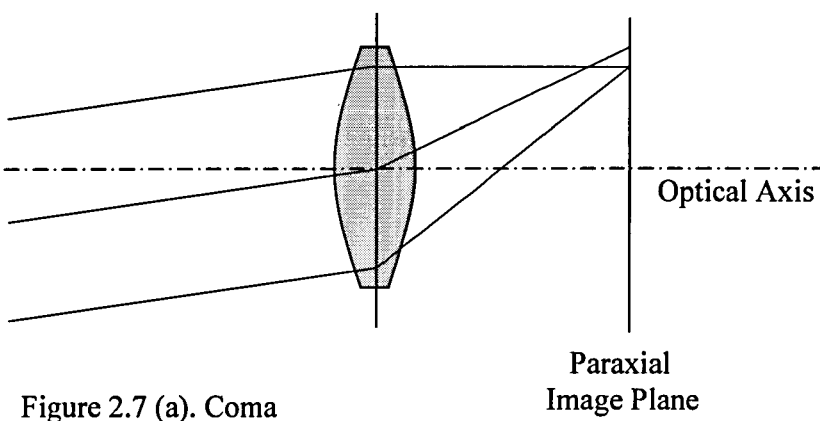


Figure 2.7 (a). Coma



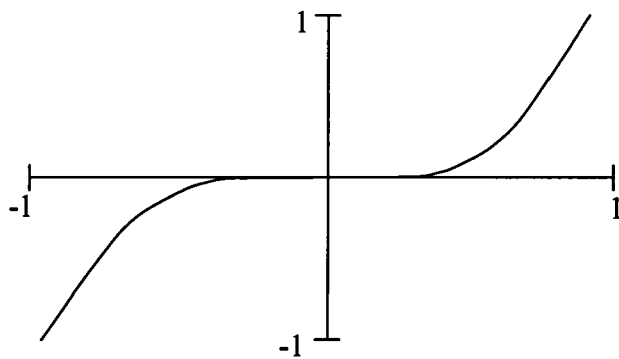


Figure 2.7 (b) Wavefront Diagram for Coma

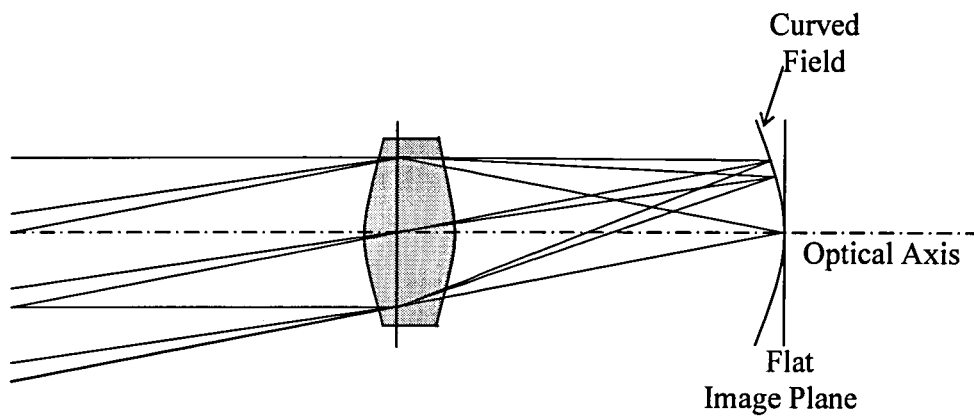


Figure 2.8. Field Curvature

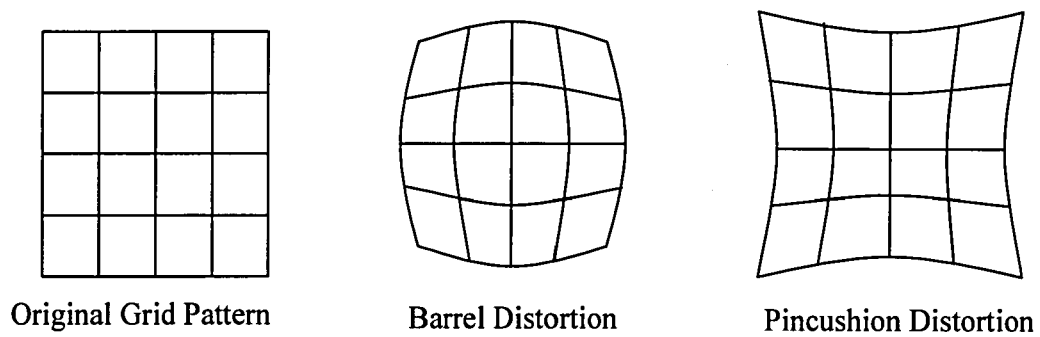


Figure 2.9. Distortion

## References

1. Robert E. Fischer , Biljana Tadic-Galeb, "Chapter 1, Basic Optics and Optical System Specification" in Optical System Design, SPIE Press & McGraw-Hill, New York, pp 1-13, (2000).
2. OSLO Optics Software for Layout and Optimisation, Version 6.1, Lambda Research Corporation, USA, (2001).
3. Robert E. Hopkins, "Optical design 1937-1988...Where to from here?", Optical Engineering, Vol. 27, No. 12, pp 1019-1026, (1988).
4. Milton Laikin, "The future of optical design", Optical Engineering, Vol. 32, No. 8, pp 1729-1730, (1993).
5. Robert E. Fischer , Biljana Tadic-Galeb, "Chapter 9, Basic Optics and Optical System Specification" in Optical System Design, SPIE Press & McGraw-Hill, New York, pp 167-180, (2000).
6. R. R. Shannon, "Chapter 5 Design Optimisation", in The Art and Science of Optical Design, Cambridge University Press UK, pp 334-353, (1997).
7. Warren J. Smith , "Chapter 2 Automatic Lens Design: Managing the Lens Design Program", in Modern Lens Design A Resource Manual, McGraw-Hill USA, pp 13-14, (1992).
8. Scott A. Lerner and Jose M. Sasian, "Optical design with parametrically defined aspheric surfaces", Applied Optics, Vol. 39, No. 28, pp 5205-5213, (2000).
9. Spencer, "A Flexible Automatic Lens Correction Program", Applied Optics, Vol. 2, pp 1257-1264, (1963).

- 
10. Warren J. Smith , “Chapter 2 Automatic Lens Design: Managing the Lens Design Program”, in *Modern Lens Design A Resource Manual*, McGraw-Hill USA, pp 5-7, (1992).
  11. Lambda Research Corporation, “Chapter 8 Optimisation”, in *OSLO Optics Reference Version 6.1*, pp 189-216, (2001).
  12. John Blackwell, Shane Thornton. “Chapter 1 Basic Optics”, in *Mastering Optics*, McGraw-Hill USE, pp 1-34, (1996).
  13. Warren J. Smith, “Chapter 2 Image Formation (First Order Optics)”, in *Modern Optical Engineering 3<sup>rd</sup> Edition*, McGraw-Hill USA, pp 21-59, (2000).
  14. E. Hecht, “Chapter 5 Geometrical Optics”, in *Optics 3<sup>rd</sup> Edition*, Addison-Wesley, USA, pp 148-246, (1998).
  15. Frank L. Pedrotti, Leno S. Pedrotti, “Chapter 4 Matrix Methods in Paraxial Optics”, in *Introduction to Optics 2<sup>nd</sup> Edition*, Prentice Hall USA, 62-86, (1996).
  16. Max Born, Emil Wolf, “Chapter 5 Geometrical Theory of Aberrations”, in *Principles of Optics: Electromagnetic theory of propagation interference and diffraction of light 6<sup>th</sup> Edition*, Cambridge University Press, pp 203-230, (1997).
  17. Frank L. Pedrotti, Leno S. Pedrotti, “Chapter 5 Aberration Theory”, in *Introduction to Optics 2<sup>nd</sup> Edition*, Prentice Hall USA, 87-107, (1996).
  18. A.E.Conrady, “Chapter 2, Spherical Aberration”, in *Applied Optics and Optical Design Part One*, Dover Publications Inc, New York, pp 63-66, (1957).

- 
19. Bruce Walker, "Chapter 5, Optical design with OSLO MG" in Optical Engineering Fundamentals, McGraw Hill, New York, pp 116, (1995).
  20. Hecht, "Chapter 6, More on Geometrical Optics", in Optics 3<sup>rd</sup> Edition, Addison-Wesley, USA, pp 267-269, (1998).
  21. Bruce Walker, "Chapter 6, Primary Lens Aberrations" in Optical Engineering Fundamentals, McGraw Hill, New York, pp 138, (1995).
  22. Leo Levi, "Chapter 9, Lenses and Curved Mirrors", in Applied Optics Volume 1 A Guide to Optical System Design, John Wiley & Sons Inc. New York, pp 410-411, (1968).
  23. Abraham Szulc, "Improved solution for the cemented doublet", Applied Optics, Vol. 35, No. 19, pp 3548-3557, (1996).
  24. A.E.Conrady, "Chapter 4, Chromatic Aberration", in Applied Optics and Optical Design Part One, Dover Publications Inc, New York, pp 147-150, (1957).
  25. Warren J. Smith, "Chapter 5, Review of Specific Geometrical Aberrations", in Modern Optical Engineering 3<sup>rd</sup> Edition, McGraw-Hill USA, pp 90-91, (2000).
  26. Daniel Malacara, "Appendix 1, An Optical Surface and its Characteristics", in Optical Shop Testing 2<sup>nd</sup> Edition, John Wiley & Sons Inc, New York, pp 743-745, (1992).
  27. Ding-Qiang Su, Ya-Nan Wang, "Some ideas about representations of aspheric optical surfaces", Applied Optics, Vol. 24, No. 3, pp 323-326, (1985).

- 
28. E. Heynacher, "Aspheric Optics: How are they made and why are they needed?", *Phys. Technol.*, Vol. 10, p 124-139, (1979).
29. R. R. Shannon, "Chapter 7 Design Examples", in *The Art and Science of Optical Design*, Cambridge University Press UK, pp 388-602, (1997).
30. K. Becker, B. Dorband, R. Locher, M. Schmidt, "Aspheric Optics at Different Quality Levels and Functional Need", *EUROPTO Conference on Optical Fabrication and Testing, Proc. of SPIE*, Vol. 3739, pp 22-33, (1999).
31. Harvey M. Pollicove, "Next Generation Optics Manufacturing Technologies", *Advanced Optical Manufacturing and Testing Technology, Proc. of SPIE*, Vol. 4231, pp 8-15, (2000).
32. Warren J. Smith, "Chapter 12 The Design of Optical Systems: General", in *Modern Optical Engineering 3<sup>rd</sup> Edition*, McGraw-Hill USA, pp 393-438, (2000).

CHAPTER 3  
TOLERANCING AND THE INCLUSION OF A COST  
FUNCTION WITHIN OPTIMISATION

## Chapter 3. Tolerancing and the Inclusion of a Cost Function within Optimisation

### 3.1 Introduction

As discussed in Chapter 2, the traditional approach to optimisation is to complete the lens design on the grounds of optical performance before examining its production tolerances and inherent costs. Tolerancing is the technique of calculating and distributing the manufacturing and assembly errors throughout the optical system, to ensure that the system will perform to the required standard after it has been manufactured. It is usually the case that it is the tolerances that are placed upon an optical design that greatly affect its cost of manufacture. Clearly, the need to repeat the design process if the manufacturing costs exceed permissible levels is an inefficient and costly process in itself. With the minimisation of all costs such an integral part of the make up of any successful business, it would be very useful to have an element of cost included within the lens design optimisation function. Crude cost controls do exist, such as limiting the curvatures within the design to those for which the company already owns test plates, and not allowing the design to include the more exotic and expensive glass types. However, any workable and useful cost function would have to be far more complex including such elements as edge to centre thickness ratio, curvature to centre thickness ratio, an appreciation of the relative difficulties of generating the curves based on the available manufacturing set up, glass type, the radius of curvature, the lens centre thickness, lens diameter, and of course, the associated production tolerances which have such a large effect on the final cost. These are discussed in the following section.

### 3.2 The Tolerance Parameters

Before discussing how tolerancing is carried out and subsequently implemented into the manufacturing process, it is useful to introduce the parameters that are toleranced and, in some cases, the conventions governing how these tolerances are expressed. A useful place to begin is the standard tolerances specified within ISO 10110<sup>1</sup>, a

section of which is displayed as Table 3.1. These are the default tolerances that are to be used if none are specified on a drawing. A typical production drawing for an optical component is reproduced as Figure 3.1, showing many of the tolerances that will be discussed in this section. Note that the tolerances vary as the diameter of the lens alters, even though they are designated for the same nominal level of precision. The tolerance parameters specified in ISO 10110 will now be discussed, with reference to the lens drawing in Figure 3.1, in order to show how each of the tolerances are expressed and specified. The dimensional tolerances, such as diameter and centre thickness, are self-explanatory and appear in all engineering applications in some form. The width of the protective chamfer, ground around the edge of the optical element, is generally pertinent only to optical applications, due to the inherent brittleness of the materials, and it is employed to reduce the likelihood of edge damage when the lens is handled during the production and assembly stages.

Property	Maximum dimension of part (mm)			
	Up to 10	Over 10 Up to 30	Over 30 Up to 100	Over 100 Up to 300
Edge length, diameter (mm)	$\pm 0.2$	$\pm 0.5$	$\pm 1.0$	$\pm 1.5$
Thickness (mm)	$\pm 0.1$	$\pm 0.2$	$\pm 0.4$	$\pm 0.8$
Angle deviation of prisms and plate	$\pm 30'$	$\pm 30'$	$\pm 30'$	$\pm 30'$
Width of protective chamfer (mm)	0.1 – 0.3	0.2 – 0.5	0.3 – 0.8	0.5 – 1.6
Stress birefringence (nm/cm)	0/20	0/20	–	–
Bubbles and inclusions	1/3x0.16	1/5x0.25	1/5x0.4	1/5x0.63
Inhomogeneity and striae	2/1;1	2/1;1	–	–
Surface form tolerances	3/5(1)	3/10(2)	3/10(2) 30 mm test diameter	3/10(2) 60 mm test diameter
Centering tolerances	4/30'	4/20'	4/10'	4/10'
Surface imperfection tolerances	5/3x0.16	5/5x0.25	5/5x0.4	5/5x0.63

Table 3.1. ISO 10110 Tolerances.



The following three tolerances to be discussed all appear in the Material Specification section of the tolerances, as they are uniquely linked to the quality of glass that the lens is made from. The bubbles and inclusions tolerance<sup>2</sup> defines how many, and what size defects can be present within the glass that the lens is made from. It is defined using the form  $1/N \times A$ , where the 1 identifies that it is the bubbles and inclusions tolerance, N is the maximum permissible number of bubbles and inclusions of maximum permitted size allowed, and A is the grade number that defines the maximum permitted size of the inclusions. A is equal to the square root of the projected area of the maximum permissible inclusion expressed in millimetres. Referring to the example given in Figure 3.1, the tolerance is  $5 \times 0.25$ , which translates as a maximum of 5 bubbles and inclusions of a maximum size of 0.25mm.

The stress birefringence tolerance<sup>3</sup>, also specified on Figure 3.1, is again uniquely related to the optical medium. The 0 at the start of the tolerance identifies it as the birefringence tolerance. The number following is the maximum permissible stress birefringence, specified as an Optical Path Difference in nanometres per centimetre of path length. In the example in Figure 3.1 the tolerance is 20nm per cm of path length.

The inhomogeneity and striae tolerance<sup>4</sup> is identified by the code number 2 and is presented in the form  $2/A;B$ . Where A is the class number for the inhomogeneity and B is the class number for the striae. Inhomogeneity is defined as a variation of the refractive index of the lens as a function of position. The class numbers for inhomogeneity are based upon the maximum permissible variation in refractive index and the striae class numbers are based upon the OPD caused. The class number for this tolerance relates to two tables published in ISO 10110-4, and reproduced below as Tables 3.2a & b.

Class	Maximum permissible variation of refractive index within a part (ppm)
0	±50
1	±20
2	±5
3	±2
4	±1
5	±0.5

Table 3.2a. Inhomogeneity Classes

Class	Percentage of striae causing an optical path difference of at least 30nm %
1	≤10
2	≤5
3	≤2
4	≤1
5	Extremely free of striae Restriction to striae exceeding 30nm does not apply Further information to be supplied in a note to the drawing

Table 3.2b Classes of striae

The following sets of tolerances relate to the surface shape and quality of the lenses, and as such, there are always two tolerances specified per lens, one for each surface. The surface form tolerance<sup>5</sup>, identification number 3, is concerned with the shape of the surfaces that have been generated on the lens. This tolerance method requires the formation of an interference pattern between the surface under test and a reference surface of the inverse form. These patterns can be generated by the direct application of a test plate illuminated by monochromatic light such as sodium light, resulting in the formation of Newton's rings<sup>6</sup> (see Figure 3.2 for a schematic of the test layout), or by a number of different interferometric methods such as the Fizeau

interferometer<sup>7</sup>. A discussion, of a variety of surface form testing methods is provided in Chapter 4 and in Chapter 5, where new methods are explored. In ISO 10110, surface form error can be abbreviated to a code of the form N(A), where N is the number of (circular) fringes of power difference between the tested surface and a reference surface, and A is the number of fringes of difference between the section of the aperture of the surface with maximum curvature, and that with the minimum curvature. Examples of fringe patterns along with the corresponding tolerance that they satisfy are displayed in the drawing shown in Figure 3.3<sup>8</sup>. It is possible to specify a surface form tolerance where the non-circular value is higher than the number of complete fringes permitted, as in the front surface in Figure 3.1. This situation occurs when the surface may be astigmatic, but error in curvature should for some reason be particularly small, Figure 3.4 shows the surface form interferogram for this case.

The tolerance on centration<sup>9</sup> is given the identification number 4. The centring tolerance on a single spherical surface, as in the example in Figure 3.1, is defined as the maximum permitted angle,  $\sigma$ , between the optical axis and a normal to the surface that passes through the centre of curvature of the surface (see Figure 3.5). There is no need to include a decentration for a single spherical surface as the effect on the surface is identical to a tilt. In all other cases, such as complete elements, lens assemblies and aspheric surfaces, the centration tolerance must be expressed as a tilt,  $\sigma$ , and a decentration,  $d$ , measured from a specified datum point. Figure 3.6 shows these two properties. Centration of lenses is considered in greater detail in Chapter 6, where each lens in the system is considered individually and the datum is specified at the middle of the lens centre thickness in each case. The conventional way of specifying optical tolerances is  $4/\sigma$ , for tilt alone and  $4/\sigma(d)$  for tilt and decentration tolerances, where tilt is expressed in minutes or seconds of arc, and decentration in millimetres.

The surface imperfection tolerance<sup>10</sup>, code number 5, is expressed much like the bubbles and inclusions tolerance,  $1/N \times A$  used before. But, in this case, N

corresponds to the number of surface imperfections of the maximum permitted size allowed, and  $A$  is equal to the square root of the surface area of the maximum permissible defect in mm.

The surface texture tolerance<sup>11</sup> is specified on the drawing of the lens itself. The letter G, in Figure 3.1, indicates that the edge of the lens is to be ground. This is common practice to reduce internal reflection. The letter P on both surfaces indicates that the surface is to have a *specular* surface texture; in the vast majority of cases this means that the surface is to be polished. The stand-alone use of P means that no indication of quality is given. If more information is required, then P can be quantified by a grade number, 1 to 4, which indicates the number of permissible microdefects (small isolated pits in the lens surface) as defined in Table 3.3. Including the required frequency spectrum of the surface roughness or the R.M.S. surface roughness can provide more detail on the surface texture.

Class	Number N of microdefects per 10mm of sampling length
P1	$80 \leq N < 400$
P2	$16 \leq N < 80$
P3	$3 \leq N < 16$
P4	$N < 3$

Table 3.3. Surface Texture Classification

The tolerances on the radii of curvature are simply specified a  $\pm$  value. This is determined by the lens' position within a system, its power and the magnitude of the curvature involved. The tolerance on the surface radii is closely linked to that on the surface form. The tolerance on the lens centre thickness is also given as a plain  $\pm$  value. The tolerance on the refractive index is again a  $\pm$  value, but it is specified at a particular wavelength and ambient temperature.

### 3.2.1 Introduction to Tolerancing

The aim of tolerancing is to derive the largest possible tolerances for the optical system and still meet the required optical performance<sup>12</sup>. The design, however complex, must have a degree of robustness and insensitivity to manufacturing errors or it will be prohibitively expensive to manufacture. The highest performance lens system may not always be the design chosen for manufacture, as these systems often incorporate steep lens curvatures, high angles of incidence and very powerful optical elements, which make an optical system sensitive to manufacturing and assembly errors. A less efficient, but more tolerant, design is often chosen for manufacture.

There are two different approaches that can be taken when tolerancing a lens system. In the OSLO lens design software these approaches are termed sensitivity tolerancing and inverse sensitivity tolerancing. The sensitivity tolerancing analysis allocates every component in the system, both optical and mechanical, a tolerance and then calculates how these tolerances affect the optical performance of the system. In the inverse sensitivity method, the minimum acceptable level of optical performance is decided upon and then the routine calculates the allowed tolerance on each parameter such that this minimum level of performance is satisfied. S. Rosin suggests that a 10% change in error function would give a conservative tolerance level and a 25% change a moderate tolerance level<sup>13</sup>. These levels are dependent on the type of error function being used, and it is assumed that the error functions are based solely on optical performance and are not heavily weighted in other areas such as edge thickness. The sensitivity approach is more widely used than the inverse sensitivity method and there are a number of different systems for tolerancing lenses that fall under the banner of sensitivity tolerancing.

Sensitivity analysis will now be discussed in more detail, as it is the more commonly used approach in industry. This method is used to predict the net system performance of the completed lens systems. Every time a batch of lenses is manufactured, each lens will have a different set of 'errors' inherent to its optical

and mechanical components and in the way that these components are assembled. This will give each lens differing performance characteristics from other lenses of the same production run and from its original theoretical design. If the design has been toleranced correctly then the results can be used to predict the percentage of the manufactured lenses that will fall into the performance band predicted by the sensitivity tolerancing carried out. In order to achieve this, a model has to be developed which sums all the manufacturing errors within a system and gives an accurate prediction of performance. Each separate tolerance parameter affects the performance of the system to a differing degree, and these perturbations must be combined to predict the performance of not just a single lens, but a batch of lenses.

One of the most common tolerancing techniques used to combine the individual tolerances is the root sum square method, RSS<sup>14</sup>. This method takes the square root of the sum of the squares of the effect of each of the tolerances, as long as they are of the same form. Difficulties can arise with this method when the performance degradations caused by the tolerances are not of the same form. Performance changes caused by errors in element thickness and airspaces can be accurately combined in this method, as they both cause a change in the spherical aberration in the system. In addition, decentration and tilt can be combined as these both contribute towards coma and astigmatism. The effects of each tolerance may be expressed, for example, as an OPD (Optical Path Difference), change in RMS Spot Size, MTF (Modulation Transfer Function) or the error function calculated by the optical design software. The error function employed here is often the error function used during the optimisation phase of the design, and so will already be tailored to the system being analysed. The method chosen to express the results is largely dependent upon the use for which the system has been designed. If the lens system was to be used in a high quality photographic application, where the image plane is flat piece of film, it may be wise to choose the OPD as the performance measure, as it is a direct measure of the wavefront aberration. Within the OSLO lens design package, the RSS totals can be classified by aberration and also by perturbation class, where the example headings are radius, thickness/airspace, refractive index

and surface tilt. Combining the information under these classifications eases the task of tolerancing a lens by clearly highlighting particular areas of concern within the design.

In order to obtain more accurate predictions of performance after manufacture, more complex tolerancing methods have to be employed. The Monte Carlo tolerancing method is one such example<sup>15</sup>. As before, tolerances are assigned to all the parameters within the system. The Monte Carlo analysis then uses random numbers to generate a number of perturbed lenses all incorporating different combinations of tilts, decentrations etc., maximum values of which are determined by the assigned tolerances. These random numbers are generated using probability density functions that have been prescribed to each tolerance. The probability density functions have to be carefully arrived at to ensure they accurately reflect the likely distribution of errors within each tolerance. Examples of different distribution models can be seen in Figure 3.7. The distribution model chosen depends upon the parameter in question. For example in the case of the internal bore of a lens mount the dimension may be presented as a minimum level below which the lens will not fit so the distribution model of these internal bores will display a degree of kurtosis.

Within the Monte Carlo method, all of the selected parameters are perturbed at the same time making it a very powerful tolerancing tool. Then, after all the parameters have been perturbed, the performance of the optical system is calculated, based upon the error function that has been constructed for the lens within the optical design software. This process is repeated a number of times, set by the designer, based upon the complexity of the lens system, the available computing power and the production run that is anticipated for the lens. It would be unusual for the analysis to be carried out fewer than 25 times as this could result in misleading data. The resulting output can then be used to predict the performance of the lenses being produced. The results from the Monte Carlo analysis can be interpreted in a number of ways such as plots of performance versus cumulative probability, from which it is easy to calculate the likely optical performance of 95% of the lenses produced.

A brief example of Monte Carlo tolerancing using OSLO lens design package is now discussed, to give an appreciation of how this step fits into the lens design process. The lens being toleranced is a triplet lens of approximately 100mm focal length, a diagram of which can be seen in Figure 3.8. The error function used employed the RMS spot size as an indicator of performance, and the distributions and tolerances for the perturbed parameters were the defaults specified by the program. These tolerances are based on ISO 10110 which was discussed earlier in this chapter. Figure 3.9 is a plot of the cumulative probability against relative distribution of the error function for the 25 lenses evaluated during the analysis. Combined with the graphical representation of the results, the program also outputs a great deal of numerical data as part of the analysis, including information such as the maximum and minimum and mean values of the error function, and the standard deviation of this change. A sample of this data pertaining to the current example can be seen in Table 3.4.

Error Function For Nominal System		.096480	
Number of Systems Evaluated	25	Maximum Change in Error Function	0.102251
Mean Change in Error Function	.019574 ± 0.008565	Average Deviation	0.035820
Standard Deviation of Change	.042827 ± 0.006182	Skewness	0.438042
Minimum Change in Error Function	-.04815	Kurtosis	-1.094097

Table 3.4. Monte Carlo Tolerance Analysis Data

From the results of this analysis, we can see that this system is very sensitive to perturbations. The minimum change in error function is still over 20% of the nominal error function, which would have a large effect on the performance of this system. As a guideline, when manufacturing a batch of lenses, a limit on the change in error function of 10% is considered a suitable conservative tolerance level



according to the work by Rosin already discussed in this section. The maximum change in error function for this system is over 100% of its starting level, so this lens is not suitable for manufacture at this stage, and would require a degree of re-designing to make it feasible to manufacture.

### 3.3 Practical Considerations in Lens Design: The Application of Tolerancing at the Assembly Stage

After the completion of the optical design and tolerancing phases of the design procedure, the practical implementation of the design starts. The aim of the assembly process is to ensure that the individual lens elements are fixed in the correct position relative to each other and to a reference plane such as the film plane on a camera. As previously discussed, the lenses need to be centred about an optical axis and there are a number of methods used to achieve this. The tolerances have to be applied to all the mechanical and optical components within the system. In order to achieve this, the designer must be familiar with the different forms of tolerance parameter. These parameters can be split into two distinct groups, the asymmetrical and symmetrical errors.

The asymmetrical errors will be discussed first, followed by some of the design and assembly methods employed to minimize these errors. The errors include element decentration and tilt, surface irregularities on the elements, element wedge and inhomogeneity of the optical material. Figure 3.10 illustrates some of the problems listed above. Figure 3.10A shows a perfectly shaped and mounted lens. The optical axis is aligned with the mechanical axis and the image is formed on the centerline of the system. Figure 3.10B depicts a perfectly manufactured lens that is tilted in its mount. The optical axis does not run along the mechanical axis, meaning that the system is not rotationally symmetric and the image is formed off centre. When tolerancing the tilt of a lens, the diameter of the lens has to be taken into account because a tilt of 1 minute of arc on a 10mm lens will have a very different effect to the same tilt on a 100mm diameter lens. A useful expression of tilt is the total

indicator run out (TIR), as this takes into account the diameter of the lens and is therefore useful when comparing the tilt tolerances on lenses of different diameters. The TIR is calculated by multiplying the tilt in radians, by the diameter of the lens in question. Figure 3.10C depicts a wedged lens mounted in a perfect cell. The lens has not been edged correctly, and it can be seen in the diagram that the optical axis does not run along the mechanical axis. It can be seen that element wedge has, in the paraxial approximation, the same optical effect as tilting the element.

If a lens is to be mounted in a cell, then the inner diameter of the cell has to be larger than the outer diameter of the lens, otherwise the lens would not go in its holder, and it is this that is usually the cause of decentration within lens systems. Figure 3.11 illustrates this point. In Figure 3.11, the lens is decentered in the direction of the arrow. This decentration is caused by the clearance that can be seen around the outer edge of the lens and its cell. Some lens manufactures, notably in the Rank Taylor Hobson zoom lenses serviced by the author, have countered this problem by mounting the lenses very tightly within their cells, so tightly indeed that the cell has to be heated up before the optical element can be released. A photograph of one of these cells can be seen in Figure 3.12. These cells hold between two and seven elements held apart by spacer rings and locked in at either end with lock rings. These groups of elements are assembled to make the complete lenses by mounting them to the body of the lens with a ring of small screws, typical around M2x6. The screw holes in the lens cells are normally slotted so that the assembler has even more scope to reduce any effects of decentration or other asymmetrical error. Once the cell has been positioned to the assembler's liking, the screws are tightened and the slots are filled with cement to set the elements in position. Tolerances on the centration of zoom lenses can be as little  $7.5\mu\text{m}^{16}$ . The tolerances on zoom lenses can be especially restrictive because, in many cases, the zoom unit will rotate when it is driven and, if it is not correctly centered, the image will not remain stable as the cameraman zooms in and out.

A method for accurately assembling complex lenses within their specified tolerance budgets was presented by Carnell et al<sup>17</sup> in 1974. In this case, the lens under consideration was a wide-angle objective lens that incorporated a high degree of optical distortion within the design. This distortion had to be very tightly controlled if the lens was to perform to expectations. The method employed involved mounting each lens element individually in a brass cell that had been very accurately machined on an air bearing lathe. The clearance between the lens element and the internal diameter of the cell was of the order of 100 $\mu$ m. A rounded knife-edge was turned inside the cell onto which the lens was placed, and was held in position by a weak vacuum. The lens element was centred by holding a test plate above the exposed lens surface and examining the fringe pattern produced as the element was slowly rotated. The set-up used is reproduced in Figure 3.13. This method can ensure that the lens surface runs true to a centred sphere to accuracies in the order of the laser wavelength. The lens is then fixed to the cell using epoxy cement. The individual cells are then mounted inside a cylindrical barrel. There is almost an interference fit between the lens cells and the barrel to ensure that centration is maintained, and spacers are used to control the air spaces between elements.

A second manufacturing and assembly method is known as the Lathe Assembly Technique<sup>18</sup>. This technique involves the accurate measurement of each optical component, followed by the machining of mechanical component(s), lens barrels, with their inside diameters tailored to the individual elements. Images of an example lens barrel from a Rank Taylor Hobson zoom lens can be seen in Figure 3.14. The clearance between the outside diameter of the optical element and the internal diameter of the housing can be as little as 0.005mm, though this can cause problems if the system is exposed to extremes of temperature. With this method the centration and alignment of the elements is controlled solely by mechanical means. The lenses are locked in position using threaded retaining rings, and the air spaces between elements are controlled to 0.015mm using carefully manufactured spacing rings. This is a very labour intensive method of assembling multi-element lens

systems, requiring high degrees of measurement and machining accuracy, and as such will have a large impact on the overall production cost of the system.

A third approach to multi-element lens assembly, presented by R. E. Hopkins<sup>19</sup>, requires lower degrees of accuracy when manufacturing the optical and mechanical components, and relies on optical rather than mechanical methods to align the elements. In this method, a laser is aligned perpendicular to an optical reference surface, and then a spacer is temporarily fixed to the reference surface such that the laser passes through its centre. The first optical element is then placed on the spacer and aligned so that the optical axis of the lens and the laser are parallel. Positioning is checked by observing the fringes generated by reflections from the reference surface and the front and rear surfaces of the optical element being aligned. Once in position the lens element is cemented to the spacer, and then a second spacer is placed on the top of the first lens. The second lens in the optical system is then placed on top and aligned in the same fashion, except that the fringes formed are created by two elements plus the reference surface. Once the lens is aligned, it is cemented into position as before. This process continues until all the lenses have been aligned. A diagram of a three-element lens system that has been aligned in this manner is presented in Figure 3.15. The figure shows that the lens system can still be well aligned if the lenses are wedged or poorly centred and so do not require as exacting and costly production standards. This method can align lenses to a tolerance of 2 microns in centration.

In the Hopkins method oversized elements are required as the spacers sit on the surface of the lens. A new approach to lens assembly that uses the full aperture of the lens, mounting and testing are discussed in more detail in Chapter 6 and employs a method of active alignment during the build phase to ensure the best possible optical performance is achieved in the shortest possible time thus reducing costs.

### 3.4 Lens Building Example

During the course of research the author designed, commissioned and assembled a four element lens system to be used as part of a strain gauge measurement tool. The desired lens specifications were a focal length of 40mm, speed of around  $f/5$  and the lens was to be athermalised over a range of approximately  $40^{\circ}\text{C}$ . The lens was designed and toleranced utilising the OSLO lens design package. The approach taken to the athermalisation was to choose optical glasses whose refractive index changed slowly with temperature, and which had a relatively low thermal coefficient of expansion. The lens was assembled in a traditional manner, utilising a stepped cylindrical outer casing and threaded locking rings. A schematic of the lens system is presented at Figure 3.16. To aid clarity in the diagram only the top section of the housing is depicted.

A number of points were noted during the design and assembly of this system, and are listed below.

- (i) The athermalisation requirement of the design restricted the glass selection available and had a tendency to push the design towards more exotic and costly glass types.
- (ii) The lack of adjustment available in the chosen assembly method caused the tolerances on the manufacture of both the optical and mechanical components to be relatively tight as it was their physical dimensions that directly controlled the optical alignment.
- (iii) The results of this exercise combined with other background research showed the desirability of a cost model that could be applied at the design optimisation stage, and the development of such a model is discussed in the following section.
- (iv) The lens was also fully assembled before testing, as for the methods discussed in Chapter 2, and this experience further reinforced the requirement for a method of aligning optical systems as they are assembled.

### 3.5 The Development of a Cost Model

Now that the lens design and tolerancing processes have been established, the costing of different lens designs can be discussed. At first glance, some aspects of the optical system would appear straightforward to cost. For example, the cost of the glass or metal materials used to produce a lens or housing, though even these costs are heavily dependent upon the tolerances within which they have to be manufactured. However, generally, the major part of the cost of an optical system is incurred during the manufacture, assembly and test stage. If the relative costs of lenses are to be accurately compared, a method must be developed that estimates the additional costs incurred by having tighter tolerances on a design.

It is a very complex problem to define the cost of tightening the tolerances on lens manufacture. When designing the lens, the designer has to balance the cost of the lens with the optical performance requirements. For example, it is possible measure the radius of curvature of 25mm to 0.00625mm, and beyond dependent upon the test method employed and diameter of the surface under test/size of the area under test, and it is possible to polish a surface to this level of accuracy however in the majority of cases it would not make economic sense to do so as the component yield could be very low<sup>20</sup>.

When tolerancing the radius of a lens surface there is no simple correlation between the number of allowed fringes of deviation and cost. The function must also take into account the thickness and diameter of the lens, as well as the method by which the lens is to be manufactured. It is difficult to polish accurate radii on a very small diameter lens, especially if there is only a small number of lenses to be polished, because effects at the edge of the lens effectively have a greater effect on small lenses than on large lenses. Increasing the diameter of the lens helps, but only up to a point, where the cost of large diameter polishing tools become a problem. The centre thickness of the lens also has an effect on the polishing costs of the lens element, if it becomes too small (especially on a negative or meniscus lens) or needs

to be very accurately controlled. It is difficult to polish surfaces that approach hemispheres because of the high degree of curvature involved.

The glass type can have a large effect on the cost of generating optical surfaces on a lens. An optical glass has many more properties that the designer must take into account, than simply its refractive index and dispersion characteristics. The hardness of the glass, generally given as a Knoop<sup>21</sup> hardness, has a large bearing on the ease by which optical surfaces can be generated on it. Hard glasses can require exotic and expensive polishing abrasives and extended production times, which increase their cost accordingly. If the lens system is to be used in an environment where the ambient temperature is variable, then two more glass properties may become important especially in high precision measurement applications. The more obvious is the thermal coefficient of expansion of the glass, (TCE). This property needs to be considered alongside the thermal expansion characteristics of the materials that the lenses are mounted in. In the vast majority of cases, the optical elements are, by necessity, tightly held within their cells especially when the centration tolerances are tight. If the glass expands more quickly than the cell, then at best the lens may suffer aberrations caused by the induced stress and, at worst the lens may chip or crack. If the lens expands more slowly than the cell then it may become loose in the cell with the inherent problems this causes. These problems may be circumvented, to a degree, by fixing the lens in silicon-type cement that allows some flexibility in the mounting, though this method has additional assembly cost implications.

The second temperature related parameter is the change in refractive index with respect to temperature, that is  $\delta n/\delta T$ . This parameter can be very important in high precision, multi-element systems as optical glasses within the system will all react differently to changes in temperature which could result in disproportionately large changes in performance for some optical glass combinations. This parameter must be looked at carefully in the design of certain systems such as lens systems that must be athermal (the lens performance remaining constant, over large temperature

changes) as the  $\delta n/\delta T$  can be used to compensate for positional changes occurring from the TCE effects.

The final important properties to bear in mind when selecting an optical glass type are its chemical properties, climatic, stain, acid, alkali, and phosphate resistance. These properties are given numerical values corresponding to 'look up' tables that give more information on their properties. The climatic and stain properties are important in many applications as they may necessitate special handling care during the manufacture and assembly stages as well as during the normal operation of the optical system. If the lens is especially vulnerable to climatic conditions or stains, it may require special optical coatings that will add to the cost of the system. The acid, alkali and phosphate parameters are generally linked to more specialised system applications. The OSLO lens design package provides some cost information on glass types relative to BK7, which is a very commonly used optical glass, but little information about how it is calculated is provided, and it appears to be simply based on the purchase cost of the glass which, as has been discussed, may only be a small part of the overall cost of the element.

In order to estimate the increase in cost of tightening the tolerances, it is necessary to establish a base-line starting point and the ISO 10110 tolerances specified Table 3.1 seem reasonable. However, the appropriate tolerances depend heavily on the system being developed and it is therefore useful to look at baseline tolerances suggested by other authors in the field. A number of different tables, by a variety of authors, will now be presented and discussed, often with reference to ISO 10110, to establish a better understanding of the cost implications of different tolerances. Table 3.5, shows the differing tolerances applied to the same parameters depending on the required level of accuracy<sup>22</sup>. The percentages below the tolerances are estimations of the increased level of cost incurred by tightening the tolerances.



Quality level	Thickness (mm) ±	Radius (mm) ±	Refractive Index ±	Abbe Number ± (%)	Homogeneity	Decen. (mm) ±	Tilt (arc sec)	Sphericity (fringes)
Commercial	0.1 100%	1.0 100%	0.001	1.0	0.0001	0.1	60	2 100%
Precision	0.01 150%	0.1 125%	0.0001	0.1	0.00001	0.01	10	1 125%
High Precision	0.001 300%	0.01 150%	0.00001	0.01	0.000002	0.001	1	0.25 150%

Table 3.5. Typical Tolerances and their Associated Costs

At first glance, it can be seen that the tolerances specified in Table 3.5 for thickness and tilt are tighter than those specified by ISO 10110, even for a commercial level of performance. A difficulty arises when attempting to compare the data in Table 3.5 with other sources of information, due to the fact that it does not give any indication of the diameter of the lens being toleranced, a factor that has a large effect on the other tolerances such as those placed on thickness, radius, and sphericity as discussed earlier in this chapter. For some of the above parameters, following discussions with lens manufacturers, it has been possible to estimate the cost implications of tightening the tolerances. If we take the commercial quality level to have a cost value of 100% for each of the parameters, then the percentages (below values in the table) indicate the extra costs involved in tightening the tolerances to precision and high precision levels. It can be seen that the stated high precision tolerance on element thickness triples the cost of this process and, further more, at this tolerance the manufacturing process becomes almost *hit and miss* with lens rejects increasing rapidly. The cost of tightening the restrictions on the radius is less dramatic. However, a great deal depends upon the radius being polished and the diameter of the lens being worked. From discussions with the glass manufacturers, the average tolerance placed on the refractive index is  $\pm 0.0001$ , which agrees with the precision quality level. However, the average tolerance placed upon the Abbe number was  $\pm 0.5\%$  which lies somewhere between the commercial and precision quality levels. The cost implications of tightening the tolerances on the refractive index and Abbe number are hard to estimate, as these depend heavily on the glass type under consideration and how often that type of glass is melted to the higher

tolerances. Because there was no more information on the sphericity tolerance provided than that shown, the cost implications of tightening the tolerances have been based upon a nominal number of four fringes, and on the assumption that it is a relatively simple curve being generated. The implications of this are that, for the commercial quality level, two out of the four fringes are allowed to be oval, meaning a small amount of asphericity can be tolerated.

Table 3.6 lists typical tolerances and is taken from a larger table printed in *Modern Optical Engineering* by Warren J. Smith<sup>23</sup>:

Quality Level	Diameter (mm)	Thickness (mm)	Radius (Fringes)	Regularity (Sphericity) (Fringes)	Centration (concentricity) min
Commercial	0.07 100%	0.25	10	3	3-10
Precision	0.02 110%	0.1	5	1	1-3
Extra Precision	0.01 130%	0.05	1	0.2	<1

Table 3.6. Typical Tolerances

This table, again, gives no indication of the diameter of the lens in question or the radii being generated, which makes it difficult to compare directly with the data presented in Table 3.5 or with the ISO 10110 tolerances given in Table 3.1. It can be seen that, in this table, the radius and sphericity have been presented in the same way as discussed in the tolerancing section. However, the centration refers to a complete lens element rather than a single spherical surface. In Table 3.5 the radius of curvature tolerance was specified in millimetres rather than in fringes as it is in Table 3.6 and subsequent tables. When the tolerance is specified in millimetres it is an absolute tolerance based on a  $\pm$  change in the radius generated on it. When the tolerance is specified in fringes it describes the departure of the lens surface from the

surface of the test plate. Each fringe indicates a difference between the lens surface and the test plate of half a wavelength of the incident light. The tolerances placed on the radii of curvature in ISO 10110 are broadly similar to those specified for the commercial lens quality, but they cannot be directly compared with those in Table 3.5 as they are specified differently. The costs of increasing the tolerance on the diameter have been estimated in the same manner as before, and again are displayed in the table below the tolerance values. It can be seen that tightening the tolerance on the diameter of the lens, even quite dramatically, does not have the same effect upon the manufacturing costs as tightening the tolerance on the radius or, especially, the lens thickness. This is because generating the diameter of the lens is a much simpler process to control than that of achieving the correct thickness. Once the lens has been roughed out it has to be polished to its correct radius of curvature. By definition, this polishing process removes thickness from the lens, so it is obviously a more complex process to ensure that the correct radii of curvature, surface finish and lens thickness are reached at the same time. Once the curved surfaces have been generated, the lens is edged to the correct diameter. In a discussion related to Table 3.6, Smith also makes the point that if the thickness tolerance is too tight then the rejection rate can increase substantially. First the lens is mounted on to a chuck (pitch or vacuum mounting methods are the most common) and then it is rotated. A grinding wheel is introduced from one side (much in the same way as a cutting tool on a lathe) and the lens is ground to the correct diameter. Care must be taken, when mounting the lens on the chuck, to ensure that the lens is centrally fixed and the centres of curvature of the two surfaces lie along a single axis. Once this is achieved, grinding the lens to the specified diameter is a relatively simple process.

Table 3.7 showing generic tolerances, is part of a table taken from Optical System Design by Fischer and Galeb<sup>24</sup>. These are the tolerances recommended by the authors as necessary to achieve “*reasonable lens performance*”.

Parameter	Tolerance	Parameter	Tolerance
Radius (Fringes)	3	Decentration (mm)	±0.05
Thickness (mm)	±0.05	Refractive Index	±0.001
Air Space	±0.05	Abbe Number	±0.8%
Tilt	0.05 mm TIR	Homogeneity	±0.0001

Table 3.7. Tolerances for Reasonable Lens Performance

In comparison with the tolerances in Table 3.5, the tolerances presented by Fischer and Galeb correlate quite closely with those specified for a commercial level of quality. However, when considered alongside those presented by Smith (Table 3.6) the directly comparable tolerances agree most closely with those require for the extra precision standard. Although there is a power fringe tolerance given for the radius, there is no indication of a tolerance on the sphericity of these fringes. Again, there is no indication of the lens diameter or radii being polished, or the diameter to centre thickness ratios of the lenses. The tilt tolerance is specified as the Total Indicator Run out value, (TIR), which is a different method of expressing tilt than previously encountered. Table 3.8 is taken from work carried out by Plummer and Lager<sup>25</sup>.

Diameter (mm)	±0.1 100%	±0.05 100%	±0.025 103%	±0.0125 115%	±0.0075 150%		
Thickness (mm)	±0.2 100%	±0.1 100%	±0.05 115%	±0.025 150%	±0.0125 300%		
Stain Characteristics	0 100%	1 100%	2 103%	3 110%	4 150%	5 250%	5+ 500%
No. of lenses per block	25 100%	18 105%	11 115%	6 130%	3 175%	1 300%	
Eccen. In light dev.	6 min. 100%	3 min. 103%	2 min. 108%	1 min. 115%	30 sec. 140%	15 sec. 200%	
Figure in $\lambda$ (pow/irreg.)	10-5 100%	5-2 105%	3-1 120%	2 ½ 140%	2 ¼ 175%	1 ⅛ 300%	
Dia. To thickness ratio	9-1 100%	15-1 120%	20-1 150%	30-1 200%	40-1 300%	50-1 500%	
Beauty defects (MIL-C-13830A)	80-50 100%	60-4 110%	40-30 125%	20-10 175%	10-5 350%		

Raw Glass Cost in 1000lb lots	\$ 3.00 100%	\$ 5.00 108%	\$ 8.00 115%	\$ 15.00 125%	\$ 25.00 135%	\$ 50.00 200%	\$ 100.00 350%
Coatings Spec.	Uncoated 100%	Mg.Fl. 115%	3-4 Layer 200%	>4 layers 200- 500%			

Table 3.8. The Increasing Cost of Tightening Tolerances

In this case the tolerances are specified for a lens that is between 25 and 50mm in diameter, though no information is provided about the types of curvature involved. It can be seen that trends in the cost increases discussed earlier tie up with the information in Table 3.8. The costs incurred tightening the tolerances on element thickness incur a considerably higher cost penalty when compared to those associated with diameter. This table also includes cost associated with the tolerance placed on the surface radius of curvature. Table 3.8 also introduced the cost penalties on the stain characteristics and beauty defects, which are both directly concerned with the quality of the glass that the lenses are made from. The beauty defects tolerance can be considered as a combination of the bubbles and inclusions, striae and surface imperfection tolerances and is almost a cosmetic specification. The stain characteristics are based on a numerical scale and predict how easy the glass is to handle. At the lower end, the glass is extremely easy to use. However, at the higher end the glass may be stained by exposure to air or the breath of the worker controlling its manufacture. The handling of these glasses obviously requires special procedures and can have a dramatic increase in cost. The cost implications placed on the number of lenses per block are an interesting parameter. The radii of curvature can limit the number of lenses that can be manufactured on a single block. If the radius of curvature is too small then the lens will have to be manufactured individually. The benefits of multiple lenses being polished simultaneously on a single block are not simply the obvious timesavings that result from the simultaneous polishing. In general, it is easier to polish accurate figures on multiple lenses because of reduced problems at the edges of the polished region. The tooling costs are also reduced as multiple lenses are produced simultaneously

from each tool. Indeed, the inherent cost advantages in mounting multiple lenses on a single block can be so great that it is often more cost effective to employ a more expensive, higher refractive index glass rather than steeper curvatures, in order to increase the power of a lens element<sup>25</sup>. An in depth discussion of how lenses are manufactured, including the multiple lenses per block approach, is provided in Chapter 4. A useful method for checking the number of lenses that can be mounted on a single block is the ratio of radius of curvature to the diameter of the lens element. The limits on this ratio are presented in Table 3.9.

Radius of Curvature/Diameter	No. of lenses per block
<0.84	1
0.84-1.04	3
1.05-1.40	6
1.5-2.00	11
2.10-2.70	18
2.8-	25

Table 3.9. Number of lenses per block.

In combination with the radius of curvature to diameter there are a number of other ratios that a lens designer would do well to bear in mind. It is good practice to keep the centre thickness to edge thickness ratio within reasonable limits, in order to ease the manufacturing process. This level is dependent upon the glass types involved and the manufacturing techniques employed. It is also wise to place a lower limit on the minimum allowed lens edge thickness, during the optimisation process. The edge thickness has a bearing on how difficult the lens is to manufacture and assemble accurately. Too small a value and it becomes difficult to control during polishing, makes the edges of the lens very brittle, combined with making the lens more susceptible to tilt when assembled in the system. The default minimum edge thickness specified within OSLO is only 0.05mm, which may be a little small for many applications. It may be necessary to limit the design to certain specific curvatures for which the workshop has existing tools and test plates. In

general, it can also be problematic to generate highly accurate surface forms on elements whose centre thickness to diameter ratio is low. A guide is to keep the thickness to diameter ratio below 1:10. However, if the edge thickness of the element is sufficiently large then it can be possible to raise this to 1:30. If the surface is particularly difficult to manufacture then this ratio may have to be as low as 1:3<sup>26</sup> in order to keep production costs and rejection rates at an acceptable level. Certain curves can be more difficult and expensive to polish, such as large radius curves on small diameter lenses, especially in small batches, and equally, large radius curves and small lenses can be difficult to generate accurately. It may be wise in some cases to alter the lens design such that the surface becomes optically flat.

In order to produce a comprehensive cost function that could become a viable part of an optimisation routine, all of the data presented in this section must be combined into a single, multi-variable function that allows a comparative cost to be calculated for any lens element. The complexity of the cost function must reflect the complexity of the optical system being designed, and must take account of the manufacturing and assembly costs inherent in the competing optical elements. A simple example of this would be to combine the information in Table 3.8 with the cost implications of altering the number of elements per block presented in Table 3.9 to make a single cost function that relates the radius of curvature to the lens diameter. This error function has been calculated over a range of surface radii and lens diameters and can be seen in Figure 3.17. In order to make this a comprehensive cost model relating to radius of curvature, the cost tightening tolerance on surface form, in terms of radius and figure, must also be included, as well as the ratio of radius of curvature against centre thickness referred to earlier in this section.

An attempt has been made to collate much of the published data on manufacturing costs into a single function, which estimates the manufacturing costs of an optical element<sup>27</sup>. This function draws together the cost of tightening the tolerances work discussed previously which the cost of certain manufacturing issues such as the

effects of allowing the diameter to centre thickness ratio to increase to an unacceptable level. The cost function, MT, is presented in equations 3.1a-d. These equations are then summed to obtain an estimate of the costs involved in manufacturing a single optical element.

$$\text{Roughing Cost} = 4 + 90/LM + 0.1 \times d^2 \quad 3.1a$$

Where LM=Number of parts milled in single set-up  
d=Lens diameter.

$$\text{Part Set-up Cost} = (14 \times Y) \quad 3.1b$$

Where Y=Yield factor (defined as total number of elements manufactured divided by the number that pass inspection).

$$\begin{aligned} \text{Grinding and Polishing cost (each surface)} &= (P \times Y \times 14/N) \\ &\times \{ [1 + 0.25 \times KI/\Delta I] \\ &\times [1 + (R/d)^2 \times 8 \times KZ/\Delta R + 0.0003 \times (d/T)^3] \\ &+ 40 \times KT/\Delta T \\ &\times (1 + 10/S + 5/D) \times (1 + 0.01 \times SC^3) \} \end{aligned} \quad 3.1c$$

Where P=Polishability factor based on glass type (see Table 3.10)  
N=Number of elements per block  
KI=Cost increase factor for the lens surface form tolerance  
 $\Delta I$ =Lens surface form tolerance  
R=Radius of curvature  
KZ=Cost increase factor for the radius of curvature tolerance  
 $\Delta R$ =Radius of curvature tolerance  
T=Lens centre thickness  
KT=Cost increase factor for the centre thickness tolerance  
 $\Delta T$ =Lens centre thickness tolerance  
S=Scratch specification (Defined as per MIL-O-13830A)



D=Dig specification (Defined as per MIL-O-13830A)

SC=Stain characteristic of glass type.

The cost increase factors are defined numerically in Table 3.11.

$$\text{Edging and Centring} = \frac{(2+d+C+F)}{3} + \frac{(30+10 \times C + 15 \times F)}{LC} \times (1 + 10 \times KD/\Delta d + 0.145 \times KW/\Delta A) \quad 3.1d$$

Where C=Number of chamfers on lens element  
 F=Number of flats on lens  
 LC=Number of lenses edged and centred in one set-up  
 KD= Cost increase factor for the lens diameter tolerance  
 $\Delta d$ =Tolerance on lens diameter  
 KW=Cost increase factor on tilt  
 $\Delta A$  is the tilt tolerance.

The parameters employed in these equations will now be discussed. As already mentioned, the ease by which a lens may be ground and polished is partly dependent upon its glass type. Wiley and Parks, the authors of the above equations, have estimated the ease with which different glass types may be worked and they have termed this parameter polishability. The polishability factor of a variety of optical glasses can be seen in Table 3.10. They are presented in the same form as the tolerance costs with a base line assigned a cost of 100%.

Glass Type	Polishability Factor (%)
BK7	100
SF56	120
Germanium	130
Fused Silica	140
FK2	170
LaFN21	200
Sapphire	800

Table 3.10. Polishability factors of a variety of optical materials.

The stain characteristic, SC, is simply the stain code, as mentioned earlier in this section and is an integer value between 0 and 5 dependent upon the stain resistant properties of the glass<sup>28</sup>. The scratch and dig numbers, S and D respectively, are a different method of specifying the surface imperfection tolerance defined using ISO 10110 part 5 earlier in this section. In this case the scratch and dig imperfections are separated and defined in different ways according to a United States military specification<sup>29</sup>. The scratch tolerance is given a number corresponding to the maximum width of allowed scratches in ten thousands of a millimetre, such that a scratch value of 50 allows scratches up to 5 microns wide. The dig tolerance is defined by the maximum diameter of dig allowed in hundredths of a millimetre. In the case of non-circular digs the diameter is defined as half the length plus the width.

The various cost increase factors are based upon the estimated increase in cost per element due to tightening the tolerances, as already discussed in this section. Pooling data from authors such as Fischer and Plummer and Lagger as well as research by Wiley and Parks has derived these values for the factors. These factors can be seen in Table 3.11.

Cost Factor	Value
KI (Lens figure)	1 (if $\Delta I$ specified in fringes)
	$12.5 \times 10^{-6}$ (if $\Delta I$ specified in inches)
KZ (Radius of Curvature)	1 (if specified in fringes)
	$12.5 \times 10^{-6}$ (if specified in inches)
KT (Centre Thickness)	$12.5 \times 10^{-6}$ (if $\Delta d$ specified in inches)
	0.316 (if $\Delta d$ specified in microns)
KD Lens Diameter	$12.5 \times 10^{-6}$ (if $\Delta d$ specified in inches)
	0.316 (if $\Delta d$ specified in microns)
KW (Edging & Surface Centration)	1 (if $\Delta A$ specified in milliradians)
	$(\text{refractive index}-1)0.344$ (if $\Delta A$ specified in minutes of arc)

Table 3.11. Cost Factors for Various Tolerance Parameters.

These equations provide a method by which the relative cost of manufacturing an optical element can be derived from a combination of previously published data and experience. In order to get a true appreciation for the cost of an optical system the assembly process must also be considered. This includes the cost of manufacturing the metal work to ensure that the positioning of the optical elements is sufficiently well controlled and the costs of the assembly and test procedures required in order to fulfil the lens specification.

The ideal method of calculating the additional cost of tight tolerances is to base it on production records from the company where the lens systems are going to be manufactured. In this way the information would be based directly on their manufacturing and assembly practices and capabilities and would therefore give the most accurate predictions of optical system cost. It can be problematic to base the cost functions on other examples of published tolerance/cost analyses as often they are not consistent with each other and do not provide enough information about the types of lenses being toleranced and the manufacturing and test methods employed.

### 3.6 Existing Optimisation Tools that Include Cost

A number of attempts have been made to produce computer programs that can measure the relative cost of an optical system and therefore aim to reduce costs at the design stage. As already discussed, the OSLO lens design package has several constraints that can be applied to control costs such as limiting the curvatures to a specified set of the test plates, or using only the more common and inexpensive optical glasses. A more effective method of reducing the overall costs of an optical system would take into account the information in the previous section and estimate the cost of the tolerances placed on the system.

R. N. Youngworth<sup>30</sup> defines the relative cost of an optical system in terms of two components, the cost of the rejecting systems that do not meet the required performance parameters, and the cost of building the system such that it meets the

specified tolerances. The cost function implemented must consider the opposed interests of both the optical performance of the system, again defined as an error function, and the production costs if the best compromise is to be reached. The cost function relies on clearly defining the cost of tightening individual tolerances based on knowledge of the available manufacturing processes, published data on the cost of certain tolerances and the experience of the optical designer. The rejection rates were estimated using the Monte Carlo analysis technique based on a batch size of 25,000. Once the optical system has been designed the first stage of the cost based tolerancing process is to input the cost functions for each of the variables to be toleranced, and whether any compensation device will be employed, a common one being alterations in the back focal length of the system to maintain focus. Next, starting values for these tolerances are estimated based upon the experience of the optical designer. The total cost versus optical performance function is evaluated until a suitable solution is reached which balances both optical performance and cost of manufacture.

As opposed to tolerancing the optical system to have low production costs, a different approach to minimising the cost of optical system would be to de-sensitise the optical system to manufacturing errors at the design stage<sup>31</sup>. One method of achieving this is based on the Seidel aberrations, discussed in Chapter 2, and aims to minimise the level of aberration balancing between surfaces. Another method is to minimise the wave front change due to the individual maximum permitted manufacturing errors and it is a combination of these methods that was employed in the technique discussed here. The example presented by Dobson and Cox<sup>31</sup> is the redesign of a 6 element system to a 5 element system while reducing its sensitivity to manufacturing errors whilst maintaining a suitable level of optical performance. This was achieved along with around a 40% reduction in the system sensitivity to manufacturing errors.

### 3.7 A Global Cost Model

In order to investigate the viability of including a comprehensive cost function within the optimisation process, the design of a simple polychromatic, cemented doublet lens designed within OSLO was chosen to be used as an example. To simplify the analysis the design was restricted to only two glass types BK7, a crown glass, and SFL6, a typical flint glass. The doublet was to have a focal length of 100mm and was to operate at f10, with a beam entrance radius of 5mm and a field angle of 2.5°. OSLO contains a simple optimisation method where the variables in a design can be altered using a slider bar and the changing optical performance can be seen in real time. Experimenting with this system it could be seen that, for even a simple cemented doublet, there were two distinct design solutions affording similar optical performance. Obviously, these two designs would have different manufacturing costs and tolerances inherent in them, but it was not possible to examine them in detail without leaving the optimisation application. The two designs follow the standard form for positive focal length achromatic doublets. The first, Doublet 1 is the typical crown leading design and Doublet 2 is the less typical flint leading design. The two different designs generated using the slide rule optimisation can be seen in Figures 3.18a & b.

Doublet 1 depicted as part (a) of the figure has a bi-convex positive front element and a negative meniscus rear element. Doublet 2, part (b) of the figure has a meniscus front element and a bi-convex lens as the rear element. Table 3.12 shows the surface radii of the surfaces in both of the designs.

	Doublet 1	Doublet 2
Surface Radii of Surface 1	56.452	44.31954
Surface Radii of Surface 2	-69.096	31.025537
Surface Radii of Surface 3	-158.798	-582.968

Table 3.12 Surface Radii of Doublets One and Two

In terms of the relative costs of the two competing designs, they are both made out of the same glass, and there are no major edge thickness to centre thickness problems as the centre thickness was fixed, so any difference in cost will be down to the different curvatures and manufacturing tolerances.

The optical performances of the two solutions are very similar indeed, as will be discussed, so the decision to choose one of the lenses for manufacture should be based solely on cost. Both lenses exhibit diffraction limited performance on axis. Doublet 2 has slightly higher Seidel and chromatic aberrations than Doublet 1 but they are still very close. The Strehl ratios<sup>32</sup> of the two designs are within 0.6% of each other.

The two competing designs were toleranced using a sensitivity routine measuring changes in the MTF, using the default tolerances within OSLO, which are based on those specified in ISO 10110. The tolerance analysis showed that the two lenses were very similar in most of the parameters toleranced such as lens thickness and radius of curvature, which is to be expected, as the designs are also similar. The main differences in the tolerance values related to the tilt and decentration tolerances. The front surface of Doublet 2 is significantly more sensitive to tilt than the front surface of Doublet 1. In fact the standard tilt causes a change in the performance of 0.033 on axis, 0.026 at 0.7 of the field and 0.016 at full field for Doublet 1, compared with a change of 0.539, 0.738 and 0.700 respectively for Doublet 2. The tilt tolerances for the second surface are fairly similar across both designs, and though the tilt effects on the rear surface are slightly worse for Doublet 1, than 2, they still do not compensate for the considerably worse performance of the front surface of Doublet 2. The decentration tolerances are also worse for Doublet 2 than Doublet 1, the decentration tolerance on the front elements being 14% tighter for Doublet 2 where there is a much smaller difference between the rear elements <8%. These differences are due to the fact that much of the power of Doublet 2 is concentrated in the front surface, which combines the largest curvature of all of the surfaces, combined with the largest refractive index change, from air that is

nominally 1 to a refractive index of 1.8052. The largest refractive index change in Doublet 1 is at the rear surface where the ray leaves a glass of refractive index 1.8052 and returns to air. However, in this case, it is the surface with the longest radius of curvature greatly reducing the power of the surface with respect to the front surface of Doublet 2. Overall, Doublet 1 is easier to manufacture and align because the power of the lens is more evenly distributed between the surfaces rather than being concentrated at the front of the lens as in Doublet 2. For these reasons Doublet 1 would be the cheaper to manufacture and therefore the challenge is to modify the optimisation routine error function in such a way that it optimises towards Doublet 1.

In order to simplify the optimisation procedure, the lens centre thicknesses were chosen and fixed at 3mm for the front element and 2.5 mm for the second element. This leaves the variables for the optimisation as the curvatures on the elements and the back focal distance. As the lens is a cemented doublet there is no airspace between the elements and the second curvature on the first element must be the same as the first curvature on the second element for them to be successfully cemented together. This means that there would be three curvatures and the back focal distance as the variables. Although the doublet lens has been limited to two glass types there is also the variation within the design as to whether the doublet is flint or crown leading. A simple iterative optimisation procedure is then employed, where the lens is optimised according to certain "operands" which are desired characteristics of the lens. They can define the aberration characteristics that are acceptable within the design, as well the basic information about the lens such as f-number and effective focal length. They are also used to define the type of error function. Within OSLO there are two basic types of error function, those that measure RMS spot size and those based on RMS wavefront error. Other operands can be included as standard within the error function such as those to correct colour errors within the system, and distortion at full field and edge thickness. Initially, the lens was optimised using an error function that minimises the calculated RMS spot size, appended with operands that force the design to be of crown or flint leading

type and to have the paraxial properties as defined at the start of this section. Then, they were re-optimised to minimise the aberrations using the GENII ray aberration function included within OSLO, which aims to optimise the design while holding the paraxial properties of the system as they were at the start of the optimisation. All of the operands, used within OSLO, have one of two forms. They can be the minimisation type, where the program tries to minimise the value calculated by that particular operand, and the constraint type, which uses symbols such as  $<$ ,  $>$  where parameters can be forced above or below certain values. Each of the minimisation operands is then assigned a weight, which defines the penalty term incurred by the optimisation if that particular operand is not met.

It is by appending new operands to this list that the optimisation program can be altered to optimise towards an inexpensive lens design rather than simply the lens design with the highest optical performance. Some of the operands, included within OSLO that can be used to control cost, can be seen in Table 3.13 below. It is also possible for the lens design to define new operands by programming them manually, and it is through this method that any cost models can be entered

Component type	System operand component
cv(srf,cfg)	Curvature of surface "srf"
th(srf,cfg)	Thickness of surface "srf"
ap(srf,cfg)	Aperture Radius of surface "srf"
m(srf,cfg)	Refractive Index at surface
dn(srf,cfg)	Dispersion at surface
eth(srfa,srfb,cfg)	Edge thickness from surface "srfa" to surface "srfb" at height of aperture radius
pwr(srfa,srfb,cfg)	Power between surfaces "srfa" and "srfb"
ln(srfa, srfb,cfg)	Axial length from surface "srfa" to surface "srfb"

Table 3.13 Operands Used to Influence Cost within the Optimisation

The "cfg" part of the operand refers to the current configuration and relates to systems such as zoom lenses where there can be more than one configuration of the optical elements. The contribution that these operands can make to a cost function is discussed below and appropriate values from the limits on the operands are also



suggested. In the case of the cemented doublets it is the *power* operand that can be employed to force the optimisation routine towards Doublet 1, as opposed to Doublet 2. The power of a lens surface, for parallel incident rays, can be calculated using equation 3.2<sup>33</sup>.

$$Power = (n_2 - n_1) / R \quad 3.2$$

Where  $n_1$ =refractive index of first material  
 $n_2$ =refractive index of second material  
 $R$ =radius of curvature of surface.

By employing equation 3.2 it is possible to calculate the power of each surface and these are shown in Table 3.14.

	Doublet 1, Power	Doublet, 2 Power
Surface 1	0.009154674	0.0181677
Surface 2	-0.004173636	-0.009295
Surface 3	0.00507048	0.0008865

Table 3.14. Power at each surface.

From Table 3.14 it is a simple matter to calculate the maximum power between surfaces in Doublet 1, and this is 0.013 and the corresponding minimum is 0.009. However, the maximum power between surfaces of Doublet 2 is 0.027 and the minimum is 0.01. With this information it is possible to write an operand that constrains the maximum power between surfaces to be less than 0.015 and therefore, if a sufficient weighting is applied, the optimisation routine will progress towards the cheaper solution which in this case is Doublet 1. For this simple case the power between surfaces in the system is considered to be the over riding cost consideration when comparing the production costs of the competing doublets.

If the example had been more complex, then it may have been necessary to include further operands in order to drive the optimisation towards the cheaper solution.

Some of these that can be implemented simply by employing the operands included with OSLO and listed in Table 3.13 will now be discussed. Limits on the glass types can be useful in minimising cost. The obvious way to do it is to limit the designer to only using inexpensive or readily available glasses. However, it is now possible to allow the lens design software to optimise using imaginary glasses with infinitely, and often independently, variable refractive indices and dispersions, and then, towards the end of the design process, to fit these glasses to the nearest real glass and then re-optimize the design a final time. This often results in the specification of exotic and expensive glass types that may also bring with them additional polishing or handling problems. Operands can be used to control this by applying upper and lower limits to the refractive index and the dispersion, and also by specifying permitted dispersion/refractive index ratios to ensure that the design stays within the desired region of the glass map. Figure 3.19 shows the glass map with a region added which defines a rule of thumb area of everyday, and therefore economic, optical glass<sup>34</sup>.

Some of the operands within the optimisation routine can be used to give an indication of likely manufacturing tolerances. The operand *ln*, listed in Table 3.13, calculates the axial distance between surfaces. If this difference represents an airspace as opposed to a lens thickness, then this value can have a large impact on the assembly tolerances of the design. If this distance is very small, it may be wise to alter the design and cement the lenses together, especially if the curvatures are similar. Also, if this length becomes too large, then the tolerances on decentration and tilt can become prohibitively tight, especially if the axial ray slope leaving the lens is comparatively large. The *eth* operand listed in Table 3.13 can be implemented to control the edge to thickness ratio, and other simple operands can be written that restrict the design to the regions defined by the other ratios mentioned in Section 3.4.

### 3.8 Conclusions

This chapter has outlined the optical tolerancing procedure, and a selection of the more common tolerance parameters, as well as how these tolerances can be applied to both the manufacturing and assembly phases of optical production. The main sources of cost have been highlighted and discussed and general principles of cost minimisation have been introduced. Within a large proportion of designs, costs generally arise from the tolerances that have to be applied, if the optical performance is to be met. A comparison of a number of different cost/tolerance models was undertaken with the aim of generating a comprehensive cost function. Based on this information, the error function within OSLO was altered such that for a simple cemented doublet case, which had two solutions of very similar optical performance, the optimisation routine progressed towards the cheaper solution. The ideal solution would be to have an optimisation procedure that takes an account of the real cost of these tolerances as part of the routine and optimises to find a design that provides the largest possible tolerances on critical aspects of the design while still meeting the overall performance requirements. However, this would require the program to leave the optimisation process and calculate a tolerance profile every time it changes a parameter within the design. These tolerances would then be referenced against the comprehensive cost function which takes account of the manufacturing, tooling, assembly and test techniques that are required to meet the tolerances and then calculates a cost for the design. When it is considered, except in the simplest cases, that current lens design procedures will not usually find a solution with optimum lens performance it is unlikely that the introduction of complex cost functions will be possible in the near future. Following preliminary work with the doublet lenses, it was decided that attention to the manufacture and mounting of lens elements would be more productive in reducing the cost of compound lenses. The following chapter discusses how lenses are manufactured and the different methods by which their surface form is assessed with particular reference to aspheric surfaces.

Chapter 3. Figures

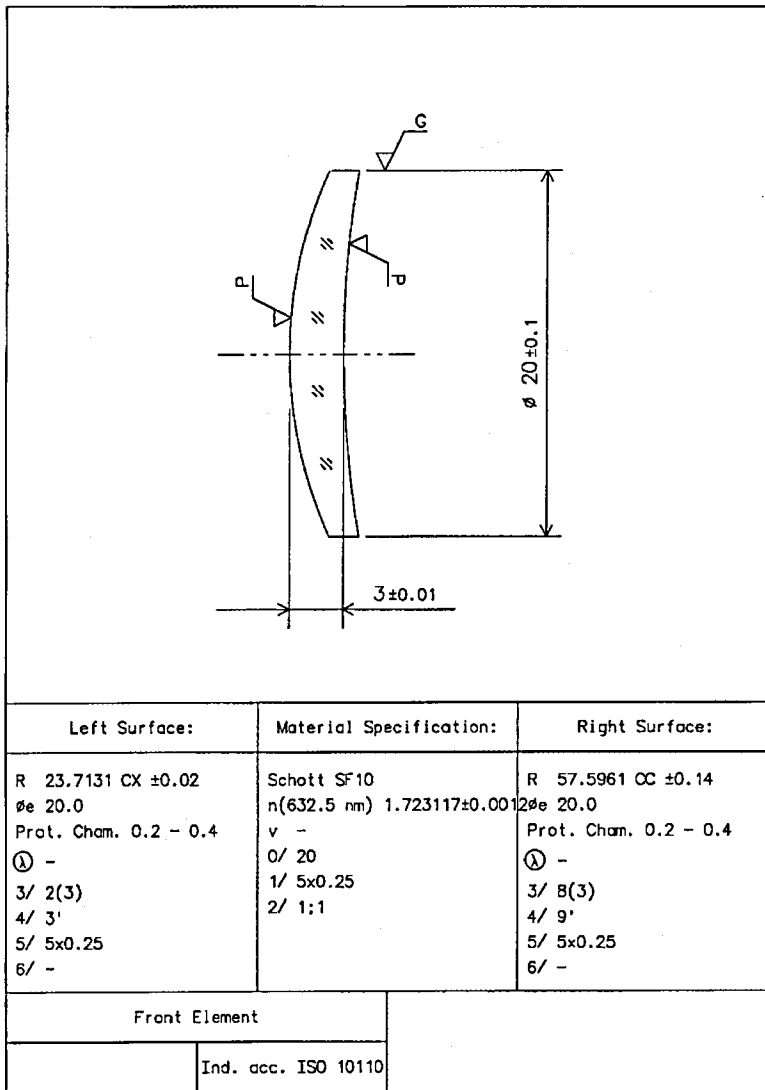


Figure 3.1. Sample Lens Drawing

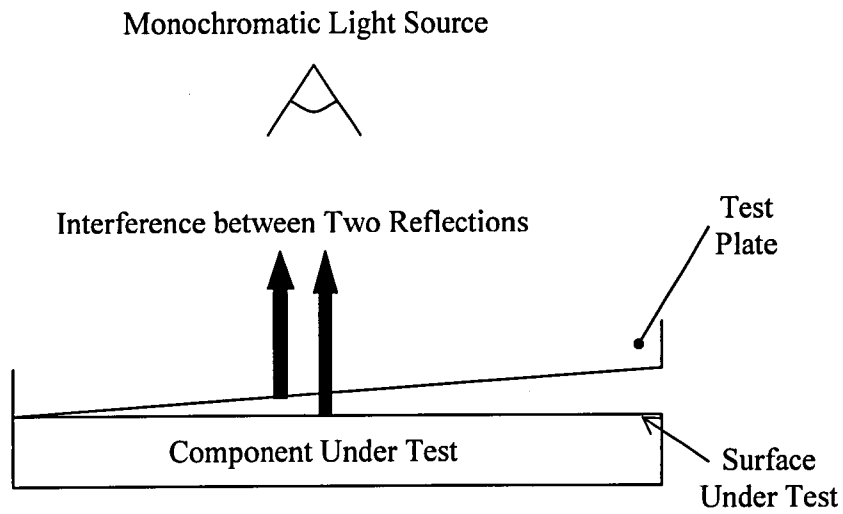


Figure 3.2. Schematic of Test Plate

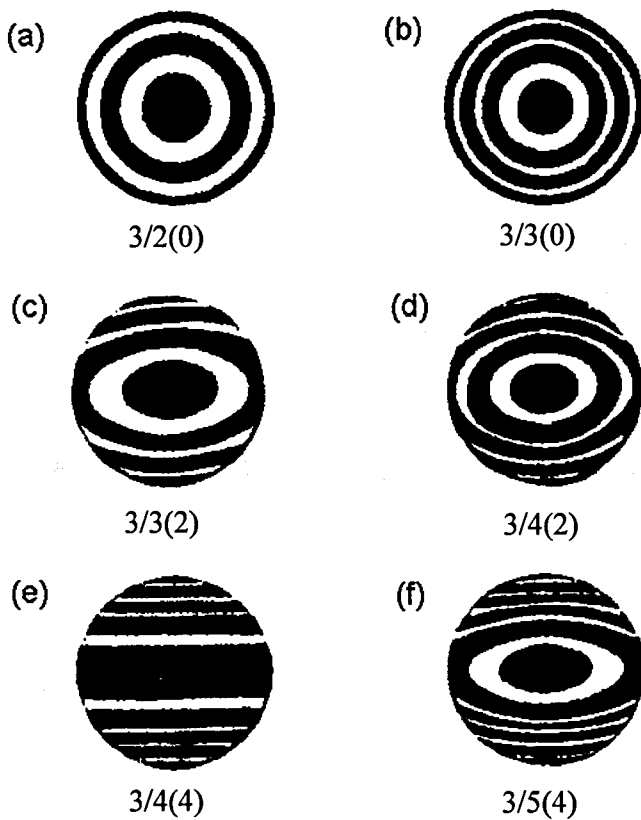


Figure 3.3. Example Fringe Patterns and Associated Tolerances



Figure 3.4. Fringe Pattern from an Astigmatic Surface where Non-Circular value is Greater than the Number of Complete Fringes Permitted

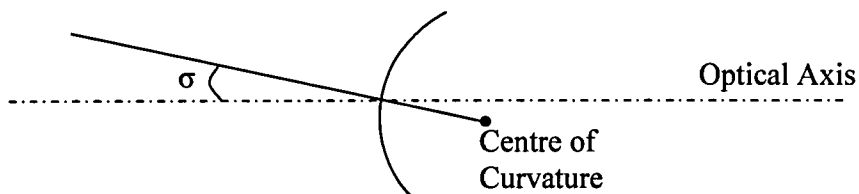


Figure 3.5. Tilt of a Single Surface

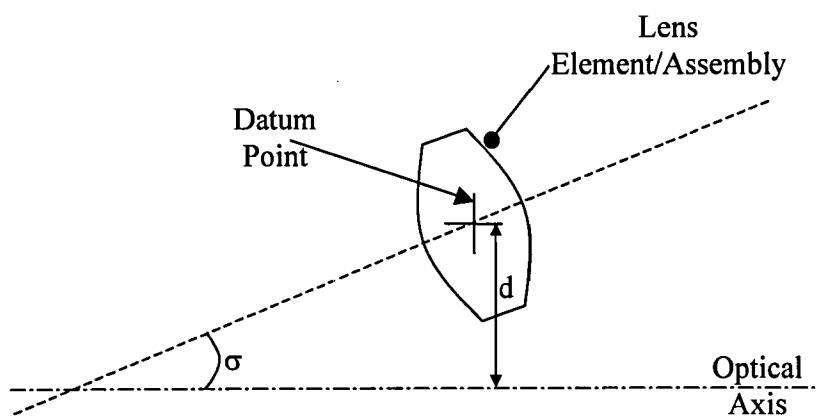


Figure 3.6. Centration of an Optical Element or Assembly

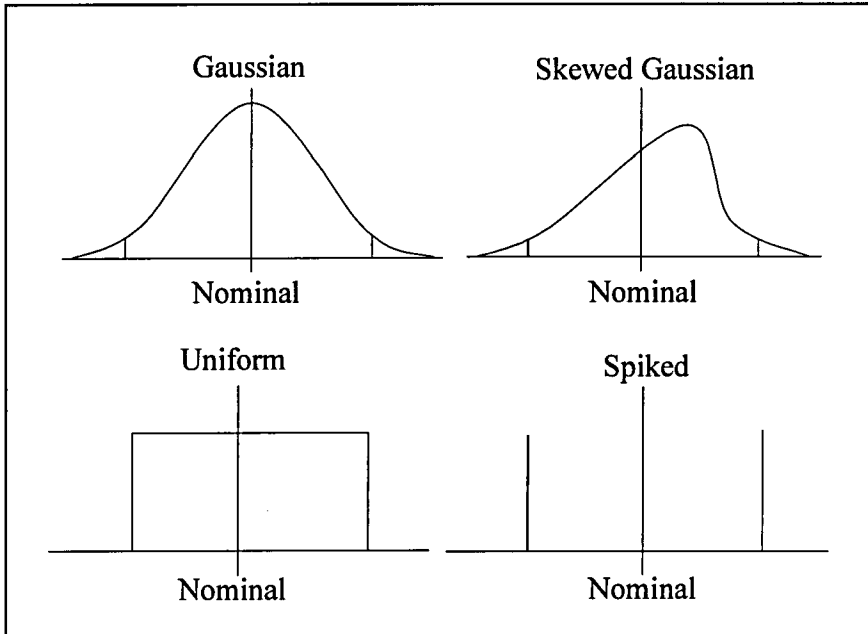


Figure 3.7. Sample Distributions

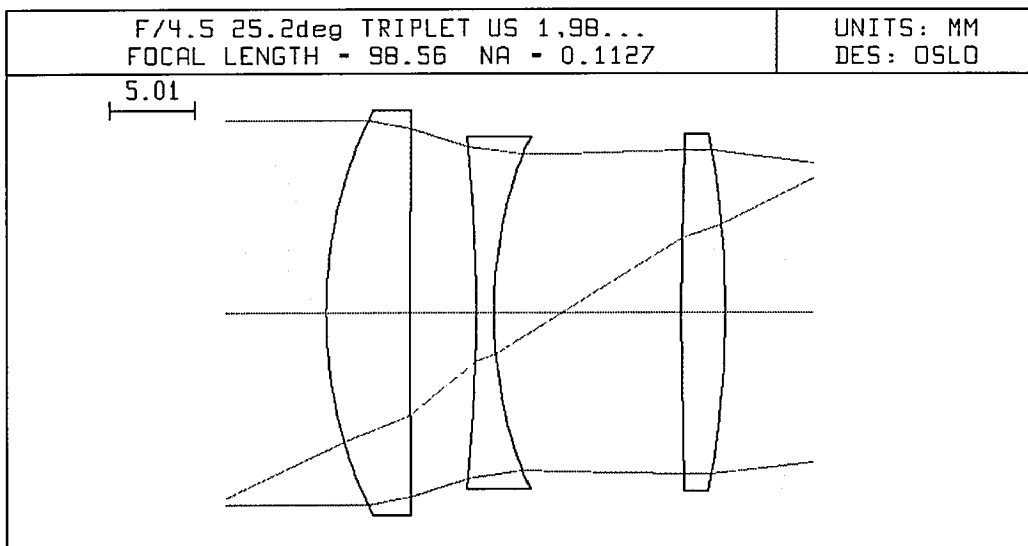


Figure 3.8. Triplet Lens Toleranced

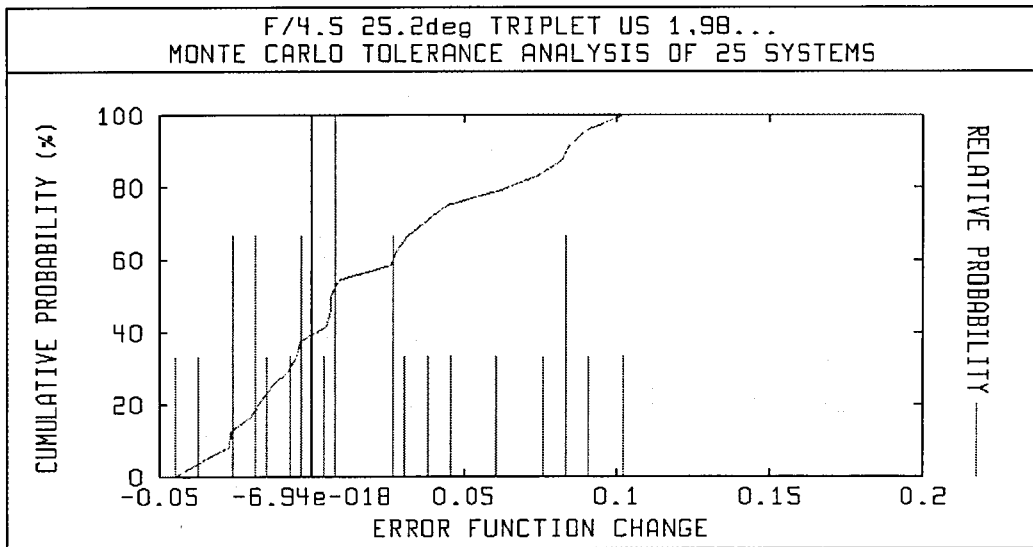


Figure 3.9. Cumulative Probability against Error Function Change

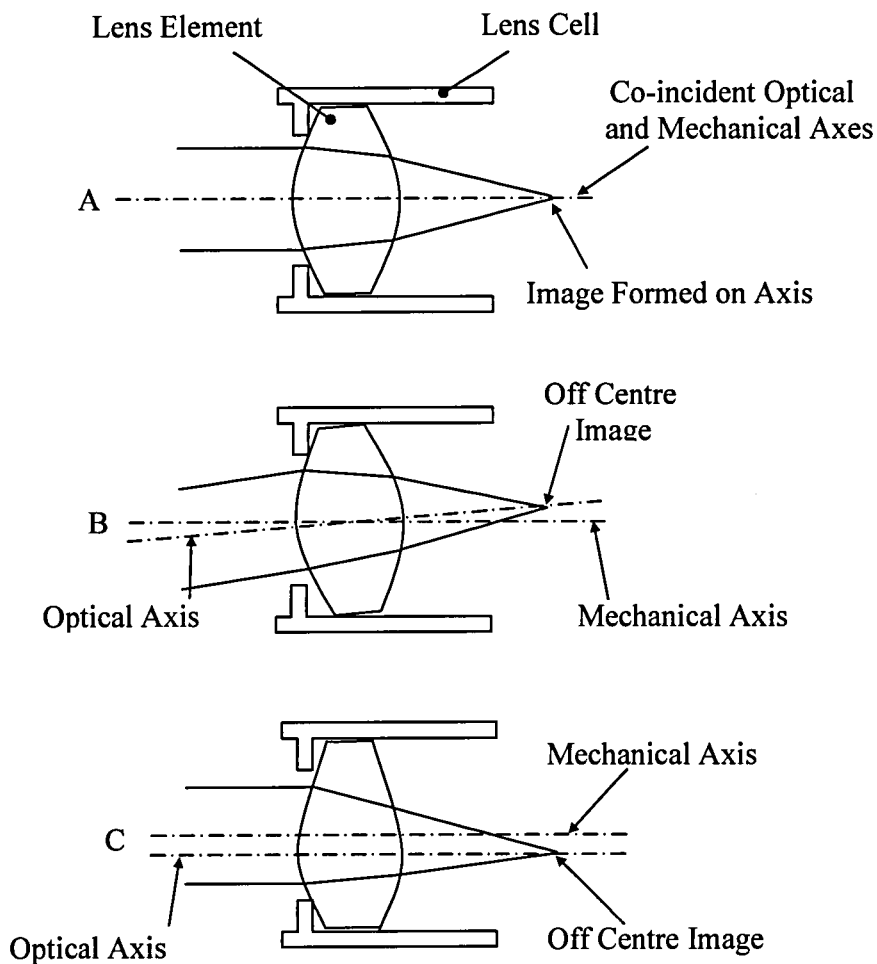


Figure 3.10. Decentrations and Tilts



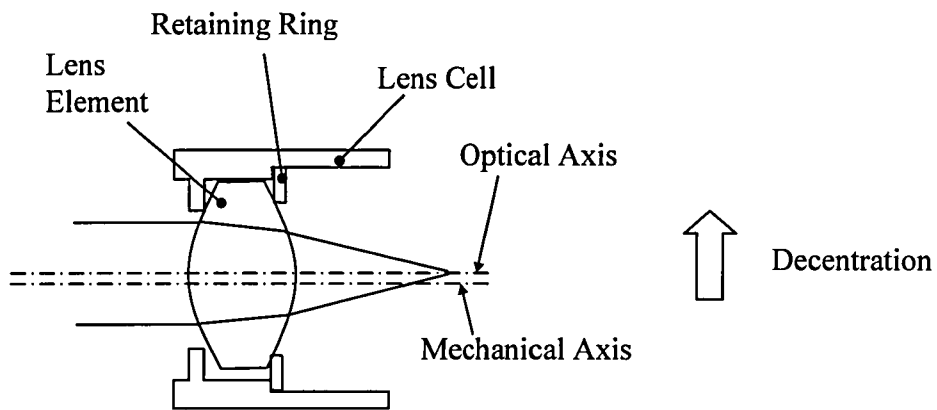


Figure 3.11. Lens Decentration within a Cell

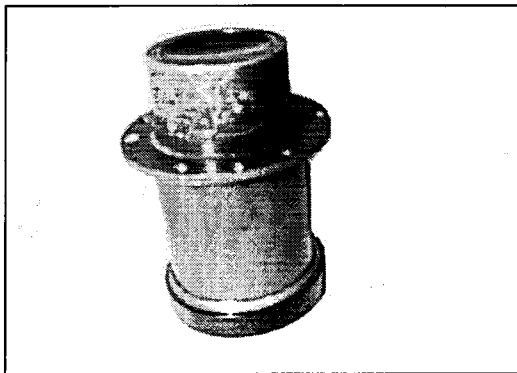


Figure 3.12 Multi Element Cell

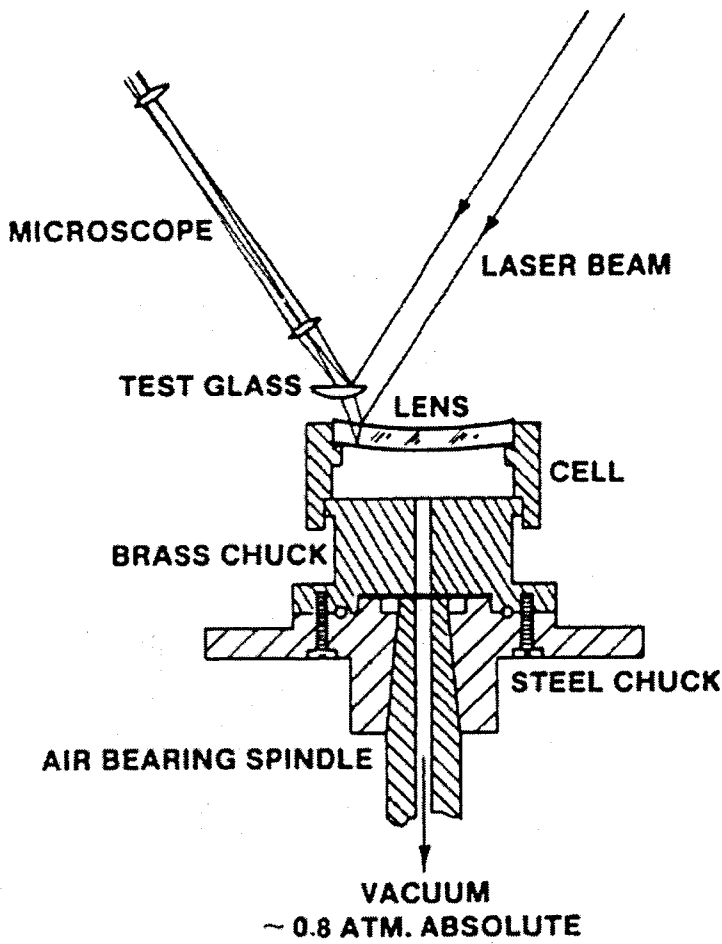


Figure 3.13. Mounting and Centring of Optical Elements (After Carnell et al.)

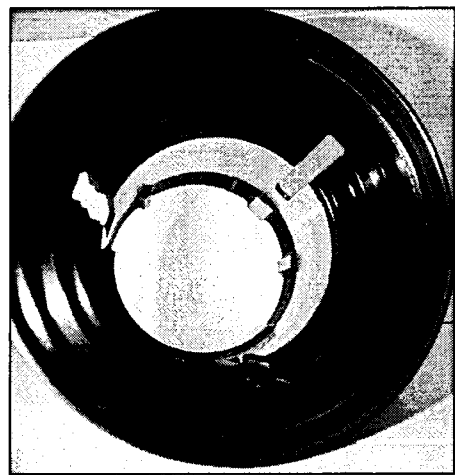
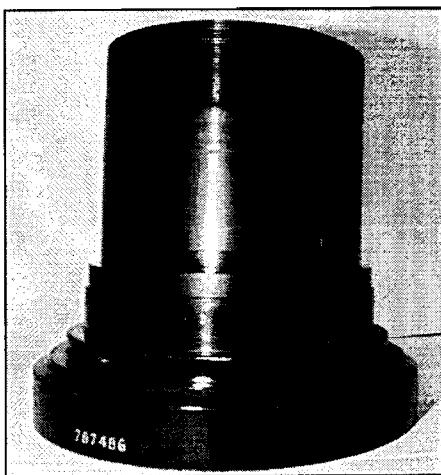


Figure 3.14. Detail of Lens Mounting Shoulders within a Lens Barrel

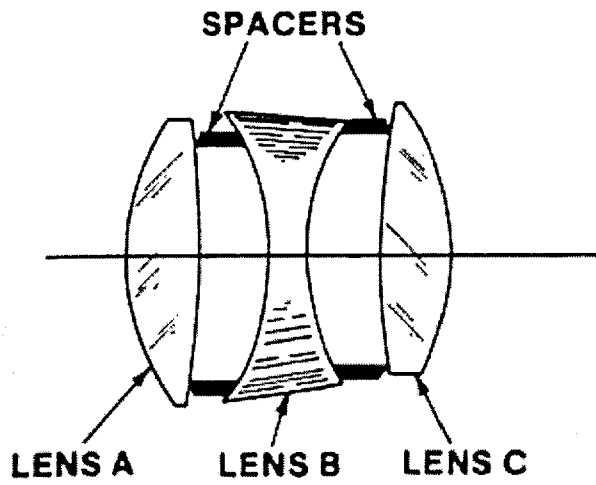


Figure 3.15. Lens Assembled via the Hopkins Method (After R.E. Hopkins).

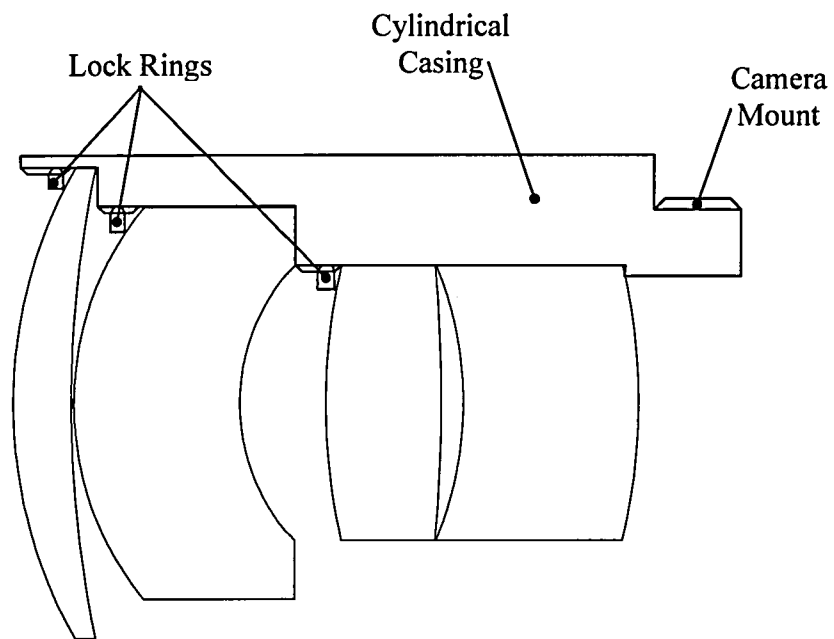


Figure 3.16. Lens System for Strain Gauge

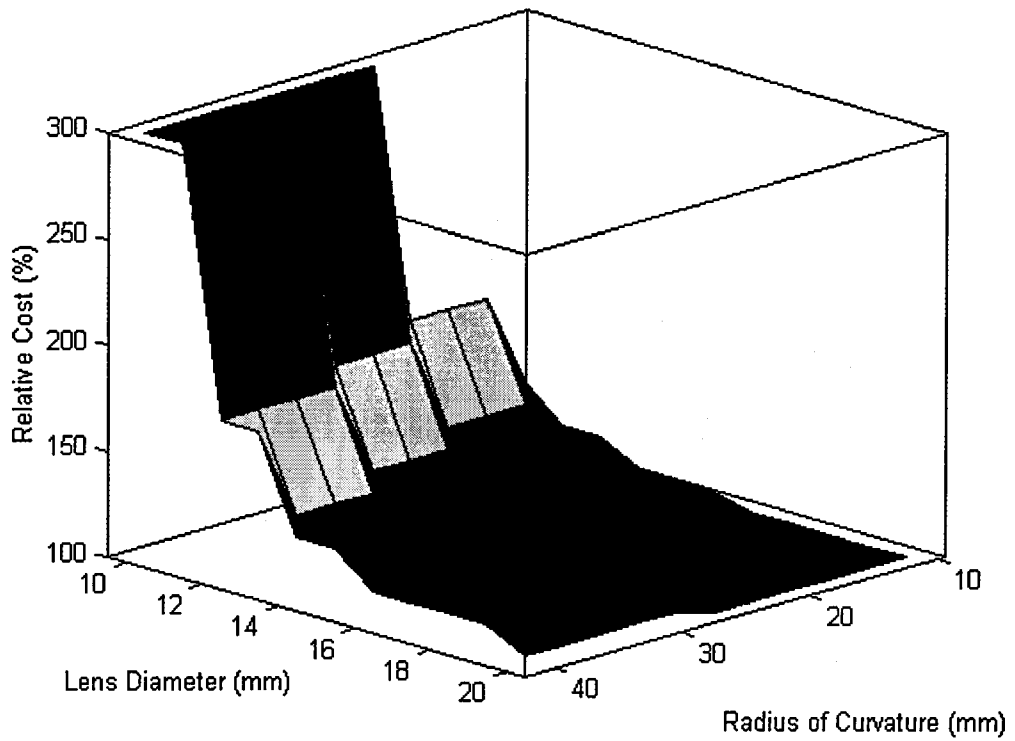


Figure 3.17. Simple Cost Model relating Radius of Curvature to Lens Diameter.

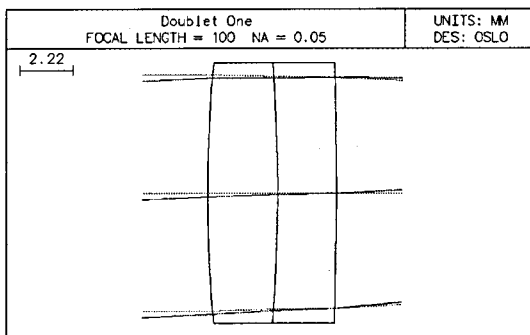


Figure 3.18a. Doublet One

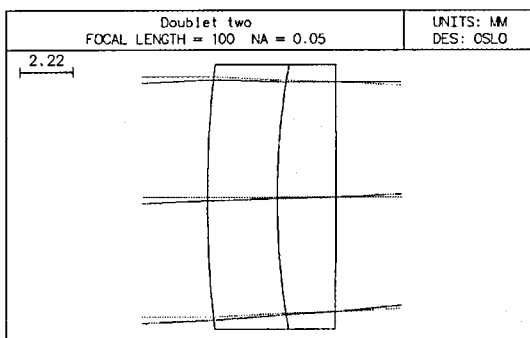


Figure 3.18b. Doublet Two

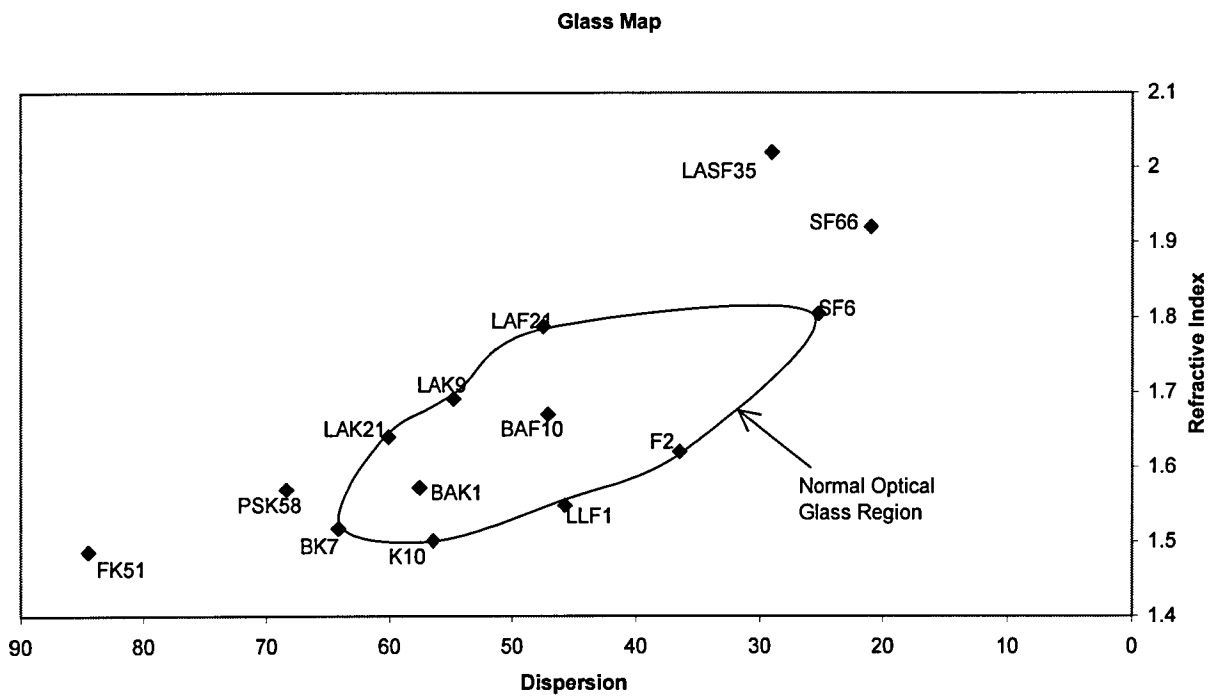


Figure 3.19. Glass Map

## References

- 
1. ISO 10110, Optics and Optical Instruments-Preparation of drawings for optical elements and systems, (1996).
  2. ISO 10110 part 3, Optics and Optical Instruments-Preparation of drawings for optical elements and systems-Part 3: Material imperfections-Bubbles and inclusions, (1996).
  3. ISO 10110 part 2, Optics and Optical Instruments-Preparation of drawings for optical elements and systems-Part 2: Material imperfections-Stress birefringence, (1996).
  4. ISO 10110 part 4, Optics and Optical Instruments-Preparation of drawings for optical elements and systems-Part 4: Material imperfections-Inhomogeneity and strain, (1996).
  5. ISO 10110 part 5, Optics and Optical Instruments-Preparation of drawings for optical elements and systems-Part 5: Surface form tolerances, (1996).
  6. Frank Twyman, "Chapter 11, *Testing Optical Work*", in *Prism and Lens Making*, Adam Hilger, London UK, pp 364-421, (1988).
  7. D. Malacara, "Chapter 1 Newton, Fizeau and Haidinger Interferometers", in *Optical Shop Testing*, John Wiley & Sons Inc, USA, pp 1-50, (1992).
  8. G. Sheehy, B. G. Brown, "Training Manual on the Blocking, Smoothing and Polishing of Glass Lenses and Prisms", internal training document for Watson, (1972).

- 
9. ISO 10110 part 6, Optics and Optical Instruments-Preparation of drawings for optical elements and systems-Part 6: Centring tolerances, (1996).
  10. ISO 10110 part 7, Optics and Optical Instruments-Preparation of drawings for optical elements and systems-Part 7: Surface imperfection tolerances, (1996).
  11. ISO 10110 part 8, Optics and Optical Instruments-Preparation of drawings for optical elements and systems-Part 8: Surface texture, (1996).
  12. Robert H. Ginsberg, "Outline of tolerancing (from the performance specification to toleranced drawings)," *Optical Engineering*, Vol. 20, No. 2, pp 175-180, (1981).
  13. Seymour Rosin, "Merit function as an aid in optical tolerancing", *Applied Optics*, Vol. 15, No. 10, pp 2301-2302, (1976).
  14. Warren J. Smith, "Chapter 23, Tolerance Budgeting" in *Modern Lens Design a Resource Manual*, McGraw Hill, USA, pp 437-438, (1992).
  15. OSLO Optics Software for Layout and Optimisation, "Chapter 9, Tolerancing", Version 6.1, Lambda Research Corporation, USA, pp 228-229, (2001).
  16. Paul R. Yoder, "Chapter 5 Mounting Multiple Lenses", in *Opto-Mechanical Systems Design 2<sup>nd</sup> Edition*, Marcell Decker Inc, USA, pp 235, (1992).
  17. K. H. Carnell, M. J. Kidger, A. J. Overill, R. W. Reader, F. C. Reavell, W. T. Welford and C. G. Wynne, "Some experiments on precision lens centring and mounting", *Optica Acta*, Vol. 21, No. 8, pp 615-629, (1974).
  18. Paul R. Yoder, "Chapter 5 Mounting Multiple Lenses", in *Opto-Mechanical Systems Design 2<sup>nd</sup> Edition*, Marcell Decker Inc, USA, pp 207-270, (1992).

19. Robert E. Hopkins, "Some Thoughts on Lens Mounting", *Optical Engineering*, Vol. 15, No. 5, pp 428-430, (1976).
20. R. E. Fisher and B. Tadic-Galeb, "Chapter 16 Tolerancing and Producibility", in *Optical System Design*, McGraw-Hill, USA, pp 315-356, (2000).
21. International Organisation for Standardisation, *Knoop Hardness Test for Glass and Glass-Ceramics*, ISO 9385:1990.
22. R. R. Shannon, "Chapter 6 Tolerance Analysis, in *The Art and Science of Optical Design*", Cambridge University Press, UK, pp 356-387, (1997).
23. Warren J. Smith, "Chapter 15. Optics in Practice", in *Modern Optical Engineering*, Third Edition, McGraw Hill, USA, pp 569, (2000).
24. R. E. Fisher and B. Tadic-Galeb, "Chapter 16 Tolerancing and Producibility", in *Optical System Design*, McGraw-Hill, USA, pp 315-356, (2000).
25. J. Plummer, W. Lagger, "Cost Effective Design", *Photonics Spectra*, Vol. 16, Part 12, pp 65-68, (1982).
26. Warren J. Smith, "Chapter 15. Optics in Practice, in *Modern Optical Engineering*", Third Edition, McGraw Hill, USA, pp 562, (2000).
27. Ronald R. Wiley, Robert E. Parks, "Chapter 1, Optical Fundamentals", in *Handbook of Optomechanical Engineering*, Edited by Anees Ahmad, CRC Press, USA, pp1-38, (1997).



---

28. Schott Glass Company, Optical Glass Description of Properties, Pocket Catalogue, Version 1.1, Mainz, Germany, pp 29-30, (2000).

29. Mil Std, MIL-O-13830A.

30. Richard N. Youngworth and Bryan D. Stone, "Cost-based tolerancing of optical systems", *Applied Optics*, Vol. 39, No. 25, pp4501-4512, (2000).

31. S. J. Dobson and A. Cox, "Automatic desensitisation of optical systems to manufacturing errors", *Meas. Sci. Technol.*, Vol. 6, pp 1056-1058, (1995).

32. Leo Levi, "Chapter 9, Lenses and Curved Mirrors", in *Applied Optics: A Guide to Optical System Design Volume 1*, John Wiley and Sons Inc, New York, pp 454, (1968).

33. R. Kingslake, "Chapter 6, Basic Geometrical Optics", in *Applied Optics and Optical Engineering Volume 1, Light: its Generation and Modification*, Academic Press, New York and London, pp 215-216, (1965).

34. SIRA Course Literature, *Optical Design: A Practical Introduction*, "Chapter 6, The Design of Specific Systems", pp 44, at Imperial College London, (27-29<sup>th</sup> March 2000).

CHAPTER 4  
OPTICAL ELEMENT PRODUCTION AND TESTING

## Chapter 4. Optical Element Production and Testing

### 4.1 Introduction

Once the lens design has been completed and the tolerance analysis carried out, the information is passed onto the production facility and the optical elements are manufactured. In this chapter traditional and more modern manufacturing techniques will be discussed and contrasted, and a discussion of the various methods of surface form testing that are available in the modern optical workshop will be presented. The advantages and disadvantages of these methods are considered and the characteristics of an ideal system are then assessed. It is noted that the elements considered here have two spherical or aspherical curved surfaces, as opposed to single surface working such as mirrors, although many of the techniques discussed are suitable for both cases.

### 4.2 The Manufacture of Optical Elements

The manufacture of optical components is a multi stage process. It begins with the melting of a batch optical glass to the required quality levels as specified in the lens element tolerances. Next, the block of glass has to be roughed out into an appropriate blank by either moulding or cutting the block. If the glass is to be cut, then it is likely that the correct aperture diameter of the blank will be achieved by trepanning. Glass can also be roughed out by hand (though this is becoming less common), or moulded into a blank. A cylindrical grinder employing an abrasive wheel can also achieve the desired diameter on the blank. In this case, the lens blank is either blocked onto a chuck using pitch, or is held using a vacuum chuck. The chuck is then mounted in the grinder and rotated (much as on a conventional lathe). The grinding wheel, which is also rotating, is then traversed in from the side until the desired blank diameter is reached. A suitable lubricant/coolant and correct cutting speeds, should be selected when grinding and trepanning, if damage to the glass is to be avoided.

The curvatures can then be generated on either side of the lens as specified in the drawing. There are many different methods now available for generating these curved surfaces, from the traditional roughing and polishing stages to more modern single point techniques, and the selection of the most important depends upon the curvature type, glass type, the required accuracy of manufacture, size of the optical component and the cost constraints on the design.

#### 4.2.1 The Production of Curved Optical Surfaces

Traditionally, spherically curved surfaces were manufactured by a roughing and polishing process, managed by a highly trained and experienced technician<sup>1</sup>. After the blank has been produced, it is roughly shaped to remove unwanted material more quickly than would be achieved by polishing. In general, during the roughing stage, the blank is mounted in a rotating chuck and a rotating circular diamond impregnated tool is introduced at an angle to the rotation axis of the blank and a radius is generated on the lens blank. Once the surface has been roughed out, the lens is blocked onto a curved holder using pitch as an adhesive. When producing spherically curved surfaces, it is usual to block multiple lenses around the same holder so that they are polished simultaneously. This has a number of benefits including the obvious cost benefit of reduced batch polishing times and an improvement in the surface quality of the lenses as the polishing is carried out over multiple lenses equating to a larger area. The block then passes to the polishing machines where it is again mounted on a rotating spindle. When polishing convex surfaces, the polishing tool is concave with the same radius as the desired surface being generated, and when polishing concave surfaces the reverse is true. Figure 4.1 shows a section through a block of lenses undergoing the polishing of a convex spherical surface. The tool is mounted to an arm, which precesses over the lenses in harmonic motion, and the tool rotates freely about the crank pin. The holder/blocking tool is also rotated as shown in Figure 4.1. During the polishing process the tool is usually lined with a polishing pitch, which rapidly takes on the

form of both the tool and the lenses. A slurry is introduced between the tool and the lenses being worked that to act as the abrasive. This slurry is made up of water and, generally, iron or cerium oxides. Other compounds may be added to the slurry such as anti caking agents that prevent the abrasive from forming lumps. Between the blocking and polishing stages there is often a grinding or smoothing phase that is similar to the polishing phase. However, the abrasive employed is considerably coarser, meaning the surface is generated more rapidly but the surface finish is much lower quality. During the polishing phase the shape of the lenses may be checked with test plates to ensure that the correct radius is being achieved. This method can be problematic when polishing lenses with a high degree of curvature as, when they are ground together, their radii, while both being spherical, will begin to differ and therefore the radii polished on the lenses will differ depending upon their position on the block. Once the polishing stage is complete, the lenses are removed from the block and are centred. In this process the edge of the lens is ground until the mechanical axis of the lens coincides with the centres of curvature of its two surfaces.

In addition to the traditional form of surface polishing, there are a number of new techniques, many specifically developed to aid the polishing of aspheric surfaces. The first of these to be addressed is a technique referred to as single point diamond turning, SPDT. With the advent of computer numeric control of milling machines, and especially lathes, it became possible to control the positioning of a tool to the accuracy required in optical manufacturing. The tools employed in this technique are single crystal diamonds and the method used is directly analogous to the machining of conventional engineering materials. Initially, however, the technique was only useful for the grinding stage of surface manufacture, as the surface form could be accurately manufactured but the surface finish was not suitable for optical imaging systems<sup>2</sup>. The single point method left tool marks in the lens surface that had an effect on the optical performance. Surfaces generated in this manner had to be polished by another method to remove the tool marks.

Another drawback of the early diamond turning systems was the inability to cut the full range of optical glasses. In fact the only materials that could be machined using SPDT were metals (for the manufacture of mirrors) and more exotic compounds such as silicon, germanium and zinc selenide<sup>3</sup>. The method could also be used on many plastics, which are becoming more popular in many optical applications. In less critical applications, for example in infrared optics where the wavelengths are considerably larger than the optical spectrum, then SPDT was proven to be a useful technique especially in the manufacture of axially symmetric aspheric optics, as no special tools have to be produced.

Modern SPDT is now more capable in terms of surface form accuracy and is even reaching surface roughness levels below  $Ra \leq 2$  nm especially in reflective surface applications<sup>4</sup>. This figure can be compared with the values in Table 4.1, which give an indication of the surface roughness levels that are acceptable for various optical applications<sup>5</sup>.

Application	Typical Surface Roughness (nm)
Eye Glasses	10
Illumination Optics	2
Projector Optics	1
Photo Optics, consumer devices	1
Space Optics	0.5

Table 4.1. Typical Surface Roughness Values for Various Applications

From the table we can see that without further polishing, SPDT surfaces are only suitable for eye glass and illumination applications. Progress is being made towards the goal of being able to finish optical glasses with similar diamond tools with some success<sup>6</sup>. The precise geometry generated on the surface by the diamond turning and CNC techniques is controlled by a number of factors. These include the shape and size of the tool, the hardness of the optical material, tool dwell time around the optical surface and tool wear.

A more modern method of achieving high quality surface finishes on optical components is Magnetorheological Finishing (MRF)<sup>7</sup>. This technique can result in precision polishing of even aspheric surfaces without the requirement for specialist tooling for different surface forms. A magnetorheological fluid is effectively replacing the polishing tool employed in the traditional polishing method. The position, shape and stiffness of this fluid is computer-controlled to control the shape of the optical element. The shape of the fluid is controlled by the application of a magnetic field and altering the flow rate controls the stiffness. The positioning of the jet of fluid on the optical surface is also controlled by the application of magnetic field, so there can be preferential targeting of certain high spots on the surface that consequently require higher removal rates. The technique can polish all types of optical surfaces including aspheric and completely asymmetric surfaces. The MRF method of lens polishing can produce surface form, peak to valley accuracies, of approximately 0.05 of a wave. Modern aspheric lenses can be manufactured by a combination CNC diamond tooled grinding to produce the desired lens form, followed by a polishing phase, using a technique such as MRF, to improve the surface texture to an acceptable level for visible light imaging applications<sup>8</sup>.

#### 4.2.2 The Problems Presented by Aspheric Surfaces

Whilst aspheric surfaces are useful to the optical designer in areas such as the reduction of optical aberrations, they present problems to the optical polisher. There have been attempts to quantify the difficulty of manufacture of different aspheric surfaces based on the rate at which the radius of curvature varies with distance from the optical axis<sup>9</sup>. As discussed above, the traditional method employed to generate a spherical surface is that of random polishing with an oversize tool of a single radius, as the distance from any point on the surface to the optical centre of curvature is the same. This is not the case with aspheric lenses, so alternative methods have to be used in their manufacture.

One method of manufacturing rotationally symmetric aspheric optics is to modify the nearest spherical surface<sup>10</sup>. For lower quality applications the surface form is generated with a cam guided grinding machine similar to that used in the traditional spherical polishing process. The next stage is to polish the surface up to the required surface texture level without altering the surface form too much. One method of achieving this is the use of flexible tooling, which will mould to the contours of the aspheric surface<sup>11</sup>. However, the degree of flexibility must be carefully controlled as the tool must be rigid enough to polish away the high spots on the lens surface. Repeated polishing and surface form measurement stages can produce successively more precise aspheric surfaces until the required accuracy is reached. The lenses are polished with CNC, flexible, sub-aperture tools which are used to reduce the high spots on the lens after each measurement stage. The measurement techniques used must be very high resolution and a number of different methods are discussed in the following section.

#### 4.3 Surface Form Testing with Particular Reference to Aspheric Surfaces

During and after the manufacturing stages, the lens must be measured to ensure it has both the correct surface form and finish (or texture). In the vast majority of cases, the measurement of surface finish is carried out in the same manner regardless of the type or shape of surface that has been manufactured. However, a large variety of techniques can be employed when the surface form of an optical component is to be assessed. These techniques have varying accuracies and complexities as well as applicability to the testing of a range of surfaces. Descriptions of a number of these tests are given below, along with discussions of their most suitable applications and their strengths and weaknesses.

##### 4.3.1 Simple Test Plates

Test plates are among the most common method of assessing optical surface form. A test plate is a glass optic that has been polished to a very exact radius that is the



same as the desired radius on the work piece. A concave test piece is used to examine a convex work piece and vice-versa. The lens is carefully cleaned after polishing and the test piece is placed in contact with the lens surface and illuminated with monochromatic light. The shape of the lens surface is assessed by the formation of interference fringes, known as Newton's Rings, between the light reflected off the lens surface and the test plate surface. More detailed information on the formation of Newton's rings was provided in Chapter 3, Section 3.2.1, along with examples of interference patterns in Figure 3.3. Each fringe relates to a distance of half a wavelength between the two surfaces. If the fringes are counted, the difference between the radii of curvature can be approximated by applying Equation 4.1<sup>11</sup>.

$$\Delta R \approx F\lambda\left(\frac{2R}{d}\right)^2 \quad 4.1$$

Where             $\Delta R$  = the difference in Radii  
                        $F$  = the number of fringes  
                        $\lambda$  = the wavelength  
                        $R$  = the radius of curvature of the test plate  
                        $d$  = the diameter of test area.

Whether the curvature of the work piece is too large or too small can be determined by where it contacts the test plate. If the radius is too large it will contact the test plate at the edges and if it is too small then it will contact the test plate in the centre. For large diameter spherical surfaces, the test may not be carried out over the whole surface. Smaller areas can be tested in the same manner using test plates of a smaller diameter than the work pieces. The lens surface form tolerances on the production drawing will specify whether the whole lens aperture is to be examined, or define the size of the sub aperture section to be tested. Because the reference surface is in contact with the surface being measured both surfaces have to be scrupulously clean if accurate measurements are to be taken, and the surfaces are to remain damage free. Spherically polished test plates can be used to examine rotationally symmetric aspheric surfaces provided that they do not deviate a great

deal from their nearest spherical surface. It must be noted that the test plate method of surface form evaluation is only as accurate as the radius of the test plate, so the accuracy to which it is made must be known. Test plates can also be limiting to the optical designer as they are only applicable to one radius, so the radius in the optimisation stage, instead of being a continuous variable, becomes a variable that can only occupy the discrete points that correspond to the test plates owned by the optical workshop.

### 4.3.2 Contact Techniques

The majority of surface contact profilometers are of the stylus type<sup>12</sup>. Figure 4.2 shows the layout of a generic profilometer of this type. The surface profiler is measured by moving a stylus, generally diamond tipped with a radius around 0.25mm to 1mm in radius, over it and recording how the stylus displaces. In order to have accurate control over the motion of the stylus along the measurement axis, its motion is relative to a reference datum bar. These datum bars typically have a straightness of better than 0.5 $\mu$ m over a length of 120mm or so, while the stylus has a positional accuracy along the measurement axis of 0.25 $\mu$ m. A second translation stage is often added allowing translation in the axis orthogonal to the measurement axis, such that multiple profiles can be taken over the test surface. The profilometers are known as x,y,z profilometers where the x-y are the translation axes and the z-axis corresponds to the measurement height axis. Traditionally the movement of the stylus was measured via an inductive gauging system operating along the same lines as a transformer. However this method had a limited resolution in the z-axis, and so was of limited use in the accurate measurement of optical surfaces. To improve the surface height resolution, a Michelson Interferometer can be included to measure the displacement of the stylus<sup>13</sup>. With the inclusion of the interferometer this particular measurement system has a range to resolution ratio of 600,000:1, resulting in a measurement resolution of 10nm over a surface height variation of 6mm. There are limitations to the technique including its relatively slow measurement times, the possibility of damaging the surface under test and the fact that the only part of the

surface profile that is assessed is that directly below the stylus. A typical  $x,y,z$  profilometer can take 1.5 hours for a 10mm by 10mm scan. It is obvious that if a diamond stylus is moved across an optical surface there is the potential for the surface to be scratched or marked. Allied to this, if the stylus does deform the surface, either plastically or permanently, then the accuracy of the measurement is compromised.

Wang et al.<sup>14</sup> have developed a dual gauge profilometer (DGP) that is of the  $x,\theta,z$  type, meaning that it samples the surface at points defined in cylindrical polar coordinates. The technique is known as dual gauge profilometer as it employs two measurement gauges. Gauge A measures the position of the measurement head relative to a precise granite straight edge, and gauge B measures the surface height of the part. In this case the profile gauge moves along a datum straight edge as before, but instead of employing translation in the  $y$ -axis, to facilitate the sampling of more of the surface the test surface is rotated beneath the profile gauge as it translates. The measurements are spaced such that the surface is sampled in radial strips, as spokes on a wheel. The main advantage of this method is that the time taken to sample a surface is greatly reduced. Using this method, it is possible to assess the surface profile of a 600mm diameter optic, to a surface height accuracy of 4 microns, in 40 minutes. However, this sampling is carried out at a relatively low sampling density of only 1044 data points spread over 36 radial "spokes". On each 300mm radial "spoke", there are only 29 sampled data points, which is not a suitable resolution for rapidly changing aspheric optics.

#### 4.3.3 Interferometric Techniques and other Optical Non-Contact Techniques

The majority of optical surfaces manufactured at present are tested by either interferometry or profilometry or a combination of both. Profilometry samples only the surface along the paths the measurement tool takes, and if a larger test area, or indeed the whole lens surface, is required to be tested, then interferometry is the more useful technique. When the measurement of an entire optical surface is

required to the accuracy of a few nm or less, then interferometry is the only measurement tool available<sup>15</sup>. The simplest type of interferometer involves the use of a test plate in contact with the surface to be measured which produces Newton's rings, as discussed in Section 4.3.1. The equipment used for this is known as a Newton Interferometer. A similar type of interferometer is the Fizeau interferometer, which produces similar results to those from a Newton interferometer but with an air space between the reference surface and the surface under test. A schematic of a simple Fizeau interferometer is presented in Figure 4.3. The Fizeau interferometer can also be used with a laser as the light source and this type of interferometer has been manufactured as commercial measurement tools for optical workshops.<sup>16</sup> Both the Fizeau and Newton interferometers assess the form of a surface by determining the distance between it and a reference surface. These methods work well for most spherical surface applications, especially as large numbers of spherical test plate are held in stock by optical workshops. It is possible to use the nearest 'best-fit', spherical surface in the testing of aspheric surfaces<sup>17</sup>. However, the interferometric measurement of aspheric surfaces, using these methods, can present a number of problems. Chief among these is the number of fringes that are generated when assessing aspheric surfaces. If the nearest spherical reference surface is employed then it is possible that the fringes produced will be so dense that accurate analysis becomes unfeasible because of sampling limitations<sup>18</sup>. The phase unwrapping of dense fringe patterns generated by aspheric surfaces, and deep curvatures, can also present problems in the accurate measurement of optical surface form<sup>19</sup>. The use of aspheric reference surfaces dramatically increases the cost and lead time of the measurement stage and introduces the problem of how to accurately measure the form of the aspheric reference surface.

Malacara and Cornejo<sup>20</sup> have proposed a method for increasing the fringe resolution of a Newton interferometer by the introduction of a travelling microscope, which is used to sample the fringes. By adopting this approach the Newton interferometer can be used to measure aspheric surfaces that deviate from the nearest spherical form by around 10 to 20 wavelengths. Aspheric surfaces that do not deviate too

much from the spherical form may be measured by conventional interferometric techniques, but employing IR radiation, due to its longer focal length, reduces the number of fringes generated<sup>21</sup>. This method can be used to measure the surface form of an asphere to a peak to valley accuracy of around  $\lambda/4$ . In order to obtain more accurate, generalised interferometric measurement of aspheric optical surfaces, more complex techniques have to be introduced, several of which are discussed below.

Sub-aperture interferometry, where the test is carried out over small sections of the surface and then “stitched together” to form a complete map of the surface, is one method by which the number of fringes can be reduced to a measurable level. This approach involves moving either the interferometer or the lens under test (or sometimes both), such that multiple overlapping images of the component are taken. Watt proposed a method that rotates the lens while the interferometer is moved on an x-y translation stage as the measurements are taken<sup>22</sup>. The stage and set up must be highly accurate, and Watt quotes mechanical accuracies of the planes and axes in the order of  $\lambda/10$ . The number of fringes generated in each sub-aperture measurement is minimised as the deviation from the nearest spherical surface over the tested area is limited, and the size of the test area can be altered with the aim of maintaining the number of fringes within a measurable level. An approximate limit on fringe resolution, given by Watt, is when the fringe spacing approaches one wavelength. By utilising the translation stages necessary for stitching interferometry, the technique measures absolute surface form directly, rather than simply knowing the distance between the measured surface and the reference surface<sup>23</sup>. There are inherent sources of error with this method that have to be understood and minimised if the results are to be accurate. It is very important that the measured areas overlap in order to minimise errors that could be introduced, when stitching the data back together, especially if there is tilt or vertical displacement of the surface under test<sup>24</sup>.

Another interferometric method of testing spherical and aspheric optical components is lateral shearing interferometry. Figure 4.4 shows a schematic of a typical laser

lateral shearing interferometer<sup>25</sup>. The laser light is expanded through a spatial filter, which is located at the focus of a collimating lens. The collimated light is then reflected off the front and rear surfaces of a parallel plate. As the plate has a finite thickness there is a lateral shear in the wavefront. The level of shear is a function of the plate thickness and refractive index, and the angle of incidence of the impinging light. The sensitivity of the interferometer can be altered by varying the level of shear introduced, which controls the number of fringes produced in the interferograms. A useful modification to the system depicted in Figure 4.4, is to substitute two flat reflecting surfaces, with a variable airspace in-between, instead of the single reflecting plate, which gives the interferometer a greater measurement range and flexibility<sup>26</sup>. The lateral shear interferometer is susceptible to the same fringe density measurement and summation problems that afflict most types of interferometers when they are measuring steeply curved or aspheric optical surfaces. Other drawbacks of conventional lateral shear interferometers are that the interferograms do not cover the whole pupil of the test lens and the evaluation of the interferograms is laborious and time consuming<sup>27</sup>.

To date, interferometric measurements have been limited largely to situations where the fringes have been nearly "nulled out", such that there are few fringes in the interferogram<sup>28</sup>. However, when testing aspheric surfaces, the production of the aspheric null optics required to achieve this presents many problems, as already discussed. The use of a computer generated hologram (CGH) as a reference wavefront can be a very powerful tool in testing aspheric surfaces, where it is very difficult to reduce the number of fringes by conventional means. The CGH alters the wavefront produced by the aspheric surface under test into a plane or circular wavefront that is then interferometrically compared with a simple reference surface<sup>29</sup>. There are a number of advantages in using CGH to test aspheric surfaces. There is no need to manufacture costly aspheric reference surfaces, and a wide range of aspheric surfaces can be tested with CGH to a high degree of accuracy and provide an absolute description of the surface shape<sup>30</sup>. As the degree of asphericity increases, CGH do not become any more difficult to generate<sup>31</sup> as would be the case

for aspheric reference plates, and a CGH can be integrated into use with conventional interferometers such as Fizeau interferometers thus broadening their usefulness. However, it is not a general solution to the problem of testing aspheric surfaces, as individual CGH have to be produced for each aspheric surface under test, and they can be expensive especially if the batch of lenses being produced is not very large<sup>27</sup>.

There are also a number of optical non-contact surface measurement methods that are based on the optical profiling technique. This is similar in approach to the stylus type profilers discussed in section 4.2.2. Non-contact, optical profilers can be broken down into two different types of probe, the laser range probe and the triangulation probe<sup>32</sup>. The basic laser range probe moves over the test surface on a precision x-y translation stage taking measurements at a predetermined resolution. Alternatively the sensor can be kept still and the surface under test can be moved on the translation stage. At each measurement point the sensor projects a laser spot onto the surface and then auto-focuses until the reflection is in focus on a photodiode sensor. The distance between the sensor and the test surface can then be accurately determined from the amount the sensor has had to refocus. The surface is sampled in a grid pattern and its profile is built up from each of the separate height measurements. This method has the advantage that there is no requirement for an optical reference surface of any kind and is a very simple technique. The effective reference surface in this case is the accuracy of the translation stage, or a granite straight edge, used to control the movement of the measurement head. However, there are a number of drawbacks with this technique. If the surface is large or requires a high resolution scan, then the process can be time consuming. The accuracy of the measurements is limited by the accuracy of the translation stages. There is a limit to the degree of surface curvature that the sensor can measure before the light reflected off the surface is no-longer able to be collected by the sensor. An approximate guide is that if the angle of the curved surface approached  $10^\circ$  then the reflected light will miss the sensor<sup>32</sup>. The laser triangulation probe works in a different manner. The x-y translation stages are again required though this time the

laser source and the sensor are at different locations above the surface. Laser light is aimed at the surface and the location of the reflected beam on a sensor allows the calculation of the distance between the laser and the surface. In its basic form this technique suffers from the same problems as the laser range probe in terms of resolution, stage accuracy and problems with surface curvature. However, there have been improvements in both the laser range probe and triangulation measurement tools that alleviate some of the problems with these techniques and some of these developments are discussed below.

Ehrmann et al<sup>33</sup>, have proposed an optical profilometer which has a sensor mounted on an  $x, y, \theta$  translation stage. The angular position of the sensor,  $\theta$ , is set before each measurement, based on an auto-focus feedback loop such that the sensor is always angled perpendicular to the test surface. The permissible range for focus error in the signal is approximately  $\pm 20\mu\text{m}$ . This means that the profilometer can measure surfaces of any given curvature instead of being limited to relatively shallow curves. The mechanical accuracy of the translation stage is better than  $0.7\mu\text{m}$ , and the combined measurement error is less than  $2.8\mu\text{m}$ . However, this is still a time consuming technique. A single profile scan along a 20mm long path, taking 1000 measurements (resolution of 20 microns) takes approximately 20 minutes. Glenn and Hull-Allen have reduced this scanning time<sup>34</sup> through mounting multiple probes around the extremity of a rotating disc. This disc is then swept over the test surface in overlapping profiles and the data from these profiles is "stitched together", much as in the scanning interferometry, to form a total surface height map.

Tsai et al<sup>35</sup>, have presented an improved version of the triangulation measurement technique. This system incorporates a zoom function for the system sensor enabling a variable resolution. With a zoom function the system can assess a larger curvature over a smaller area. The system can zoom in or out depending on the rate of change of the curvature inherent in the surface under test, thus both speeding up and increasing the resolution of the technique. Two sensors instead of one are also



included which increases the degree of surface curvature that the system can measure. The positioning repeatability of the translation stage in this technique is around 2 microns, and the average error of the surface measurement results was reported to be approximately 42 microns.

#### 4.4 An Ideal Surface Test System for Aspheric Optics

As can be appreciated from the selection presented above there are numerous different methods of assessing the surface form of aspheric optical elements. However, none of the methods discussed represent what might be considered as an ideal test system for the modern optical manufacturing environment. The following discussions will cover some of the attributes that an ideal optical surface test system would possess.

With many modern aspheric optical surfaces now being generated on SPDT machines or similar methods of CNC manufacture it is clearly desirable to have an on-machine, in-process<sup>13</sup> method of surface assessment which would allow corrective inputs into the machine whilst the optical manufacturing process is ongoing, and without having to remove and then re-mount the optic within the production tooling. The system should be non-contact in order to avoid the risk of unnecessary damage to the optical surface. Also, if the method is to be in-process, then a contact method of surface assessment would present problems due to the mechanical frequency response of the stylus assembly and the surface measurement speed<sup>13</sup>. The technique must be tolerant to vibrations. It is desirable that the method would sample the whole of the optical surface under test in order to give the most accurate prediction of its likely optical performance<sup>36</sup>. An ideal test system should include a large degree of flexibility such that it can measure a broad range of different surface profiles with the minimum number of modifications to the method or set up. This precludes the use of separate reference surfaces specific to the surface under test. As already discussed these surfaces are expensive, require long

lead times<sup>18</sup>, and in many cases can be as problematic to manufacture and test as the surface they are designed to test.

#### 4.5 Conclusions

Traditional polishing techniques are no-longer able to produce the deeply aspheric surfaces that are now becoming more common in the optical industries. New manufacturing techniques have been developed including SPDT and MRF, which do not require the rigid form tools of previous methods. These new manufacturing methods would benefit greatly from an in-process on-machine measurement technique that would enable an iterative process of test and form correction without taking the optical component from the polishing machine. In the field of optical testing there a number of different methods that are suitable for measuring the surface form of aspheric optics though many have large cost implications, resolution problems, or are inherently unsuitable for the on-machine applications. The following chapter will present a new optical surface measurement method for aspheric surfaces that is flexible enough to measure many different aspheric forms without modification, or the need for separate reference surfaces, and is suitable for on-machine applications with in the manufacturing environment.

Chapter 4. Figures

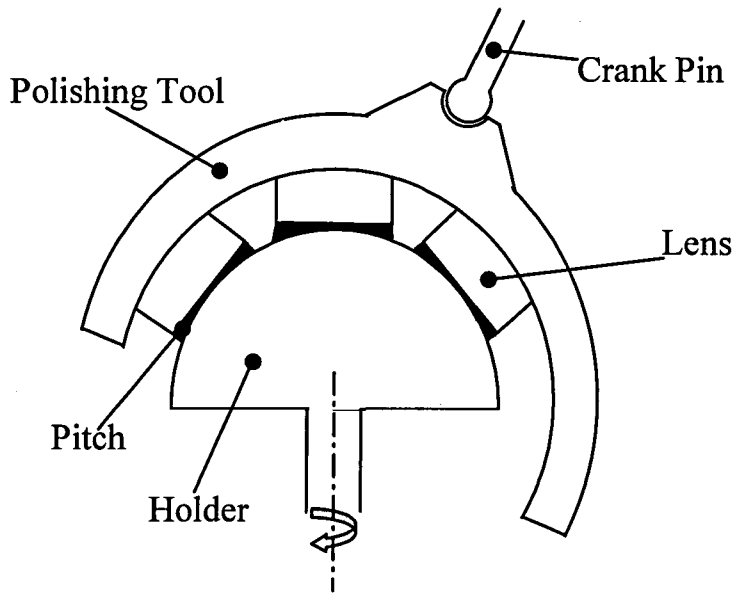


Figure 4.1. Traditional Lens Polishing

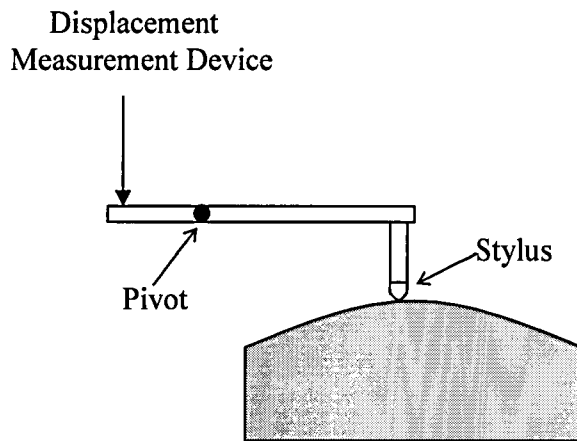


Figure 4.2. Stylus type Contact Profilometer

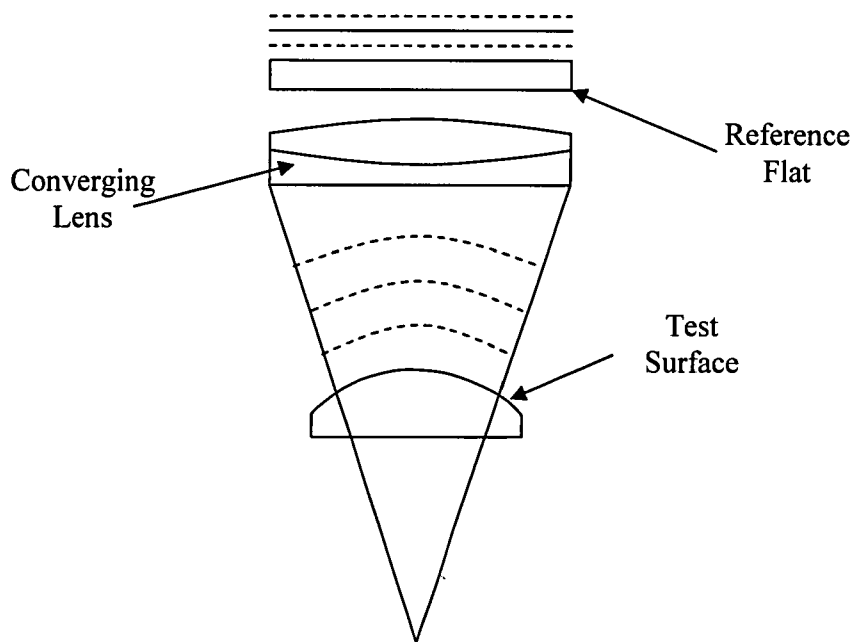


Figure 4.3. Fizeau Interferometer

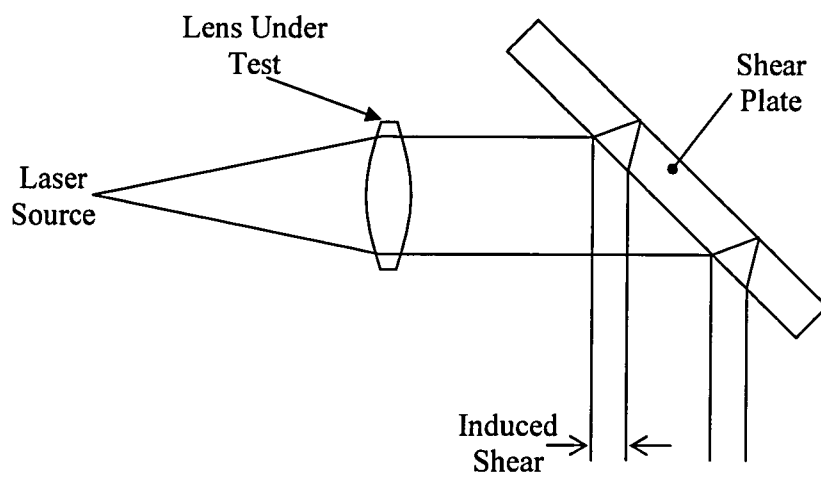


Figure 4.4. Lateral Shear Interferometer

## Chapter 4. References

- 
1. Frank Twyman, "Chapter 3, The Nature of Grinding and Polishing", in *Prism and Lens Making*, Adam Hilger, London UK, pp 49-66, (1988).
  2. Gordon Doughty & James Smith, "Microcomputer-controlled polishing machine for very smooth and deep aspherical surfaces", *Applied Optics*, Vol. 26, No. 12, pp 2421-2426, (1986).
  3. Sergey Solk, Sergey Shevtsov & Alexi Iakovlev, "Designing of optical elements manufactured by diamond turning", *Advanced Optical Manufacturing and Testing Technology, Proceedings of SPIE Vol. 4231*, pp 181-188, (2000)
  4. Han Rongjiu & Gavin F. Chapman, "Results achieved in the generation of complex surfaces using deterministic ultra-precision machining systems and processes", *Advanced Optical Manufacturing and Testing Technology, Proceedings of SPIE Vol. 4231*, pp 175-179, (2000)
  5. K. Becker, B. Dorband, R. Locher & M. Schmidt, "Aspheric Optics at Different Quality Levels and Functional Need", *EUROPTO Conference on Optical Fabrication and Testing, SPIE Vol. 3739*, pp 22-33, (1999).
  6. Zhang Feihu, Li Wei & Qiu Zhongjun, "Application of ELID grinding technique to precision machining of optics", *Advanced Optical Manufacturing and Testing Technology, Proceedings of SPIE Vol. 4231*, pp 218-223, (2000)
  7. Harvey M. Policove, "Next Generation Optics Manufacturing Technologies", *Advanced Optical Manufacturing and Testing Technology, Proceedings of SPIE Vol. 4231*, pp 8-15, (2000)

- 
8. S. Jacobs, J. Ruckman, E. Fess, D. VanGee, C. Cotton, S. Moore, E. Cleveland & D. Golini, "Real world examples demonstrate manufacturing of aspheres" *Convergence*, pp 1-3, January/February (2000).
  9. J. William Foreman Jr., "Simple numerical measure of the manufacturability of aspheric optical surfaces", *Applied Optics*, Vol. 25, No. 6, pp 826-827, (1986).
  10. Feng Zhijing, Wu Hongzhong, Guo Zhengyu, Zhao Yan, "Fabrication of free-form lens with computer-controlled optical surfacing", *Advanced Optical Manufacturing and Testing Technology, Proceedings of SPIE Vol. 4231*, pp 194-201, (2000)
  11. Warren J. Smith, "Chapter 14, Optics in Practice", in *Modern Optical Engineering the Design of Optical systems 2<sup>nd</sup> Edition*, pp 463-514, McGraw-Hill Inc. (1990).
  12. Daniel Malacara, "Chapter 17, Contact and Noncontact Profilors", in *Optical shop Testing 2<sup>nd</sup> Edition*, John Wiley & Sons Inc, USA, pp 687-714, (1992).
  13. David M. G. Stevens, "The application of optical techniques to aspheric surface measurement", *Int. J. Mach. Tools Manufact.*, Vol. 32., No. ½, pp 19-25, (1992).
  14. Wang Quandou, Zhang Zhongyu, Zhang Xuejun and Yu Jingchi, "Novel profilometer with dual digital length gauge for large aspherics measurement", *Advanced Optical Manufacturing and Testing Technology, Proc. SPIE, Vol. 4231*, pp 39-47, (2000).
  15. Franke Shillke, "Critical aspects on testing aspheres in interferometric setups", *EUROPTO Conference on Optical Fabrication and Testing, Berlin, SPIE Vol. 3739*, pp 317-325, (1999).

- 
16. Daniel Malacara, "Chapter 1 Newton, Fizeau and Hadinger Interferometers", in *Optical Shop Testing 2<sup>nd</sup> Edition*, John Wiley & Sons Inc, USA, pp 1-50, (1992)
  17. J. D. Briers, "Best-fit spheres and conics as an aids in the manufacture and testing of diamond-turned aspheric optics", *Optica Acta*, Vol. 32, No. 2, pp 169-178, (1985).
  18. Ho-Jae Lee, Seung-Woo Kim. "Precision profile measurement of aspheric surfaces by improved Ronchi test", *Optical Engineering*, Vol. 38, No. 6, pp 1041-1047, (1999)
  19. K. Creath, Y-Y. Cheng and J.C. Wyant, "Contouring surfaces using two-wavelength phase-shifting interferometry", *Optica Acta*, Vol. 32, No. 12, pp 1455-1464, (1985).
  20. D, Malacara and A, Cornejo, "Testing of Aspheric Surfaces with Newton Fringes", *Applied Optics*, Vol. 9, pp 837, (1970)
  21. Mauro Melozzi, Luca Pezzati, Alessandro Mazzoni, "Testing aspheric surfaces using multiple annular interferograms", *Optical Engineering*, Vol. 32, No. 5, pp 1073-1079, (1993)
  22. Gordon J. Watt, "Aspheric measurement by scanning interferometry", *SPIE Vol. 508, Production aspects of single point machined optics*, pp 46-53, (1984).
  23. Michael Bray, "Stitching Interferometry and Absolute Surface Shape Metrology: Similarities", *Optical Manufacturing and Testing, Proc. Of SPIE*, Vol. 4451, pp375-383, (2001).
  24. Masashi Otsubo, Katsuyuki Okada, Jumpei Tsujiuchi, "Measurement of large plane surface shapes by connecting small-aperture interferograms", *Optical Engineering*, Vol. 33, No. 2, pp 608-613, (1994).

- 
25. Daniel Malacara, "Chapter 4 Lateral Shearing Interferometers", in *Optical Shop Testing 2<sup>nd</sup> Edition*, John Wiley & Sons Inc, USA, pp 123-172, (1992)
26. P. Hariharan, "Simple laser interferometry with variable tilt and shear", *Applied Optics*, Vol. 14, pp 1056-1057, (1975).
27. P. Hariharan, B. F. Oreb and Zhou Wanzhi, "Measurement of aspheric surfaces using a microcomputer-controlled digital radial shear interferometer", *Optica Acta*, Vol. 31, No. 9, pp 989-999, (1984).
28. Paul E. Murphy, Thomas G. Brown, Duncan T, Moore, "Interference imaging for aspheric surface testing", *Applied Optics*, Vol. 39, No. 13, (2000).
29. J. C. Wyant and P. K. O'Neill, *Computer Generated Hologram; Null lens test of aspheric wavefronts*", *Applied Optics*, Vol. 13, No. 12, pp 2762-2765, (1974).
30. Bernd Dorband and Hans J. Tiziani, "Testing aspheric surfaces with computer-generated holograms: analysis of adjustment and shape errors", *Applied Optics*, Vol. 24, No. 16, pp 2604-2611, (1985).
31. Steven Arnold, "CGH null correctors enable testing of aspheric surfaces using standard interferometers", *SPIE oemagazine*, pp 40, (August 2002).
32. K.J. Cross and J. W. McBride, "3-D laser metrology for the assessment of curved surfaces", in *laser metrology and machine performance*, editors D.M.S. Blackshaw, A. D. Hope, G.T. Smith, Southampton, UK, (1993).



- 
33. Klaus Ehrmann, Arthur Ho and Klaus Schindhelm, "A 3-D optical profilometer using a compact disc reading head", *Meas. Sci. Technol.*, Vol. 9, pp 1259-1265, (1998).
34. Paul Glenn and Gregg Hull-Allen, "Self-referencing, motion-insensitive approach for absolute aspheric profiling of large optics to the nanometer level and beyond", *Optical Manufacturing and Testing IV*, Proc. SPIE, Vol. 4451, pp 313-325, (2001).
35. Tung-Hsein Tsai, Kuang-Chao Fan and Jong-I Mou. "A variable-resolution optical profile measurement system", *Meas. Sci. Technol.*, Vol. 13, pp 190-197, (2002).
36. Frank Twyman, "Prism and Lens Making", Chapter 11, *Testing Optical Work*, Adam Hilger, London UK, pp 364-421, (1988).

CHAPTER 5  
SYNTHETIC APERTURE INTERFEROMETRY

## Chapter 5. Synthetic Aperture Interferometry

### 5.1 Introduction

In the previous chapters, methods used in optical design and manufacture have been reviewed. In Chapter 2 it was noted that the aberration correction properties of aspheric optics make them very attractive for the optical designer. Although the benefits of aspheric optics are clear, their manufacturing, and test costs are often prohibitive, particularly for small batch production and large aperture elements. In Chapter 4 it was noted that traditional spherical polishing techniques that produce elements with both accurate spherical form and a high standard of surface finish are not appropriate to the generation of aspheric form. The generation of accurate aspheric form can be achieved using single point diamond turning. However, even the most sophisticated machines cannot achieve the required surface finish with most optical glasses. The generation of high quality aspherics for use in the visible spectrum therefore requires a final polishing step and the quality control during this step that introduces significant costs.

Clearly, it is important that the polishing process removes enough material to provide adequate surface finish without causing deviation from the required aspheric form that has been generated using a different technique such as single point diamond turning. As discussed in Chapter 4, standard Fizeau or Newton interferometers are not usually appropriate to aspheric testing since any significant deviation from a spherical form results in high frequency fringes that cannot be resolved using standard cameras. For this reason the testing of aspheric optics is almost exclusively done by scanning single point measurement techniques along one or more radial tracks usually using a contacting probe. In effect these devices measure deviation from a reference surface (or line) that is defined by the path of the traverse and temperature stabilized, precision mechanics are required.

It is clear that the manufacture of aspheric optics would greatly benefit from a measurement technique that could be implemented on the machine and used to control the polishing process. This chapter describes a scanning interferometer that produces two-dimensional fringe patterns in a manner analogous to a Fizeau interferometer. However, an essential feature of the interferometer is that the optical field reflected from the surface of interest is not recorded simultaneously but is recreated from the coherent superposition of signals obtained from a scanning single point detector. In this way a synthetic aperture is sampled at a rate that can be adjusted to suit the spatial bandwidth of the interference pattern and no null plates are required. For the case of ideally rotationally symmetric aspheric optics, this is particularly advantageous since the surface can be conveniently scanned whilst rotating the optic on the polishing machine.

In the following sections the synthetic aperture interferometer concept is discussed in detail. Scanning source and detector configurations are described and data processing methods are discussed. The method is demonstrated for the measurement of a small aspheric deviation from a flat. The extension of this method to measure optics with large surface gradients is considered.

## 5.2 Background to the Synthetic Aperture Technique

The technique of aperture synthesis has been known and employed for some time, in an application known as Synthetic Aperture Radar (SAR). In this technique high-resolution images of the ground are constructed by illuminating the target area many times whilst moving the radar's send and receive antennas, generally combined into one antenna. Other uses of SAR include the identification of military vehicles from the air, and terrain following radar. The technique effectively *synthesises* a large antenna by knitting together the returns from a smaller array that is moving relative to the target area. The distance between the antenna and the target is logged, known as the range and the azimuth, which is perpendicular to the range is also logged. Repeating this procedure many times, whilst moving the send and receive antennas

between measurements, results in a set of data that can be combined together to form an image of the area being sampled. This technique has been used to produce 3-D maps of the earth's surface from space to a resolution of  $25\text{m}^1$ .

### 5.3 Synthetic Aperture Interferometer Configurations

Initially, let us consider the testing of an axis-symmetric form that is nominally spherical. Traditionally this type of optic would be tested on a Fizeau interferometer as shown in Figure 4.3. A practical measurement would require illumination of the object with a converging wavefront that is nominally concentric with the surface of interest. The resulting interference pattern, imaged from any surface (real or virtual) can then be considered as the interference between the reflected wavefront and an ideal spherical reference wavefront<sup>2</sup>. The interference observed, for example, in a nominally concentric circular arc in the meridional plane, is shown schematically in Figure 5.1. It is clear that, providing the arc is close to the surface, the optical path difference (OPD) is twice the surface deviation. Using a traditional Fizeau interferometer it is also clear that both the illuminating wavefront and the resulting interference pattern are generated simultaneously.

Since coherent detection is implicit in interferometry it is not necessary to measure a time-stationary wavefront simultaneously and because of this, a larger or more detailed interferogram can be synthesised over the aperture covered by a scanning detector. In its simplest form a synthetic aperture interferometer suitable for the measurement of the optic described above would consist of a single (mono-mode) send/receive fibre as shown in Figure 5.2. This configuration is similar to that proposed by Bradley and Jeswiet as a means to measure surface texture<sup>3</sup>. The fibre delivers the light from a HeNe laser and is scanned along a nominally concentric circular arc in the meridional plane. The interference between light reflected from the surface of interest and the fibre termination is detected by a remote photomultiplier as a function of fibre position. Providing the distance between the fibre and the surface is small, it is clear from Figure 5.2, that the OPD is once again

equal to twice the surface deviation. In this case the interference pattern is generated point by point along the circular arc, depicted in Figure 5.2 by a dashed line, but it is identical to that obtained by the Fizeau interferometer.

Although greatly simplified the fundamental advantages of synthetic aperture interferometry are apparent in the example above. First, the path of the scanning fibre can be adapted to suit the optic of interest. The path of the fibre termination can be thought of as the "test plate" since it defines the reference surface. In this way, to test an axially symmetric aspheric surface, the spatial bandwidth of the interference pattern will be minimised if the fibre moves along a path defined to be a small distance from the ideal form. In addition, any form that is ideally, axially symmetric will result in an interference pattern that is also symmetric. Practically, this means that it is only necessary to sample the interference pattern sparsely as the object is rotated about the axis of (nominal) symmetry.

It is noted, however, that in the basic synthetic aperture configuration of Figure 5.2, the surface measurement is made relative to the fibre path. As such the measurement is inherently sensitive to vibration and the accuracy is ultimately determined by the accuracy of the fibre path.

Figure 5.3 shows a more robust and practical type of synthetic aperture interferometer. To avoid unwanted reflection from the fibre termination, the configuration consists of separate source and receive-fibres that are rigidly mounted together to form a probe that travels along a defined path in the meridional plane. The two fibres were clamped into grooves cut into a rigid steel tool. This tool, complete with send and receive fibres attached, is approximated diagrammatically in Figure 5.3. Light reflected from both the front and rear optical surfaces of the element under test is collected at the detector fibre where it is passed to a remote photomultiplier tube. In this case, if the form of either the front or the rear surface is known the form of the other can be deduced. Since a differential measurement is

made the method is less sensitive to the path taken by the probe and is inherently tolerant to vibration. We now analyse this set-up in detail.

#### 5.4 Theory

With reference to Figure 5.3, let the origin of the fibre probe be defined as,  $(x_p, y_p)$ , such that the source and receive fibres are separated by a distance,  $2d$ , and located at positions  $(x_p - d, y_p)$  and  $(x_p + d, y_p)$  respectively. If it is assumed that the intensities of the reflections from the front and rear surfaces are approximately equal then the interference signal can be written as,

$$I(x_p) = I_0 \left( 1 + \cos \left( \frac{2\pi \text{OPD}}{\lambda} + \phi_0 \right) \right) \quad 5.1$$

where  $\lambda$  = the wavelength  
 OPD = the optical path difference at a given probe position  
 $I_0$  and  $\phi_0$  = intensity and phase at the origin, respectively ( $x_p=0$ ).

Let us assume that the exact functional form of the probe path is known and it will be defined as,  $y_p = g(x_p)$ , and that the exact form of one of the surfaces is also known. In effect, the latter provides the reference surface and without loss of generality it will be assumed that it corresponds to the rear surface defined by  $y_r = g(x_r)$ . From this, and the probe intensity data, the exact functional form of the front surface given by  $y_f = h(x_f)$ , can be calculated. The first step is to invert equation 5.1 to find the OPD such that,

$$\text{OPD} = \text{OPD}_0 + \frac{\lambda}{2\pi} \left[ \cos^{-1} \left( \frac{I}{I_0} - 1 \right) - \phi_0 \right] \quad 5.2$$

Where  $\text{OPD}_0$  = the optical path difference at the origin.

Since the absolute phase of the interference pattern is not recorded in our basic configuration the fact that most aspheric optics are relatively small perturbations to a large spherical sag, is recognised and made use of. In this case, the phase of equation 5.1 is usually monotonic and the inverse cosine in equation 5.2 should be interpreted as a phase unwrapping operator<sup>4</sup>.

In general the OPD can be written as the difference of the optical path lengths,  $OPL_f$  and  $OPL_r$ , corresponding to reflections from the front and rear surfaces respectively,

$$OPD = OPL_f - OPL_r \quad 5.3$$

These paths can be expanded to give,

$$OPL_f = \left[ (x_p - x_{f1} - d)^2 + (y_p - y_{f1})^2 \right]^{1/2} + \left[ (x_{f1} - x_p - d)^2 + (y_{f1} - y_p)^2 \right]^{1/2} \quad 5.4$$

and,

$$OPL_r = \left[ (x_p - x_{f2} - d)^2 + (y_p - y_{f2})^2 \right]^{1/2} + n \left[ (x_{f2} - x_r)^2 + (y_{f2} - y_r)^2 \right]^{1/2} \quad 5.5$$

$$+ n \left[ (x_r - x_{f3})^2 + (y_r - y_{f3})^2 \right]^{1/2} + \left[ (x_{f3} - x_p - d)^2 + (y_{f3} - y_p)^2 \right]^{1/2}$$

Where  $n$  = the refractive index

The co-ordinates  $(x_{f1}, y_{f1})$ ,  $(x_{f2}, y_{f2})$ ,  $(x_{f3}, y_{f3})$  and  $(x_r, y_r)$  correspond to the ray intersections at the front and rear surfaces as shown in Figure 5.3. According to Fermat's principle these coordinates are those that minimise the optical path lengths defined by equations 5.4 and 5.5. Therefore, the additional equations can be derived,



$$\frac{\partial \text{OPL}_f}{\partial x_{f1}} = \frac{\partial \text{OPL}_r}{\partial x_{f1}} = \frac{\partial \text{OPL}_r}{\partial x_{f2}} = \frac{\partial \text{OPL}_r}{\partial x_{f3}} = 0 \quad 5.6$$

Although in principle equations, 5.4, 5.5 and 5.6 are sufficient to deduce the required surface form as a function of probe position, we have been unable to formulate a general analytic solution to the problem. However, in practice the desired aspheric form is known and it is relatively straightforward to use this as an initial guess to the true form and then to use numerical methods to iterate onto a consistent solution.

The method employed at present is a two-stage process and proceeds as follows. First the initial estimate of the aspheric surface is used to calculate the ray intersections  $(x_{f1}, y_{f1})$ ,  $(x_{f2}, y_{f2})$ ,  $(x_{f3}, y_{f3})$  and  $(x_r, y_r)$ , and the OPLs from equations 5.4 and 5.5. Figure 5.4. shows the x- coordinates of ray intersections calculated for a plano-spherical optic with a radius of curvature of 30mm and a centre thickness of 10mm and a refractive index of  $n=1.5$ . In this case, the probe consisted of source and receive fibres that were separated by 0.2mm and moved along a straight line defined by  $y_p=1$ mm. The ray intersections were calculated using the Nelder-Mead Simplex method<sup>5</sup>. It can be seen that, for this convex surface, the point of reflection from the front surface increasingly lags behind the probe position as the latter increases. Conversely the ray intersections corresponding to the path of the ray reflected from the rear surfaces lead the probe position. The reverse of these observations would be true if the surface was concave.

Figure 5.5a shows the OPLs corresponding to the front and rear ray paths. It can be seen that the path corresponding to reflection from the front surface increases as a function of probe position while that from the rear surface decreases. Figure 5.5b shows the change in OPD ( $\text{OPD} - \text{OPD}_0$ ), which in this case, is approximately 5mm or 8000 fringes at a wavelength of 632.8nm.

Once the ray intersections have been found, the difference between the ideal OPD and that measured by the interferometer is calculated. We assume that deviation from the surface form causes a relatively large change in the OPD and a relatively small change in the position of the ray intersections. Differentiating equation 5.3 gives the change,  $\Delta OPD$ , as a linear function of changes to the y co-ordinates,  $\Delta y_{f1}$ ,  $\Delta y_{f2}$ , and  $\Delta y_{f3}$ , of the ray intersections at the front surface.

$$\begin{aligned} \Delta OPD = & \Delta y_{f1} \left[ \frac{(y_{f1} - y_p)(x_p - x_{f1} - d)^2 + (y_p - y_{f1})^2}{+(y_{f1} - y_p)(x_{f1} - x_p - d)^2 + (y_{f1} - y_p)^2} \right]^{-1/2} \\ & + \Delta y_{f2} \left[ \frac{-(y_p - y_{f2})(x_p - x_{f2} - d)^2 + (y_p - y_{f2})^2}{+n(y_{f2} - y_r)(x_{f2} - x_r)^2 + (y_{f2} - y_r)^2} \right]^{-1/2} \\ & + \Delta y_{f3} \left[ \frac{-n(y_r - y_{f3})(x_r - x_{f3})^2 + (y_r - y_{f3})^2}{+(y_{f3} - y_p)(x_{f3} - x_p - d)^2 + (y_{f3} - y_p)^2} \right]^{-1/2} \end{aligned} \quad 5.7$$

Since equation 5.7 is linear it is relatively straightforward to invert to find the deviation from ideal form for example using the sparse least squares method of Paige and Saunders<sup>6</sup>. The process can then be repeated until the required accuracy is found. In practice it has been found that it is rarely necessary to perform greater than one iteration unless the deviation from ideal form is very large. To illustrate this we consider the 30mm radius spherical form described above with a fourth power deviation that might be used to correct spherical aberration. In this case the deviation from form is about 0.06mm at the edge of the lens. Figure 5.6 shows the calculated deviation from form in a single iteration. The maximum error here occurs at the extreme of the aperture and here it still remains within 1%. A 1% error over a range of 0.06mm is not a trivial error, relating as it does to an excursion from form of around a wavelength. However, in this example as the error is at the extreme edge of the lens then it is in an area that is likely to be obscured by the fixturing employed to mount and secure the lens.

### 5.5 Implementation and Experiment

In order to assess the feasibility of the technique, a fibre probe was constructed and used to measure optics that were polished on a standard CNC lathe. The general layout of the system was that of Figure 5.3, employing a HeNe source laser. The fibre probe was mounted in the turret of the lathe to traverse the test optic in a closely controlled fashion. During the measurement, the test optic was rotated at a constant speed and the fibre probe traversed the optic from the centre to the edge of the aperture. The receive fibre was connected to a photo-multiplier and the output signal was digitized on a PC equipped with data capture hardware.

Initial measurements were performed on a 25mm diameter optic, manufactured from BK7 and nominally flat. The optic was squarely mounted in the chuck. The alignment in the chuck was checked by illuminating the lens surface with a laser source and then directing the reflected light off a mirror onto a screen located around three metres from the lens. The lens was then adjusted such that when the chuck holding the lens was rotated, the laser spot imaged on the screen remained stationary. The lens was then rotated at 1000rpm (16.66Hz) while the fibre probe translated at a feed rate of 23mm/min. In all 30,000 data points were recorded during the test at a sampling rate of 1000Hz. In essence this means that the optic was sampled along 60 radial 'spokes' and corresponds to a radial distance between samples of 0.023mm.

Figure 5.7 shows the raw interference data transformed into Cartesian coordinates. The parallel fringes show that the optic is not a parallel flat but has a small wedge. For a nominally flat optic it is straightforward to show that each fringe corresponds to a deviation of approximately  $\lambda/2n$  where  $n$  is refractive index and in this case corresponds to a wedge angle of 64  $\mu$ rads. It would have been useful to have produced a corroborative interferometric pattern for the same flat produced on a conventional interferometer. However, as described below the optical element was aspherised after the test measurements were taken.

Figure 5.8 shows the raw data from the same optical flat after it was modified by polishing an annular groove approximately 7mm from the optic's centre using cerium oxide polish powder and a soft polishing tool. The bottom of this groove can clearly be seen on the fringe pattern as the lighter area between the two closely spaced sets of fringes that represent the sloping sides of the groove. The fringes towards the edge of the optic are closer together than those approaching the centre, which indicates that the groove has steeper sides at the edge of the optic and flattens out towards the centre. It can be seen that there is a nominally flat area in the centre of the optic which remained unpolished. The fringes are largely symmetric which means that the groove running around the optic is symmetric. The slight asymmetry in the fringes is due to the wedge of the flat (approximately one fringe in this case) that was observed before polishing.

Finally the fringe data in Figure 5.8 was unwrapped to give the OPD along each spoke. Since the surface form is not monotonic the bottom of the groove had to be inferred from a-priori knowledge and was taken to be the point of minimum fringe frequency approximately 7mm from the centre of the optic. Following the processing described in the previous section, the surface form of the optic was calculated and is shown as a greyscale image in Figure 5.9. The groove can clearly be seen in this image and the smoothness of the data around any circumferential path indicates that the random errors are of the order of a few nanometres.

## 5.6 Discussion of Synthetic Aperture Interferometry and Further Improvements

This chapter has introduced the concept of synthetic aperture interferometry as a means to measure the surface form of aspheric optics. Although more complicated to analyse than single-fibre systems (combined send and receive), a two-fibre (separate send and receive) synthetic aperture interferometer is more straightforward to use in practice. Since the configuration records the interference between light reflected

from the front and rear surfaces it is very robust and sufficiently tolerant to vibration to be used as an in-process measurement technique on standard machine tools.

The preliminary results clearly show the potential of the method to measure a small deviation from flat. However, it is worth considering the problems that occur when applying the method to curves of small radius.

In terms of ray optics, the first point to note is that at each point along the probe path the fibres must be capable of sourcing and collecting the rays corresponding to front and rear reflections. For the case of a single send/receive fibre (or closely aligned pair) this effectively means that the front surface normal must be included within the cone defined by the numerical aperture (NA) of the fibre. For typical fibres, this means that the surface normal must remain within a 15 degree cone.

Alternatively, if the fringe patterns resulting from the superposition of the front and rear reflected fields are considered, it is clear that the entrance pupil (exit pupil) of the fibres should be less than the fringe spacing at all points along the probe path. Since the NA of a monomode fibre is inversely proportional to its entrance (or exit) pupil diameter, this leads to a similar conclusion to that formed from consideration of ray optics. However, if the front and back surfaces of the optic are nearly concentric (or parallel), multimode fibres can be used to increase the NA and the light gathering power of the probe (as discussed below).

Finally, it is worth commenting on the light efficiency of the system. Here traditional interferometers that use cameras to record the whole interference pattern simultaneously have a significant advantage over the synthetic aperture configuration proposed here since the latter collects only a small fraction of the light emerging from the source. From the analysis above it is tempting to use specialist drawn fibres with a reduced entrance (exit) pupil and therefore an increased NA to make the technique applicable to the widest possible range of aspherics. However, it is straightforward to show that the light efficiency of the system falls as the fourth

power of the pupil diameter and so it is better to increase the system NA extrinsically. Since the NA need only be large in the radial direction an anamorphic lens system is most appropriate and this is the subject of further work.

### 5.7 Conclusions

In this chapter a synthetic aperture interferometric method has been introduced which has the potential to provide in-process measurement of the surface shape of aspheric lenses. The method does not require the use of null or test plates and is inherently tolerant of machine vibration. A mathematical basis that defines the technique and that describes how surface profile data can be extracted from the interferograms generated, has been provided. Proof of principle, is provided through the measurement of a small aspheric deviation polished on the front surface of a nominally flat form and random errors of a few nanometers have been observed. The application of the method to more general aspheric optics, and limitations of the present apparatus is discussed. Further work to develop and test the synthetic aperture technique is discussed in chapter 7.

## Chapter 5. Figures

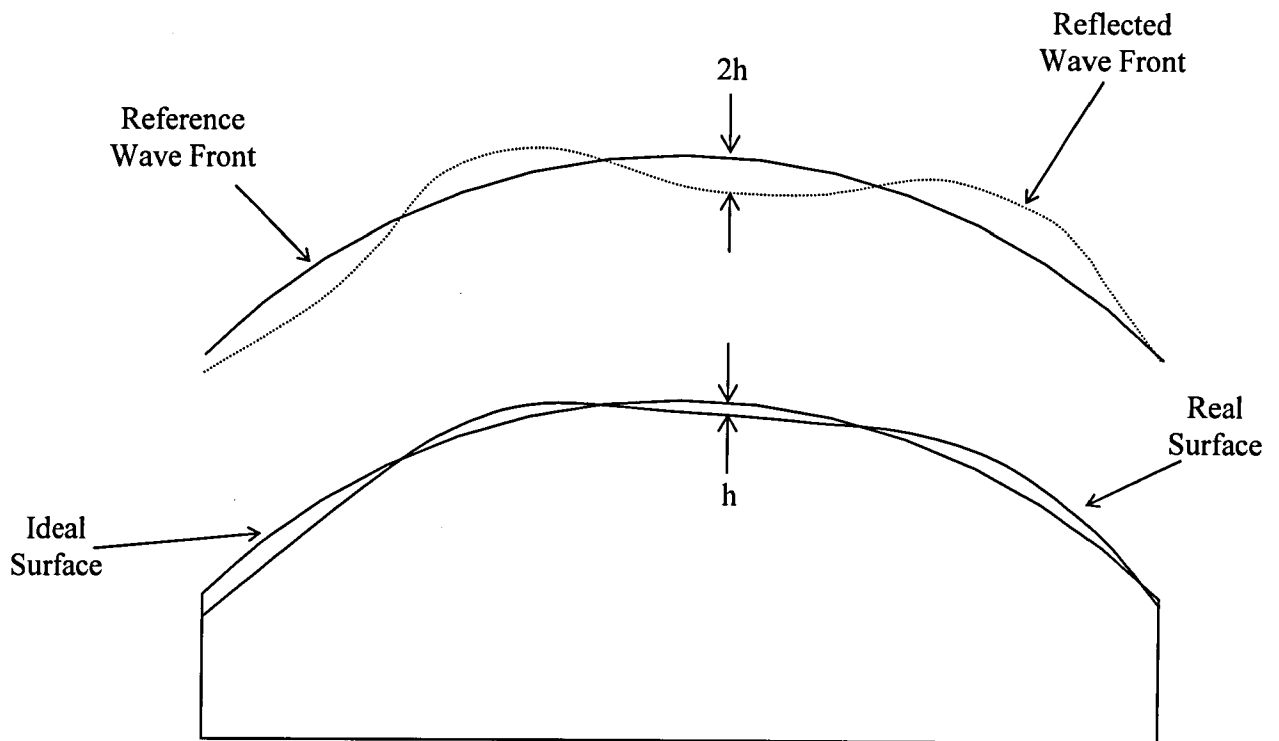


Figure 5.1. Schematic of Interference Pattern

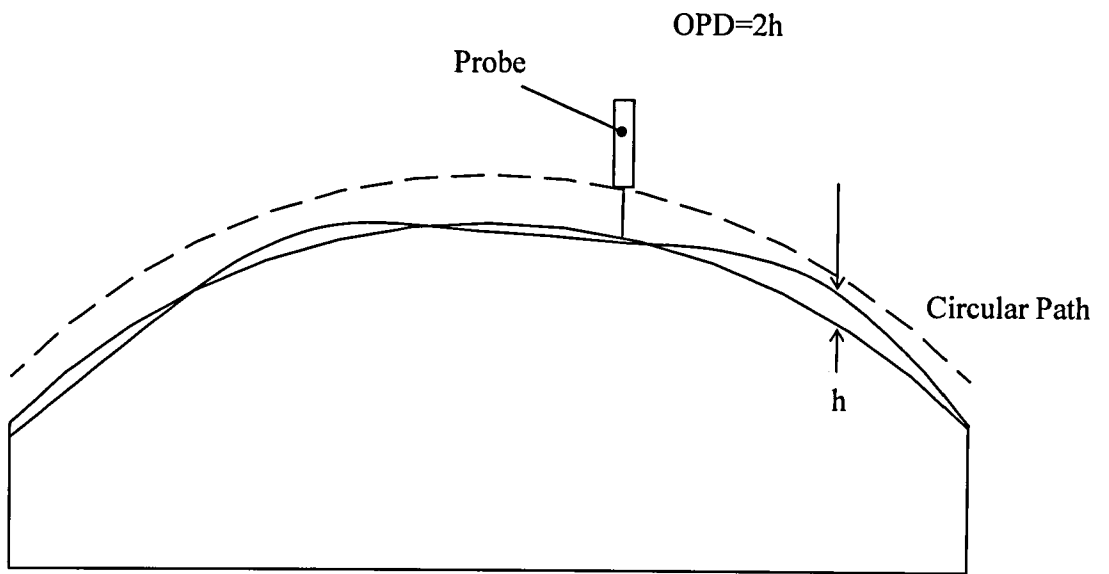


Figure 5.2. Simplest Form of Synthetic Aperture Interferometry



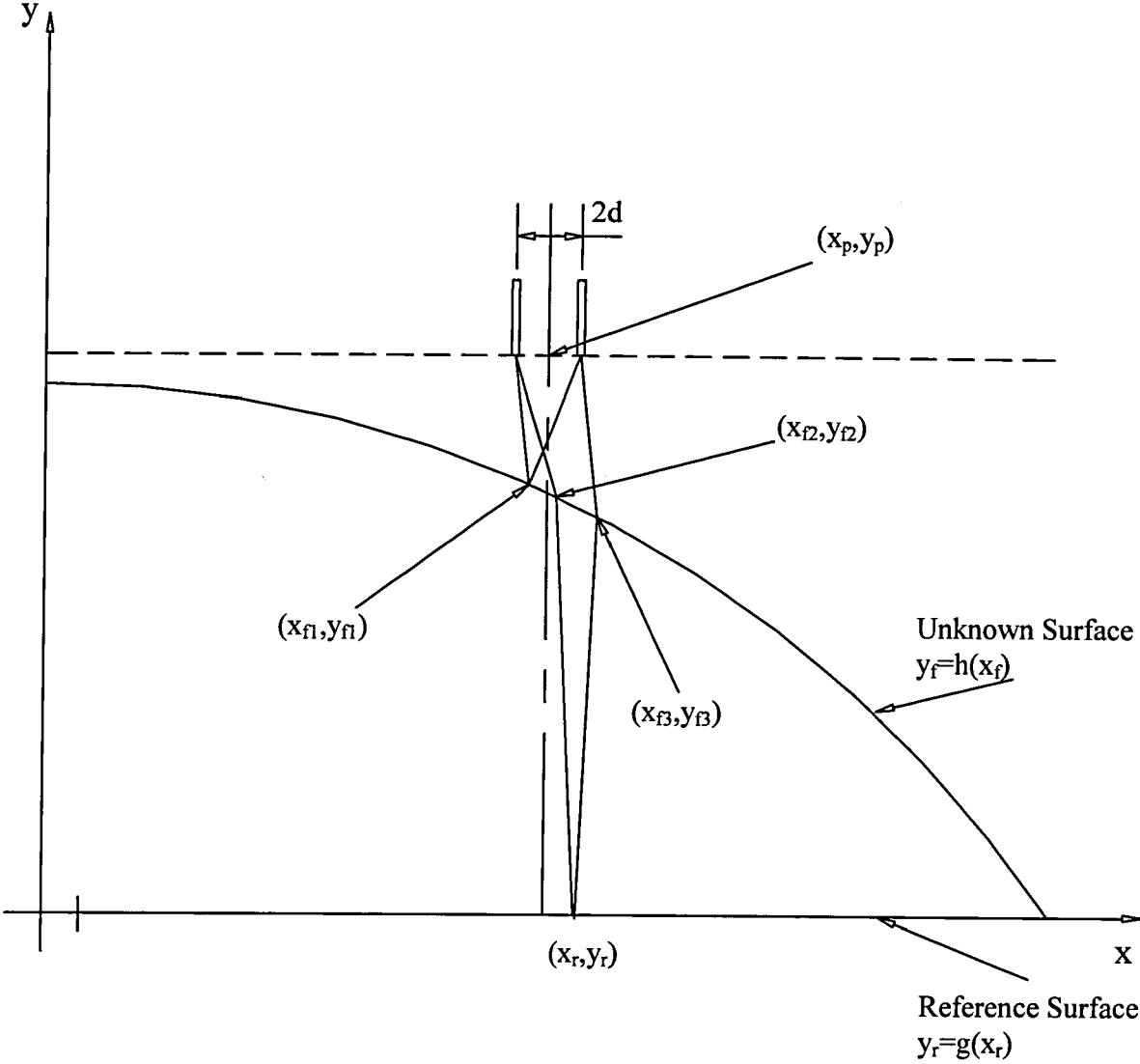


Figure 5.3. Practical Synthetic Aperture Interferometer

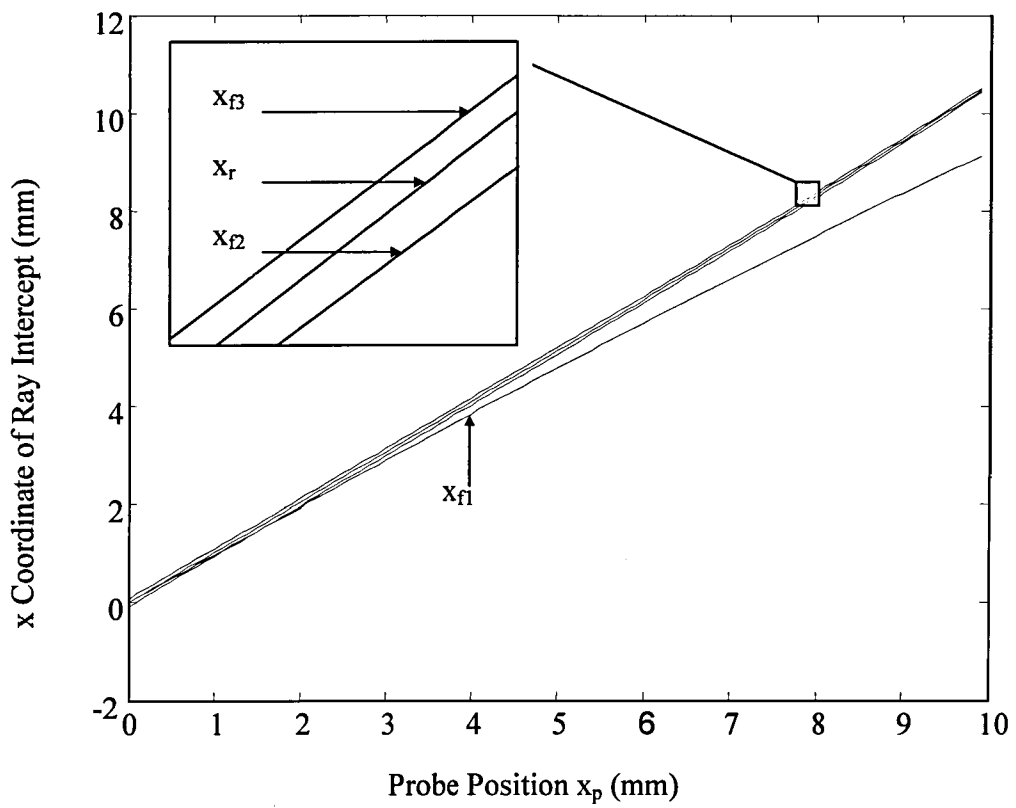


Figure 5.4. x-co-ordinates of Ray Intercept for a Plano-Spherical Optic

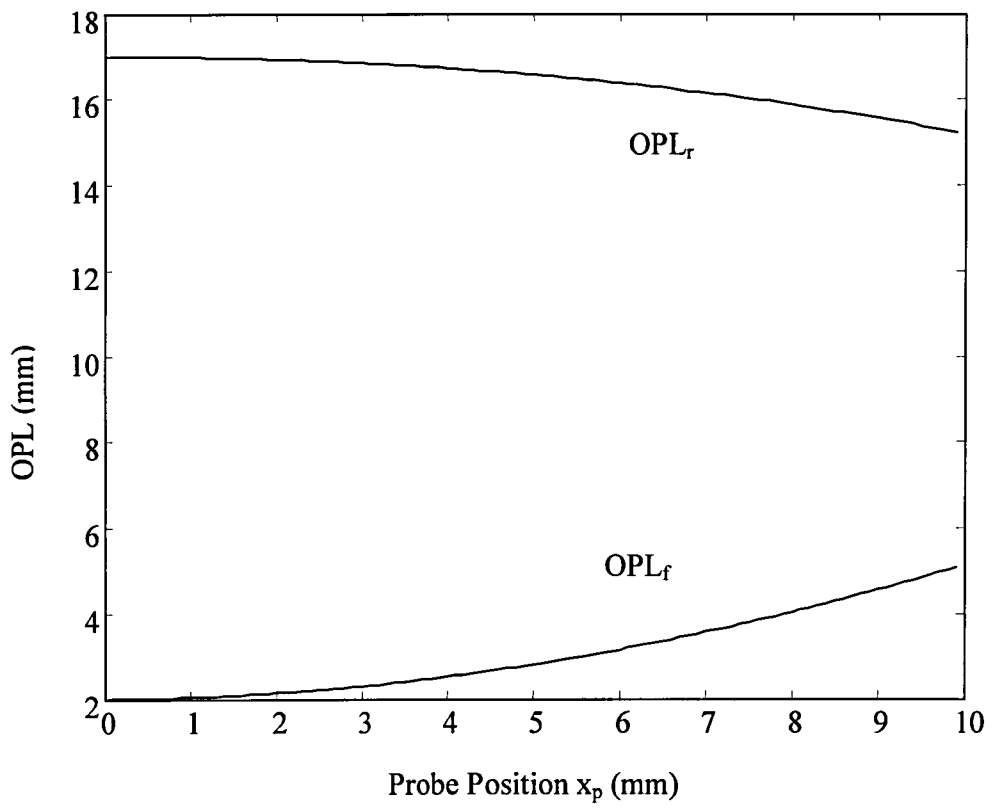


Figure 5.5a. Optical Path Length for Front and Rear Paths

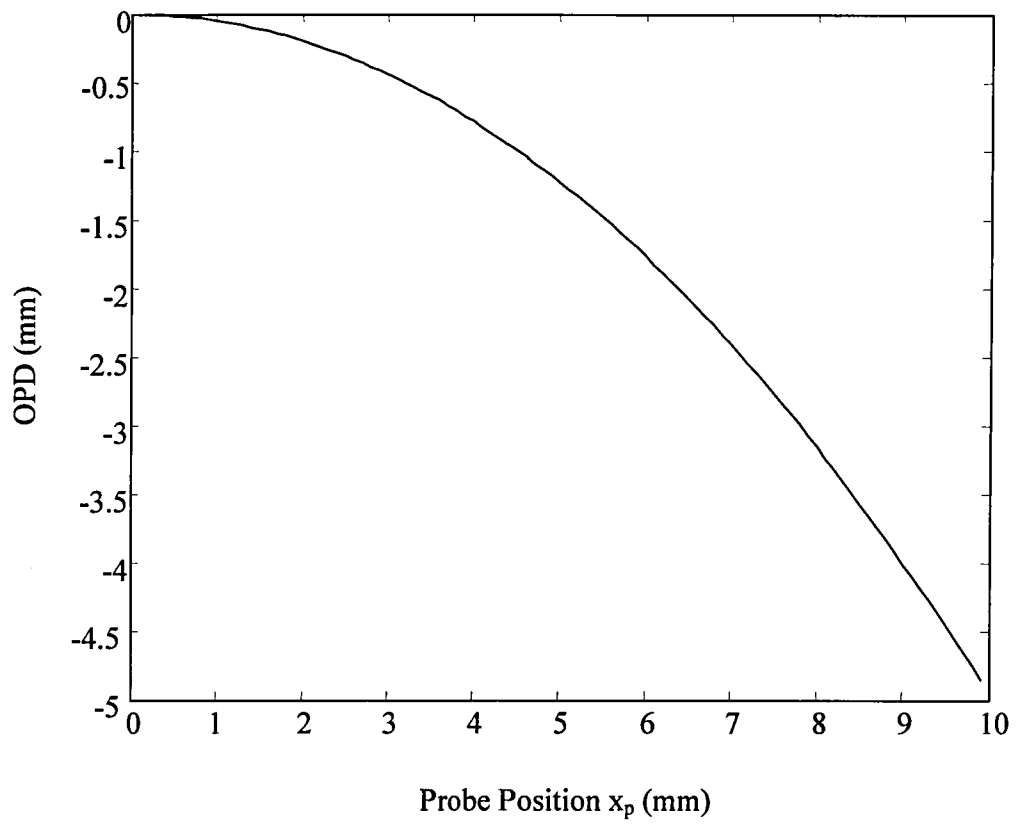


Figure 5.5b. Change in Optical Path Difference

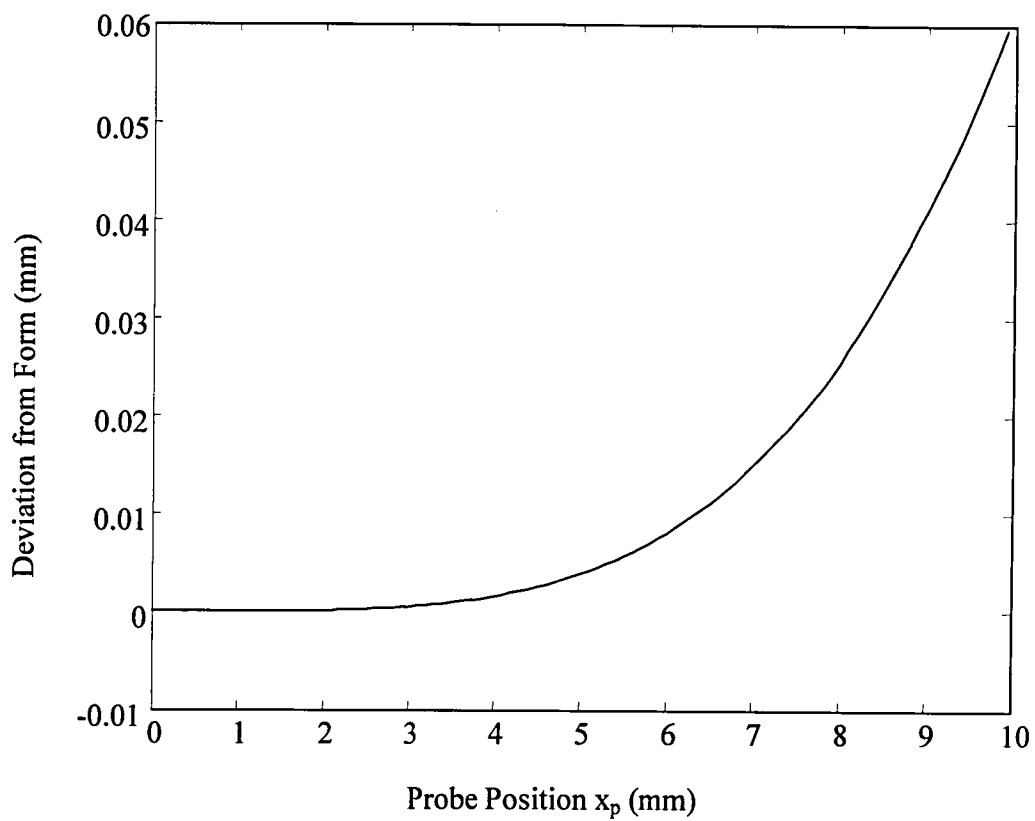


Figure 5.6. Calculated Deviation from Form After One Iteration

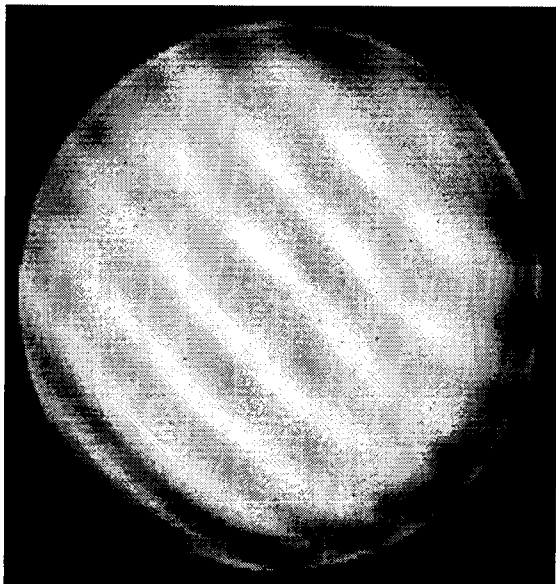


Figure 5.7. Interference Data for an Optical Flat

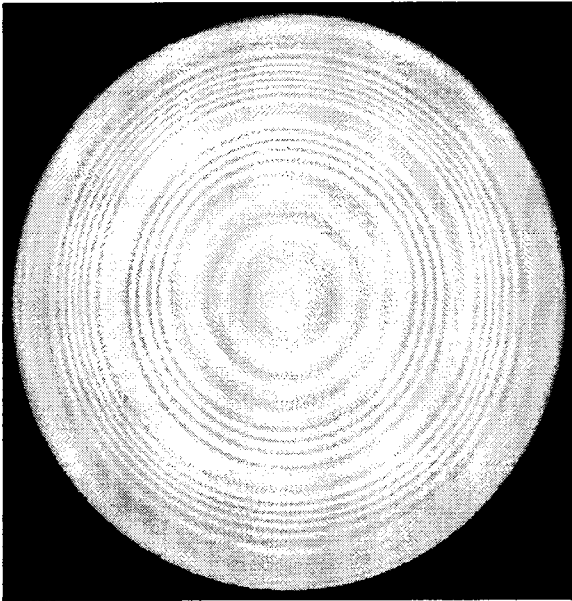


Figure 5.8. Interference Data for a Grooved Lens

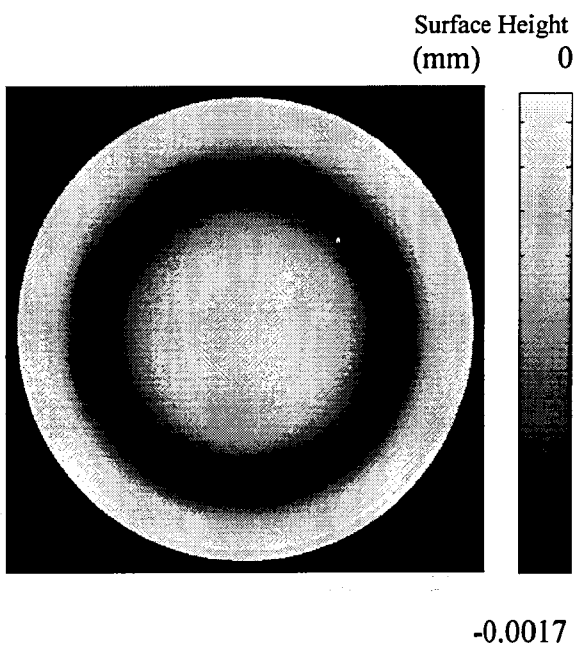


Figure 5.9. Greyscale Image of Lens Surface.

## References

1. J.P. Fitch, Synthetic Aperture Radar (Springer-Verlag, Berlin, 1987).
2. Max Born, Emil Wolf, "Elements of the Theory of Interference and Interferometers," in *Principles of Optics*, (Cambridge University Press, Cambridge, 1997), ,Chap. VII, pp 256-367.
3. C. Bradley, J. Jeswiet, "An Optical Surface Texture Sensor Suitable for Integration into a Coordinate Measuring Machine," *Annals of the CIRP*, Vol.48 No.1, pp.459-462 (1999).
4. D.C. Ghiglia, L.A. Romero,"Robust two-dimensional weighted and unweighted phase unwrapping that uses fast transforms and iterative methods," *Applied Optics* Vol.11, No.1, pp 107-117 (1972).
5. Lagarias, J.C., J. A. Reeds, M. H. Wright, and P. E. Wright, "Convergence Properties of the Nelder-Mead Simplex Method in Low Dimensions," *SIAM Journal of Optimization*, Vol. 9 No.1, pp. 112-147, 1998.
6. Paige, C. C. and M. A. Saunders, "LSQR: An Algorithm for Sparse Linear Equations  
And Sparse Least Squares," *ACM Trans. Math. Soft.*, Vol.8, 1982, pp. 43-71.

CHAPTER 6  
COMPUTER-AIDED LENS ASSEMBLY (CALA)



## Chapter 6. Computer-Aided Lens Assembly (CALA)

### 6.1 Introduction

The alignment of compound lenses was discussed in chapter 3. It can be concluded that currently, most multi-element camera lenses are manufactured on a “right first time” basis. For complex, high performance systems it is usually cost effective to check the form of individual lens elements, but the compound system is usually fully assembled before it is tested as a whole. Since the positional tolerances of lens elements are often very small, the cost of mechanical fixturing, especially in high precision applications, is correspondingly high and can quite easily overwhelm all the other costs. For this reason, tolerancing must be considered at an early stage in the optical design process and “right first time” assembly is rarely achieved in practice for high performance systems.

In many branches of optical engineering, the active alignment of components is now routine. That is, the system performance is measured in some way during the alignment and the position of components is varied to optimise this parameter. For example, single mode optical fibres are manipulated in this way before they are fused<sup>1</sup>. Although some attempts at active alignment have been made [see section 3.3] these methods usually require spacers or other high precision fixturing to be made. In principle, however, it should be possible to produce flexible fixturing to hold and manipulate individual elements during alignment, and once aligned the relative position of the elements can be retained in position by fixing them to a low precision split casings. This concept is illustrated in Figure 6.1. For the case of compound lenses the advantage of this approach would be significantly reduced costs in the production of precision metalwork and less time wasted during the test/modification cycles.

The work by Rafael Navarro and Esther Moreno-Barriuso<sup>2</sup> demonstrated that aberrations in optical systems can be measured by introducing narrow laser beams

into the optical system and recording the position of each at the image plane, effectively making the system a physical realisation of numerical ray tracing. In the system described in this chapter, an array of physical rays in the form of Gaussian laser beams is generated and their path is measured to assess the performance of the system being aligned. In a similar manner to ray tracing packages used for design optimisation, a computational or geometric ray trace is then used to find the positional errors most likely to account for the path of the physical rays, and the system is improved by making iterative adjustments. We refer to this method as computer aided lens alignment (CALA) and will now discuss it in detail.

## 6.2 The CALA Method

The aim of the CALA method is to actively align the elements in a compound lens system to achieve performance goals. The alignment process begins by loading the lens elements into a jig that allows position and orientation of each element, (in terms of decentration, tilt and axial position) to be adjusted independently. Adjustments are then made according to the results of a physical ray trace and once satisfactory performance has been achieved, the elements are cemented into shells to form compound assemblies or lens groups as required.

With reference to Figure 6.2, it is clear that each element requires five variables to define its position  $(x,y,z)$  and orientation  $(\theta_x, \theta_y)$  in three-dimensional space. Let us define  $x_{n,j}$ , as the  $j$ 'th degree of freedom of the  $n$ 'th element such that for a compound lens consisting of  $N$  rotationally symmetric elements,  $n = 1$  to  $N$ ,  $j = 1$  to  $5$ , such that there are  $5N$  degrees of freedom.

Let the performance of the lens system be measured by the propagation path of  $M$  rays through the system as shown in Figure 6.3. In general, a ray can be completely defined by the co-ordinates of its intersection in two planes, that is by 4 variables. In a similar manner to the degrees of freedom, we represent the ray set in suffix notation by  $r_{m,k}$ , where  $m = 1$  to  $M$  and  $k = 1$  to  $4$ . Following propagation through

the system we measure the intersection of the return rays in two planes A and B as shown in Figure 6.3. If  $A_{m,i}$  represents the  $i$ 'th co-ordinate ( $i = 1$  to 2) of the  $m$ 'th ray in plane A

$$A_{m,i} = f(x_{n,j}, r_{m,k}) \quad 6.1$$

$$B_{m,i} = g(x_{n,j}, r_{m,k}) \quad 6.2$$

In general then, given knowledge of the system variables such as the materials and profiles of the individual optical elements, it is possible to calculate the ray intersects that correspond to a given ray set and positional variables using computational ray tracing techniques. The problem, here, is to invert the process to find the positional variables of the lens elements, given a set of ray intersects. Since  $f$  and  $g$  are non-linear functions, this is best done using an iterative process. To this end we define an error function  $E$ , such that,

$$E = \sum_{m=1 \text{ to } M} \sum_{i=1 \text{ to } 2} (A_{m,i} - A'_{m,i})^2 + \sum_{m=1 \text{ to } M} \sum_{i=1 \text{ to } 2} (B_{m,i} - B'_{m,i})^2 \quad 6.3$$

where

$$A'_{m,i} = f(x'_{n,j}, r_{m,k}) \quad 6.4$$

$$B'_{m,i} = g(x'_{n,j}, r_{m,k}) \quad 6.5$$

and  $x_{n,j}$  and  $x'_{n,j}$  are denoted the ideal (design) position variables and an estimate of the real position variables respectively. The design values would usually be used as starting estimates of the real position variables and, for the case discussed in the experiment section, progressive estimates were obtained using the Nelder-Mead

Simplex method of optimisation<sup>3</sup>. Following iteration, the values of  $x'_{n,j}$  that minimise the error are used to calculate the required positional change given by

$$\Delta x_{n,j} = x_{n,j} - x'_{n,j} \quad 6.6$$

The process can then be repeated until the positional errors are within the allowed tolerances. The speed at which the process converges depends on the complexity of the system the number of rays traced and the precision to which they are measured.

In order for the optimisation routine to identify the positional errors within the system it is clear that there must be more independent measurements of the system performance than there are degrees of freedom. If, as above,  $M$  ray intercepts are measured in both A and B planes there are at most,  $4M$  independent measurements of system performance. It is clear therefore that a rotationally symmetric system with  $N$  elements and  $5N$  degrees of freedom requires an integer number of rays to be traced such that,

$$M > 5N/4 \quad 6.7$$

The central feature of the CALA approach is the physical ray trace that is used to measure system performance. Although other methods could be employed, such as interferometric testing<sup>4</sup> or Shack-Hartmann wave-front sensing<sup>5</sup>, the method was chosen due to its simplicity. There are, however, limitations to the technique. In a geometrical (or computational) ray trace there is no restriction to the number of rays that can be traced. However, a physical ray is a pencil beam of finite cross section that, due to diffraction, must diverge as it propagates. In addition, it is clear that the power of each surface will also affect the beams divergence and higher order aberrations will affect the distribution of intensity as the ray passes through the system.

In this investigation it is assumed that the path taken by the centre of intensity of a physical ray closely approximates that of a geometric ray. A further assumption was that to ensure this the physical rays must not overlap each other within the lens system under test. This second assumption might not be necessary in practice and it clearly restricts the number of physical rays that can be traced simultaneously. However, it means that the physical rays sample independent regions of each surface and for this reason the generation of the physical rays were based on this criterion.

Figure 6.4 shows a single physical ray passing through a unit magnification, imaging lens system. The ray has been chosen since it crosses the optical axis at the design conjugates and would therefore be expected to be relatively free of aberration. The ray is generated such that it has a Gaussian profile with a beam waist at the first (and second) principle plane of the lens system. With the beam waist in this position it is straightforward to show that the lens system has no effect on the beam divergence and the beam radius at the measurement plane, A, is due exclusively to free space propagation from the second principle plane, PP2. According to the laws governing the propagation of Gaussian beams<sup>6</sup>, at a wavelength  $\lambda$ , the beam radius,  $r_z$ , at a distance  $Z$ , from the waist of radius  $r_0$ , is given by

$$r_z = r_0 \left[ 1 + \left( \frac{\lambda Z}{\pi r_0^2} \right)^2 \right]^{1/2} \quad 6.8$$

If we assume that the beams are readily identifiable providing their spacing is at least four times their radius in the measurement planes, the minimum beam spacing,  $S_{\min} = 4r_z$  and is plotted as a function of beam waist at a wavelength  $\lambda = 500\text{nm}$  for a number of path lengths ( $Z = 10, 20, 50$  and  $100\text{mm}$ ) in figure 6.5. It can be seen that if the propagation length is of the order of  $50\text{mm}$  the minimum separation of the beams is approximately  $0.6\text{mm}$ . For a typical camera lens with a clear aperture of  $15\text{mm}$  this means that around 600 rays can be traced.

### 6.3 The Design of the Test Set-up

The mechanical jig used to hold each of the elements is shown in Figure 6.6. Three screw driven rods hold the element inside two concentric aluminium alloy rings each of which tilts and translates on ground steel rods in phosphor bronze bushes. The translations (decentrations) are driven directly from the ends of the ground steel bars by Mitutoyo 148-201 micrometer heads opposed by springs. These micrometers have a stated accuracy of  $\pm 5$  microns. The tilting mechanisms employ spring-opposed levers, mounted on the ends of the bars, driven by similar micrometers. The length of the lever arm combined with the accuracy of the micrometers gives a positional tilt resolution of  $0.02^\circ$ . In the decentration plane the lenses have a range of movement of  $\pm 3.25\text{mm}$ , in the airspace parameter  $\pm 7.5\text{mm}$ , in the axial direction, and in tilt a range of  $\pm 12.2^\circ$  that provides adequate movement to correct even poorly aligned optical systems with ease. Each pair of rings is held on a u-section carrier that is fixed with a clamp to one of the six ground steel rods that run the length of the jig. A schematic of the rig with three carriers loaded on it can be seen in Figure 6.7. Individual carriers are fixed to different rods, and each of these rods is driven independently, by spring opposed Mitutoyo 149-132 micrometer heads, which provide the axial (airspace) adjustment for each of the lens elements. These micrometers have a positional accuracy of  $\pm 10$  microns. Each of these rods is stabilized by a combination of phosphor bronze bushes and linear bearings to ensure smoothness and accuracy of movement. These bushes and bearings are fixed into two end plates, see Figure 6.7. The endplates are then clamped to a lathe bed to ensure that they do not move and are fixed parallel to each other and that there is no height change between them. This means that the rods, supporting the carriers, are parallel to the lathe bed ensuring that when the airspace is altered, there is no need to readjust the decentration of the lenses.

## 6.4 Experimental Method

Physical ray tracing was accomplished using the configuration shown in Figure 6.8. Since the performance at a single field point is the only critical parameter, in this case, a fan of rays that diverge from this point to sample the lens aperture, is propagated through the system. Accordingly, a 1mW He-Ne laser is expanded through a 100x microscope objective and a 5 $\mu$ m spatial filter and the resulting diverging wave-front then passes through a conditioning mask. Physically, the mask is a computer generated photographic transparency that provides a 7x7 matrix of (Gaussian) apodized apertures. It is convenient (and also increases the sensitivity) to use a plane mirror to reflect the rays back through the system. A cube beam-splitter is used to separate the outward and return rays and the latter are incident on a CCD array. Figure 6.9 shows a typical image of the rays recorded by the CCD. In this case the ray intercept points were measured in a single plane defined by the CCD.

Initially, the location of each ray on the CCD array is estimated by finding the local maximum of each Gaussian beam. An area of interest that surrounds the peak is then identified and a more accurate estimate of the ray intercept is found by calculating the centre of intensity  $(\bar{X}, \bar{Y})$  given by,

$$\bar{X} = \frac{\sum I_i X_i}{\sum I_i} \quad \bar{Y} = \frac{\sum I_i Y_i}{\sum I_i} \quad 6.9$$

where  $I_i$  and  $(X_i, Y_i)$  are the intensity and coordinates of the  $i$ 'th pixel respectively and the summation is performed over the identified area of interest. Using this routine it was found that the ray intersects could be found with a repeatability of approximately 2 $\mu$ m across the whole area of the array.

Once the physical ray intercept positions are found, an iterative routine involving a geometrical ray trace is employed to solve the minimise function presented in equation 6.3, to find the corresponding positional errors in the alignment of each

element. To allow flexibility, both the geometrical ray tracing and optimisation routine was written in MATLAB. In this routine, rays are defined in a matrix from a start point (the pin-hole) and at each intersection with a surface by a position and a direction. Each curved surface is defined by its curvature and the position of the centre of curvature in a global co-ordinate system. Flat surfaces are entered as planes with their positions and orientations also defined with respect to the global co-ordinate system. In addition the two surfaces that make up the individual lens elements are linked together and move accordingly when the lens is tilted or decentered. Within the routine each lens element is tilted about the middle point of its on-axis centre thickness. The lenses are fixed into the carriers such that the mid point of their centre thickness is inline with the tilt axis of the carrier. It is worth noting that the order in which the various displacements and tilts are implemented is important. With reference to Figure 6.2 the convention adopted is that displacements are made before tilt about the x and y-axes respectively.

The geometric ray trace used 49 rays that pass through both the spatial filter (pin-hole) and each of the apertures in the mask. The ray trace includes the beam-splitter as this also affects the ray paths and introduces significant spherical aberration. Initially the lens elements were assumed to be located at their ideal locations and the corresponding ideal ray intercepts were calculated in the plane of the CCD. The error function defined by equation 6.3 was then calculated and estimates of the actual positions of each of the elements were found by using the `fminsearch` function in MATLAB (Nelder-Mead Simplex method). The elements were then moved by amounts corresponding to their estimated displacements and the process repeated until the lens system performance is within the production tolerances.

### 6.5 Results

The proof of principle evaluations of the CALA method were completed by actively aligning a displaced air spaced doublet designed as a high power laser objective. The



lens was purchased from Linos Photonics (catalogue number LP 033486), has a clear aperture of 22mm, and an effective focal length of 120mm.

Preliminary investigations concerned the correction of small decentrations of one of the elements from the ideal configuration. Initially the microscope objective, pinhole, beamsplitter and mask were removed from the system (Figure 6.8) as were the lens elements, and the mirror and CCD array were aligned along the optical axis such that the mirror plane was perpendicular to the optical axis and the laser (coincident with the optical axis) intercepted the centre of the CCD array. Next the lenses were loaded into the carriers, the microscope objective was placed in the system and the tilt, decentration and airspace of the elements were adjusted such that a single, diffraction limited beam was observed to propagate back through the system. This was taken to be the ideal configuration for the doublet lens. Once this was determined the pinhole, mask and beam-splitter were re-introduced to the system. One of the lenses was then decentered a known amount and the CALA method was employed to correct for the known assembly flaw.

The first error introduced was a +100 micron decentration in the z-direction of the rear element. In the first iteration, the optimisation routine attributed the error to a combination of front element decentration in the negative y-direction and the rear element in the positive y-direction. In this way, the program attempted to correct for the decentration by splitting the error between the elements and in effect aligned the lens along an optical axis that was approximately 60 $\mu$ m higher, yet parallel to the original axis. The corrections were implemented and the performance was reassessed as before. The program now suggested that lenses were 42 $\mu$ m from the optical axis and the iteration was run once again. When the final image was analysed the front element was predicted to be 3 microns too low and the rear element was 6 microns too high. This is within the resolution of the micrometer driven mechanical positioning rig. Using the OSLO<sup>7</sup> lens design package the residual misalignment was found to be within the tolerances allowed for diffraction-limited performance. This experiment was repeated several times with similar outcome.

The CALA method was also tested in a more complex situation. In this case the rear element was decentred by 150  $\mu\text{m}$  in the positive  $y$ -direction and by 70  $\mu\text{m}$  in the negative  $x$ -direction. The front element was decentred by 100  $\mu\text{m}$  in the negative  $y$ -direction and tilted by  $0.2^\circ$  about the  $x$ -axis. In accordance with the procedure outlined earlier the decentrations were considered first. The optimisation routine correctly identified a number of decentration errors particularly in the  $y$ -direction. The progress of the optimisation can be seen in Table 6.1.

Alignment Stages	Value of Error Function
After Misalignment	147.36
After Optimisation 1	4.02e-8
After Optimisation 2	1.53e-8
After Optimisation 3	9.38e-9

Table 6.1. The Optimisation of the Complex Multi-Error Case

The three iterative stages resulted in the system being returned to diffraction-limited performance. Figure 6.10 graphically depicts the ray incident points on the CCD array as the iterative optimisation routine progressed to a point where the optical performance reached an acceptable level. The crosses depict the ideal ray termination positions and the dots represent the actual ray terminations as measured through the alignment procedure. The resultant positional errors based upon analysis of the final ray positions, show a maximum decentration in any direction of  $2\mu\text{m}$  and a maximum tilt error of  $0.0005^\circ$ . When modelled in OSLO, these errors yield diffraction-limited performance and therefore the lens assembly is considered to be within build tolerance.

## 6.6 Discussion and Conclusions

A computer aided lens assembly method has been proposed and developed that allows concurrent test and adjustment of the position of each of the elements until satisfactory performance is reached. Results have been obtained that show that the optical system can be aligned to a high degree of accuracy within 3 iterations even when optimising a number of different positional errors. It is interesting that the process of physical and geometric ray tracing does not find the correct alignment immediately but seems to divide the error between the various elements in its initial assessment. It appears that the error surface is slowly varying and that noise and other measurement errors cause the optimisation routine to stop in local minima. When the elements are repositioned, however, small inaccuracies of the mechanical positioning system appear to introduce sufficient perturbation to move the system out of these minima and allow it to proceed rapidly along the path to correct alignment. In this way the iterative alignment method can be viewed as a closed loop control system and relieves the need for a high accuracy mechanical positioning system.

Once the optical system has been correctly aligned it is proposed that a split casing is cemented in place by applying UV curing or two-part epoxy adhesives to the edge of the lens elements to form a complete compound assembly or lens group. In this way, it is clear that the casing does not have to be manufactured to exacting tolerances and is expected to be considerably cheaper to produce than conventional lock-ring assemblies. However, this phase of the assembly process has not been tested and further work is required to assess the best adhesives and fixturing for commercial lens systems.

Chapter 6. Figures

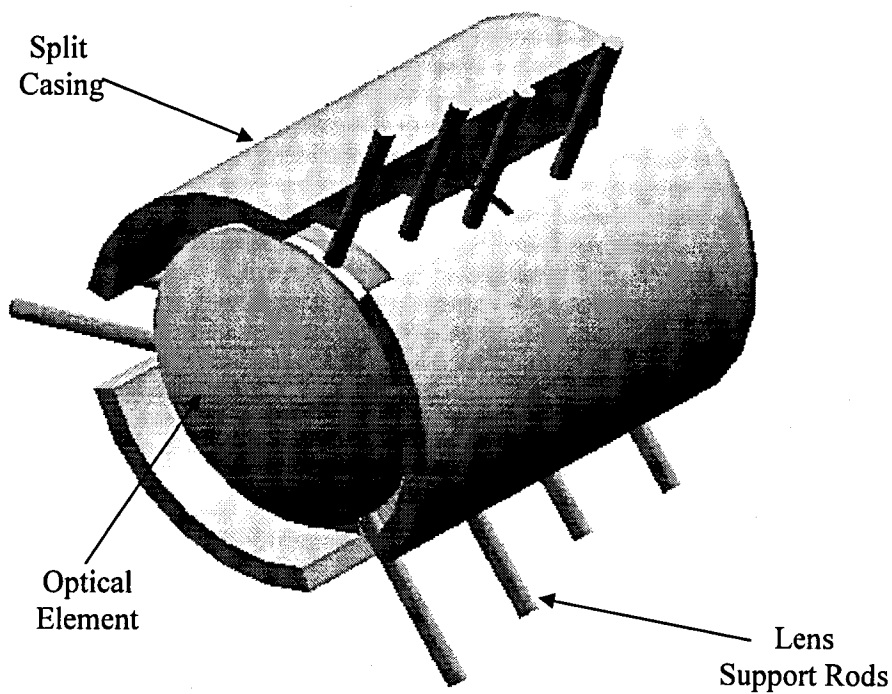


Figure 6.1. Schematic of Optical Layout

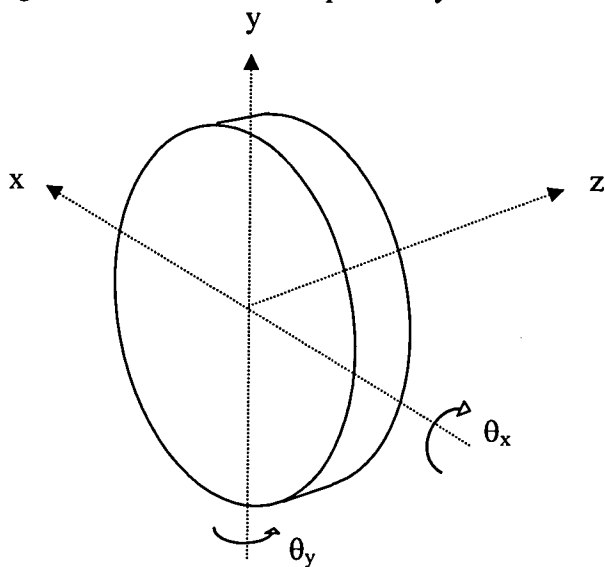


Figure 6.2. Degrees of Freedom

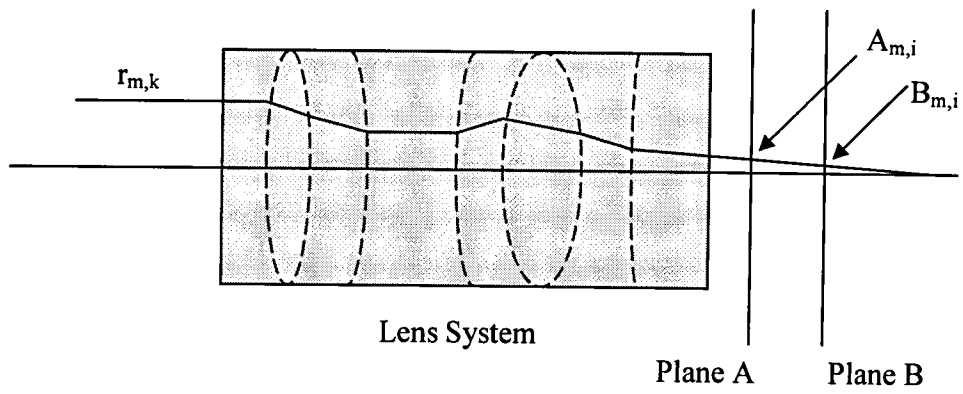


Figure 6.3. Geometric Ray Trace

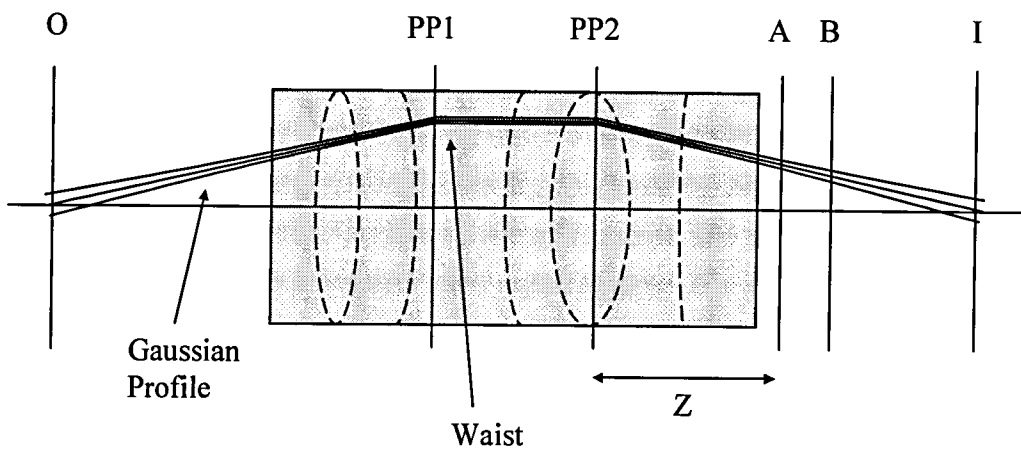


Figure 6.4. Analysis of Physical Ray Trace

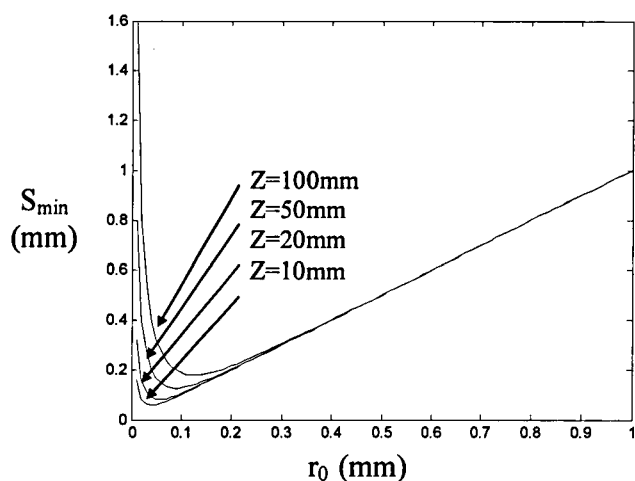


Figure 6.5. Minimum Ray Spacing as a Function of Beam Waist.

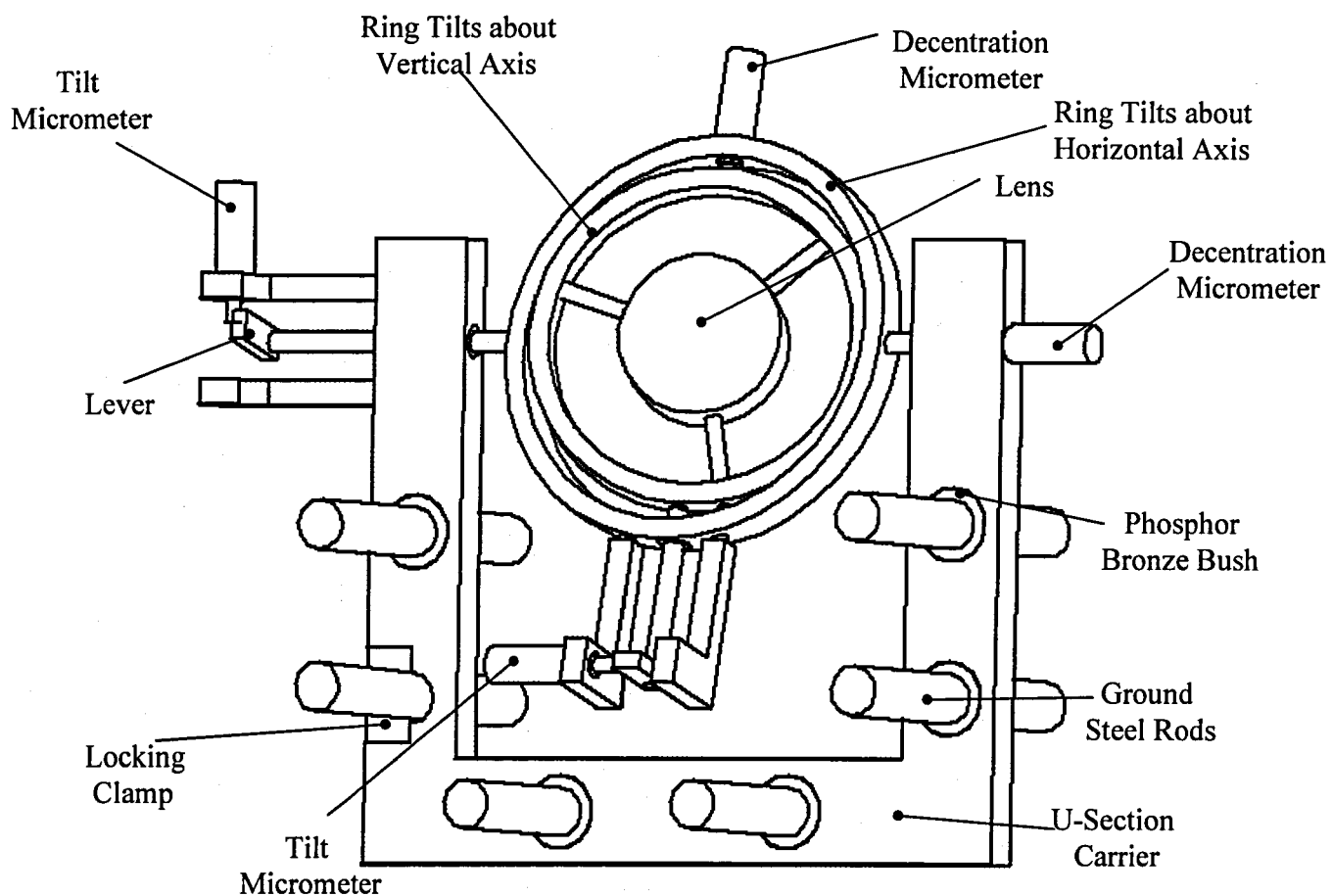


Figure 6.6. Individual Carrier and Lens Assembly

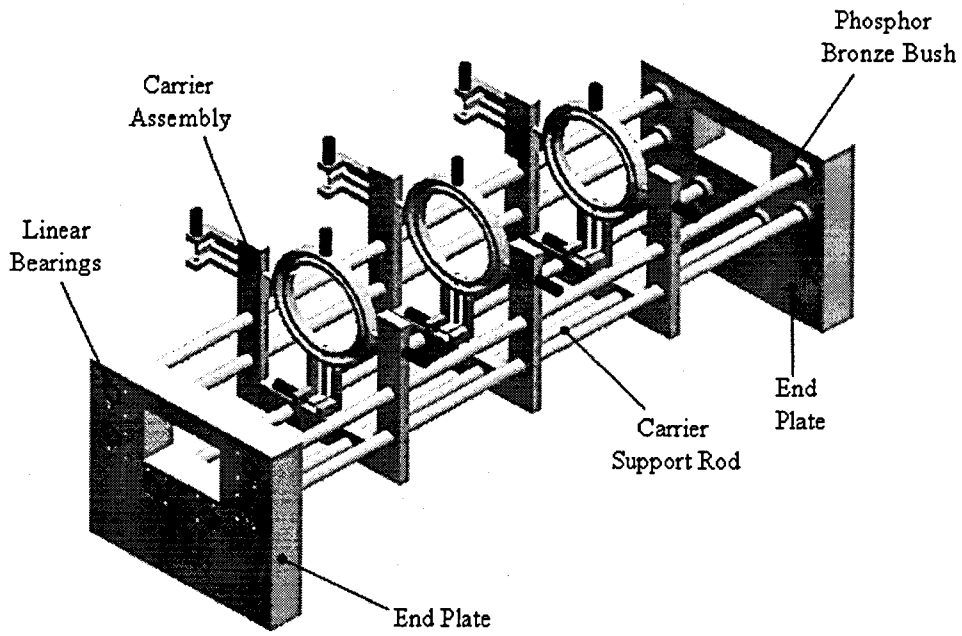


Figure 6.7. Rig Assembly

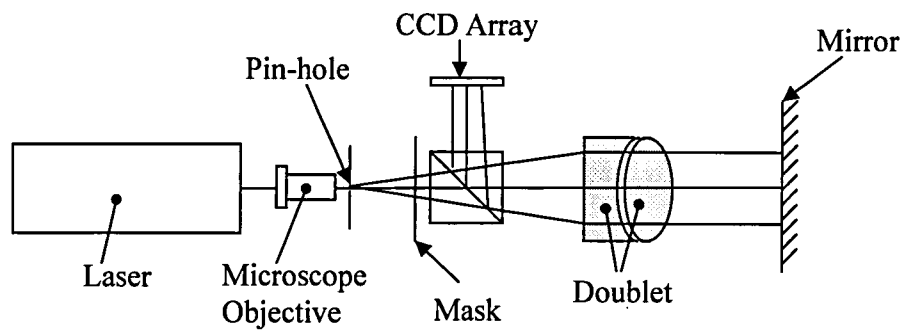


Figure 6.8 Experimental Configuration

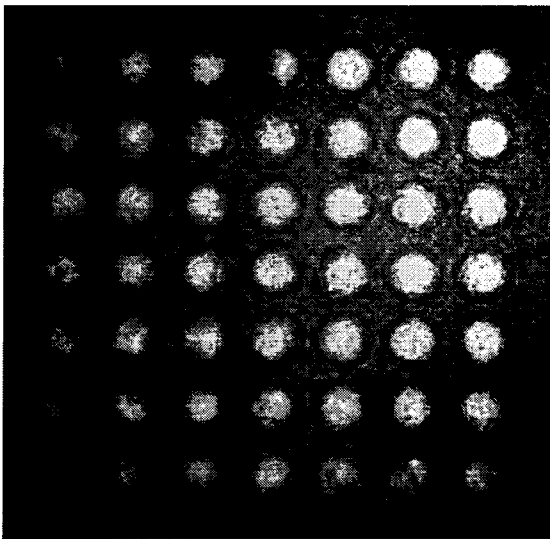


Figure 6.9. Typical CCD Image

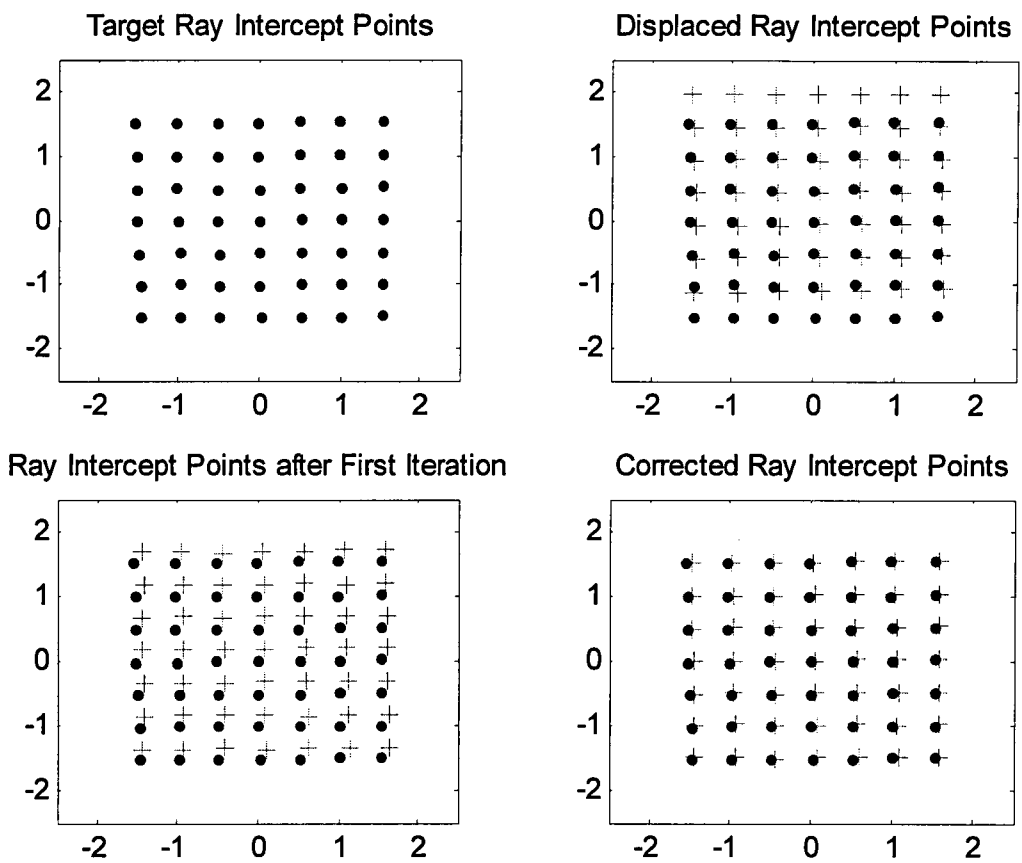


Figure 6.10. The Iterative Correction of the Multiple Error Example



## References

- 
1. D.T. Pham, M. Castellani, "Intelligent control of fibre optic components assembly", Proc. Instn. Mech. Engrs, Vol. 215, Part B9, pp 1177-1189, (2001)
  2. Rafael Navarro, and Esther Moreno-Barriuso, "Laser ray-tracing method for optical testing", Optics Letters, Vol.24, No. 1, pp 951-953, (1999).
  3. Lagarias, J.C., J. A. Reeds, M. H. Wright, and P. E. Wright, "Convergence Properties of the Nelder-Mead Simplex Method in Low Dimensions," SIAM Journal of Optimization, Vol. 9 No.1, pp. 112-147, (1998).
  4. Alberto Jaramillo-Nunez, David M. Gale, Alejandro Cornejo-Rodriguez, "Apparatus for cementing doublet lenses", Opt. Eng., Vol. 35, No. 12, pp 3432-3436, (1996).
  5. L. Seifert, J. Liesener, H.J. Tiziani, "The adaptive Shack-Hartmann sensor", Optics Communications, Vol. 216, No. 4-6, pp 313-319, (2003).
  6. Frank L. Pedrotti, Leno S. Pedrotti, "Characteristics of Laser Beams", in *Introduction to Optics 2<sup>nd</sup> Edition*, (Prentice-Hall International Inc, Upper Saddle River, New Jersey, 1996), pp 456-483.
  7. OSLO Premium Edition Revision 6.1, Lambda Research Corporation, Littleton, Massachusetts, USA, 2001.

CHAPTER 7  
CONCLUSIONS AND FURTHER WORK

## Chapter 7. Conclusions and Further Work

### 7.1 Summary

This thesis has described all aspects of the optical system production process, from the development of a specification through to the assembly of the finished article. Each stage has been discussed in detail with reference to traditional and modern practices and how these can be further improved upon. Throughout the work there has been an aim to reach a closer control of each stage of production.

At the design stage there is the desire to include the tolerances and associated cost within the optimisation stage in order to make them concurrent rather than consecutive, resulting in design towards an economic as well as high optical performance. A description of the manufacture of individual optical elements has been presented combined with how these elements are quality tested. Again the benefits of combining these two stages, such that surface form measurements can be taken while the lens is being manufactured and then any errors in the surface form can be corrected, have been highlighted. The desirability of aspheric surfaces has been detailed along with the challenges that these surfaces pose in terms of manufacture and especially test. A new type of interferometer has been developed that is applicable to on-machine and in-process optical testing without the requirement for separate purpose made reference surfaces of any kind.

The problem of optical assembly was then addressed. The current method employed for assembling multi-element optical systems involves building the complete system or at least significant sub-assemblies before testing its performance. If the system does not reach the required levels of performance then it must be disassembled and rebuilt until the performance criteria is reached. Progress has been made, during the course of this research, towards the development of a closed loop system to aid the alignment of optical systems at the assembly stage, which allows the alignment and

positioning of each of the elements within the system before they are fixed within the mechanical components that provide the body of the unit.

## 7.2 Conclusions

It can be concluded from the discussions on lens design that the optimisation of optical systems is presently carried out solely on the optical performance of the system. The application of tolerance analysis and costing are only carried out once the optical design has been completed. If the system is too costly or difficult to manufacture then it must be re-designed, and there are obvious expense and time implications in doing this. The use of aspheric surfaces within optical designs can yield a multitude of benefits in such areas as aberration control and reduction of system complexity though at present the use of aspheric lenses is considered too expensive for the majority of applications.

The investigations into optical tolerancing have provided an insight into the multitude of parameters that have to be considered. Attention has been drawn to the fact that the tolerances can have a large impact on the assembly as well as the manufacturing tolerance. Badly judged tolerances could have an inordinately large effect on the cost of an optical system especially if they cause a sharp rise in the rejection rate. In order to generate a comprehensive cost function, the base line information must be very specific to the manufacturing and assembly techniques that a given company employs and it would be best practice to develop this base line data from production data at the company. The design example presented showed that it is possible to include some cost parameters within the optimisation routines but only for simple and specific cases. A general error function that would take into account an accurate measure of lens cost as well as performance would have to be extremely complex and, as optimisation times rise approximately with the square of the number of variables involved, would require an unfeasible amount of both computing power and run time. After this rudimentary investigation, it was decided that in the near future the cost of lenses is more likely to decrease through

improvement of the manufacture and assembly processes. In terms of lens polishing it is clear that traditional grinding and polishing techniques are unable to generate the deeply aspheric surfaces that are becoming more common in lens designs. New surface generation techniques have been developed including single point diamond turning and MRF, which do not require the rigid tools of traditional methods and are more able to produce aspheric surfaces. These new techniques would benefit greatly from an on-machine surface measurement system that would enable an iterative process of test and correction until the desired surface form is reached. A specification of an ideal test system was drawn up listing such criteria as in-process measurement and flexibility without the need for costly reference surfaces (either real or computer generated).

A new type of interferometer has been developed and it has been termed Synthetic Aperture Interferometry<sup>1</sup> as it shares some principles with the established technique of Synthetic Aperture Radar. This technique is capable of producing full aperture interference patterns analogous to those produced by a Fizeau interferometer. The method is capable of measuring surface form of even aspheric lenses without the requirement for separate reference surfaces. The system is inherently resistant to vibration and is simple and robust making it eminently suitable for on machine applications.

From the literature, together with two years experience working in a lens assembly environment, it was concluded that there is also scope to improve the optical assembly process. A new assembly rig and method has been developed that employs computer-aided alignment, CALA<sup>2</sup>, of the optical system during the alignment system. This method ensures that when the elements are fixed into their respective mechanical housing they are aligned to within the tolerance required and the lens performs up to the designer's expectations.

### 7.3 Further Work

There are two main areas of thesis where there is scope for further work. The Synthetic Aperture Interferometry technique requires development until it is ready for integration into the production environment. Further investigation and subsequent trials are needed in the final stage of the CALA process where the lenses are cemented to their metal work.

In terms of the lens surface measurement, an area that needs to be looked at is increasing the variety of curvatures that can be assessed. There is a need to demonstrate the method on a highly curved surface. Testing such a surface would require the numerical aperture of the fibre probe to be increased. Noting that the NA need be increased in the radial direction only, this can be achieved by introducing an anamorphic, lens into the system in front of the fibre probes. A schematic of the optical layout of a wide-angle of acceptance probe can be seen in Figure 7.1. This should increase the acceptance angle of the fibres such that steep curves can be examined. The design of the tool needs to be re-examined and adapted such that it is suitable for integration into the current CNC optical processing machines. A process would have to be introduced to clean the lens on the machine before the measurement is taken, and a method of ensuring the measurement probe is kept clean in the polishing environment. This will ease the introduction of the technique into the production environment. The control software needed to integrate with the polishing machines must be developed and also a front end user interface for the software to enable others to use the system. There is also scope to improve the method by which the results are processed. At the current stage of development an iterative search method is used to determine the shape of the test surface. It may be better to strive for a closed form solution to the problem of inverting the path length and surface form equations, or to employ a finite-difference type approach. Further investigation is also required into the deviation from surface form error highlighted at the end of Section 5.4. The iterative search method of determining deviation from form needs to be repeated to determine whether the 1% error at the extreme of the

aperture can be reduced by employing more iterations. In addition, the method requires testing for a variety of aspheric and spherical surfaces to gain a greater level of confidence in its accuracy and if necessary refine the method.

The final stage of the CALA method also requires further investigation. Some improvements could be made to the mechanical design of the rig such as including a method by which the individual elements can be rotated about their optical axes such that the system take account of lenses that are non-rotationally symmetric. However, this would require significant changes to the optimisation software to take into account non-rotationally symmetric items and may have to include some form of trial and error optimisation routine. The structure of the rig needs to be altered to create a more solid base for the technique. This could be achieved by grouping the bushes in each yoke in a much more tightly packed arrangement thus lowering the likelihood of a twisting moment on the yoke which in turn causes uneven motion. The springs, which oppose the movement in the system, need to be stronger which will act to improve the independence of each axis of motion. The types of cement used to fix the lenses to the lens body need to be researched possibly using two-part UV curing epoxy cements, which are already widely used in the optical production environment. The cement must be carefully chosen. It must be viscous enough to stay in the casing as it is manipulated into position. At present it is envisaged that the metal work cemented around the lenses effectively be a split version of the stepped-cylindrical barrels currently used to house optical elements. The barrel would be turned as a single cylindrical unit and then split using a saw or milling machine. A method for securing the casing in place while the glue cures without disturbing the position of the lenses must be developed. This topic requires further research to see whether this technique is the most cost-effective and the accuracies to which the metal work needs to be machined. The ultimate aim is to automate the alignment procedure to a stage where the lens progresses from a misaligned to an aligned system with no operator input. This would require replacing the manual micrometers with a system that can be computer driven. This could incorporate servos, inchworm drives or electric motors to provide the motion needed to align the

lenses. An end condition would also have to be incorporated within the software to ensure that the system does not continue with infinitesimally small adjustments yielding tiny performance increases.

With the implementation of these techniques it should be possible to decrease the production costs of compound lens systems, or conversely produce higher specification systems at a similar cost to the original system.



## Chapter 7. Figures

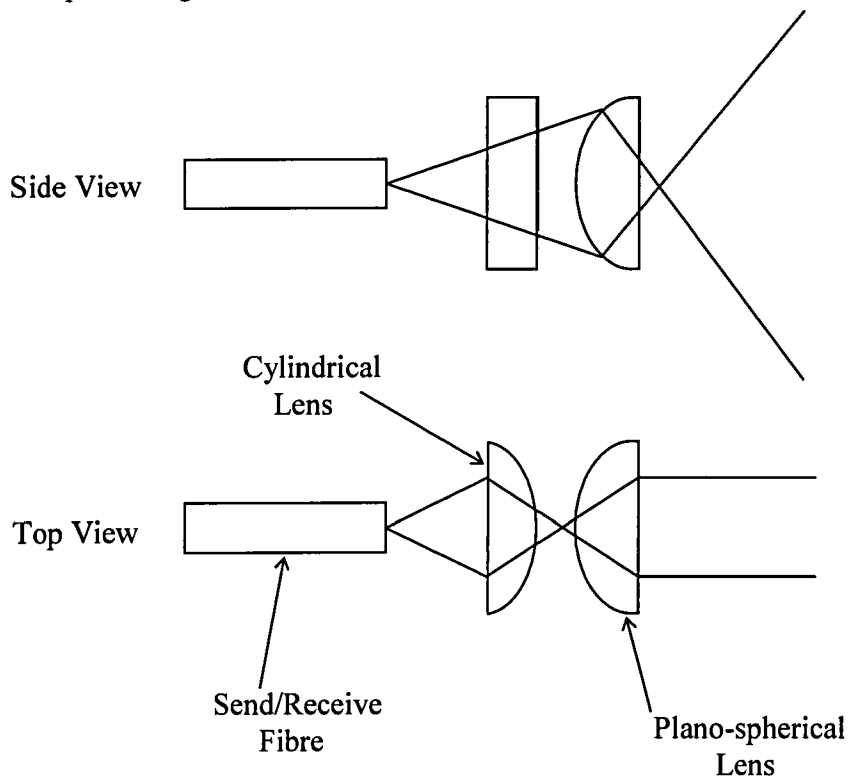


Figure 7.1. Schematic of a High Numerical Aperture Measurement Probe.

References

---

1. Richard Tomlinson, Jeremy M. Coupland, Jon Petzing "Synthetic Aperture Interferometry: In-process measurement of aspheric optics", Applied Optics, Vol. 42, Issue 4, pp 701-707, (February 2003)
2. Richard Tomlinson, Rob Alcock, Jon Petzing, Jeremy Coupland, "Computer-Aided Lens Assembly", Applied Optics, Vol. 43 Issue 3 Page 579 (January 2004)

